이학박사학위논문

Investigation of the spatiotemporal coordination mediated by SHORTROOT and NAC-REGULATED SEED MORPHOLOGY 1 for the root phloem development in *Arabidopsis thaliana.*

SHORTROOT와 NAC-REGULATED SEED MORPHOLOGY 1에 의한 애기장대 뿌리 체관 발달의 시공간적 조절에 관한 연구

2021 년 8 월

서울대학교 대학원

생명과학부

김 효 진

SHORTROOT와 NAC-REGULATED SEED MORPHOLOGY 1에 의한 애기장대 뿌리 체관 발달의 시공간적 조절에 관한 연구

Investigation of the spatiotemporal coordination mediated by SHORTROOT and NAC-REGULATED SEED MORPHOLOGY 1 for the root phloem development in *Arabidopsis thaliana.*

지도교수 이 지 영

이 논문을 이학박사 학위논문으로 제출함

2021년 08월

서울대학교 대학원
생명과학부 생명과학전공
김 효 진

김효진의 박사학위논문을 인준함
2021년 08월

위 원 장 최 연 희

부위원장 이 지 영

위 원 임 준

위 원 이 유 리

위 원 현 유 봉

Investigation of the spatiotemporal coordination mediated by SHORTROOT and NAC-REGULATED SEED MORPHOLOGY 1 for the root phloem development in *Arabidopsis thaliana.*

A dissertation submitted in partial fulfillment of the requirement for the degree of

DOCTOR OF PHILOSOPHY

to the Faculty of School of Biological Sciences

at

Seoul National University

by

Hyoujin Kim

Date Approved	Dissertation Committee	
June 29, 2021	Chair	
	Supervisor	
	Examiner	
	Examiner	
	Examiner	

Abstract

Investigation of the spatiotemporal coordination mediated by SHORTROOT and NAC-REGULATED SEED MORPHOLOGY 1 for the root phloem development in Arabidopsis thaliana.

Hyoujin Kim

Department of Biological Sciences

The Graduate School

Seoul National University

In the plant vascular system, phloem plays an important role in mediating the transportation of essential nutrients and signaling molecules. Two major phloem cell types are generated by asymmetric cell divisions (ACDs); companion cells (CCs) and phloem sieve elements (SEs). In the root apical meristem of *Arabidopsis thaliana*, CCs are generated by the ACDs of procambial cells facing the phloem SEs and pericycle cells. On the other hand, phloem SEs which are composed of the protophloem and metaphloem SEs, are originated from two sequential ACDs of a phloem SE-procambium precursor and a SE precursor.

A previous study in the lab suggested that SHORTROOT (SHR), a GRAS family transcription factor, regulates the ACDs for CCs from the endodermis and for SEs from the phloem. *SHR mRNA* is transcribed in the stele (the xylem, procambium, pericycle cells) except for the phloem pole. But, SHR protein moves into the phloem pole, endodermis, and quiescent center (QC). In the endodermis and QC, SHR activates the expression of SCARECROW (SCR), and then interacts with SCR. This protein complex promotes the expression of *microRNA 165/6* (*miR165/6*). *miR165/6* move into the stele and establish the Class III homeodomain leucine zipper transcription factors (HD-ZIP III) gradient by degrading *HD-ZIP III* mRNAs. This process specifies the identities of proto- and metaxylem. Dr. Jing Zhou, the former Ph.D. student, observed that SHR moving into the phloem pole promotes ACDs for phloem development. However, it was still unclear how movement of SHR into the phloem pole regulates ACDs for SE and CC formation. Therefore, my dissertation research was aimed to find how SHR and its downstream genes serve in phloem development. To address this goal, I performed the functional analysis of *NARS1* and *SND2*, SHR downstream target genes for phloem formation.

In this dissertation, I present that SHORTROOT (SHR) and its direct downstream genes encoding two transcription factors, *NAC-REGULATED SEED MORPHOLOGY 1 (NARS1)* and *SECONDARY WALL-ASSOCIATED NAC DOMAIN PROTEIN 2 (SND2)*, are involved in the phloem development via long-distance top-down signaling while forming a positive feedforward loop. *NARS1* is a

pivotal regulator of ACDs of phloem SE precursor in the meristem, although it is transcribed in the CCs of the root differentiation zone. Thus, NARS1 might be involved in the long-distance top-down signaling pathway. In addition, *SND2* is expressed in the protophloem SEs via NARS1 and activates *NARS1* expression, thereby setting up a positive feedback loop. Together, this study indicates that ACDs for the development of phloem SE occur via long-distance top-down signaling, which enable differentiated phloem cells to regulate the undifferentiated precursor cells. Findings from this study provide new insights into the cell type patterning and differentiation of vascular system during indeterminate plant growth.

Keyword: Phloem sieve element, Asymmetric cell division,
Long-distance signaling, SHORTROOT, NARS1, *Arabidopsis thaliana*

Student Number: 2014-25012

Table of Contents

List of Figures

List of Table

Abbreviations

ACD	Asymmetric cell division
CC	Companion cell
SE	Sieve element
SHR	SHORTROOT
QC	Quiescent center
SCR	SCARECROW
miR165/6	microRNA 165, microRNA 166
NARS1	NAC-REGULATED SEED MORPHOLOGY 1
SND2	SECONDARY WALL-ASSOCIATED NAC DOMAIN PROTEIN 2
ER	Endoplasmic reticulum
GSK3	GLYCOGEN SYNTHASE KINASE 3
HD-ZIP III	Class III homeodomain leucine zipper transcription factors
VISUAL	Vascular cell induction culture system using Arabidopsis leaves
SMXL3,4,5	SUPPRESSOR OF MAX2 1-LIKE 3,4 and 5
JUL	JULGI
UTR	Untranslated region
BRX	BREVIS RADIX

OPS	OCTOPUS
CVP2	COTYLEDON VASCULAR PATTERN2
CVL1	CVP2-LIKE1
PAX	PROTEIN KINASE ASSOCIATED WITH BRX
PIN	PIN-FORMED protein
CLE45	CLAVATA3/EMBRYO SURROUNDING REGION 45
BAM3	BARELY ANY MERISTEM 3
LRR	Leucine-rich repeat
CLV2	CLAVATA2
CRN	CORYNE
APL	ALTERED PHLOEM DEVELOPMENT
PEAR	PHLOEM EARLY DOF
TF	transcription factor
PAR	Partitioning defective protein
GSC	Germline stem cell
bHLH	Basic helix-loop-helix
SPCH	SPEECHLESS
BASL	BREAKING OF ASYMMETRY IN THE STOMATAL LINEAGE
MAPKKK	Mitogen-activated protein kinase kinase kinase
YDA	YODA

SLGC	Stomatal lineage ground cell
SDD1	STOMATAL DENSITY AND DISTRIBUTION1
ERF1	EPIDERMAL PATTERNING FACTOR 1
RAM	Root apical meristem
CEI	Cortex and endodermis initial
BIRD	INDETERMINATE DOMAIN C2H2 zinc finger
JKD	JACKDAW
NUC	NUTCRACKER
MGP	MAGPIE
CYCD6;1	CYCLIN D6;1
RBR	RETINOBLASTOMA-RELATED
CDKB1	CYCLIN DEPENDENT KINASE 1
MED31	Mediator of RNA polymerase II transcription subunit 31
SCL23	SCARECROW-LIKE23
WT	Wild type
SE-ENOD	SE nodulin-like protein
PHB	PHABULOSA
Col-0	Columbia
ABRC	Arabidopsis Biological Resources Center
MS	Murashige and Skoog
DAT	Days after transfer to the growth chamber

PI	Propidium iodide
PFA	Paraformaldehyde
RT-qPCR	RealTime-quantitative Polymerase Chain Reaction
CAL3-M	CALLOSE SYNTHEASE3
FACS	Fluorescence activated cell sorting
RT	Reverse transcription
DEX	Dexamethasone
NAC domain	NAM, ATAF1/2, and CUC2 domain
SNBE	Secondary cell wall NAC binding element
NAC 45, 86	NAC domain-containing TFs 45 and 86
YFP	Yellow Fluorescent Protein
GFP	Green Fluorescent Protein
CFDA	5(6)-carboxyfluorescein diacetate
XVE	DNA binding domain of the bacterial repressor Lex A (X), VP16 (v), estrogen receptor (E)
PRR	Pattern recognition receptor
PAMPs,MAMPs	Perceive pathogen or microbe associated molecular patterns
PEP	Plant Elicitor Peptide
DAMPs	Danger- or damage-associated molecular patterns
ChIP	Chromatin immunoprecipitation

1. Introduction

1.1. Phloem development in the root apical meristem of *Arabidopsis thaliana*.

Plants are systematically organized to optimize resource (i.e. water, sugars, hormones, essential mineral nutrients, amino acids, and other signaling macro- and micro- molecules) transport. Long-distance transport of these nutrients at the whole plant level is facilitated by vascular system in plants, consisting of two functional tissues, xylem and phloem.

Xylem transports water and essential mineral nutrients absorbed by the root, to the shoot, and plays a robust role in providing structural support to the plant, enabling it to stand firmly on the ground. In *Arabidopsis thaliana*, xylem is developed into two types in the center of the stele, the protoxylem where vessels have two strands of primary xylem in the periphery of the xylem axis, and the metaxylem where vessels have three strands of primary xylem in the center of xylem axis **(Fig 1A).** Protoxylem vessels are developed from the procambium cells specifying the narrow cells with spiral or annular cell wall thickening. Metaxylem vessels are formed by the differentiation of broad vessels with pitted or reticulate

cell wall thickening. The deposition of secondary cell walls comprising lignin, hemicellulose, and cellulose is followed by programmed cell death with removal of the nucleus and the cytoplasmic contents during xylem differentiation (Seo et al., 2020).

Phloem is responsible for transporting photo-assimilates and long-distance signaling molecules such as RNAs, hormones, and a plethora of proteins such as FLOWERING LOCUS T, a signal-promoting flowering or growth regulator. Unlike the xylem, sieve elements (SEs) of the phloem consist of the primary cell walls including a β-1,6-galactosyl substitution of 1,4-galactan (Torode et al., 2018). Unlike the xylem, phloem SEs remain alive because they are supported by the companion cells (CCs) interconnected through the cytosolic nanochannels, called plasmodesmata. Although the phloem SEs have been enucleated, these connections are essential for making phloem SE-CC complex a functional unit for transport (López-Salmerón et al., 2019; Tamaki et al., 2020). To facilitate the symplastic transportation of molecules, the apical/basal ends of phloem SEs are connected through sieve plates with sieve pores. Sieve plates are found exceptionally in angiosperms, not in gymnosperms.

Phloem loading system established an apoplastic loading mechanism, driven by plasma membrane transporter using proton motive energy in many species (Sauer, 2007). Apoplastic loading is facilitated by AHA3, a proton pump in the plasma membrane of the CCs and SUC2, a sucrose-H+ symporter carrier protein in the CCs of *Arabidopsis thaliana* (Stadler and Sauer, 1996). And in other plants, the symplastic loading system dependent on density of plasmodesmata arise from the mesophyll to the phloem driven by diffusion (Roberts, 2005; Schulz, 2005).

Phloem SEs in *Arabidopsis thaliana* show special modifications in that they are devoid of a nucleus, vacuole, rough endoplasmic reticulum (ER), and Golgi bodies. This enables mature phloem SEs to have high flow rates of up to ~ 110μm/s for long distance transport of signals and nutrients at a cellular level (Geldner, 2014). As phloem SEs are approximately 250μm long, stream of transportation could be expected to the cell in ~2sec (Sjolund, 1997). The mature phloem SEs show rapid transportation, enabling effective carrying of nutrients to all plant parts including root and shoot. During the differentiation of phloem SEs, plastids contain protein crystals or small particles of starch, instead of lacking thylakoid membranes (Sjolund, 1997).

P-protein is specially formed in the phloem SEs spanning the lumen and anchoring the periphery of mature phloem cells. When injured, SEs release P-protein from the anchoring sites. So the filaments accumulate at the sieve pore to prevent assimilate losses in injury site (Kallarackal and Milburn, 1983). Recent study indicated that varying SE/CC ratio is mainly dependent on the GLYCOGEN SYNTHASE KINASE 3 (GSK3) kinase activity based on the comprehensive gene expression in the vascular cell induction culture system using *Arabidopsis* leaves (VISUAL)-CC system (Tamaki et al., 2020).

In *Arabidopsis thaliana*'s root meristem, two major asymmetric cell division (ACD)s occur for the phloem development. CCs are generated by the ACDs of procambial cells adjoining SEs and pericycle cells. The other ACD is for SE development. The protophloem SEs and metaphloem SEs are originated from two periclinal ACDs of a SE procambium precursor and a SE precursor respectively **(Fig 1B).**

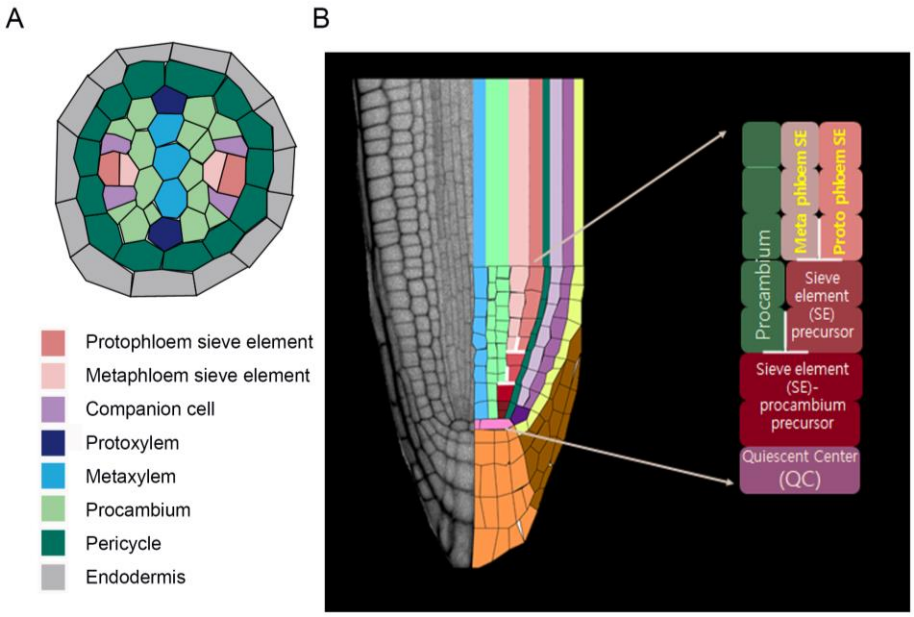

Figure 1. Schematic representation of *Arabidopsis thaliana* root tissue organization. (A) Cross sections through the meristem zones. (B) A schematic diagram showing the asymmetric cell division of two precursor cells for phloem sieve elements formation. Cell types are indicated in different colors both (A) and (B).

1.2. Recent progress in molecular mechanisms of phloem sieve element development.

Recently, many studies have been conducted on gene regulation in phloem development of *Arabidopsis thaliana*. In the earliest players of protophloem SE development, SUPPRESSOR OF MAX2 1-LIKE (SMXL) 3, SMXL 4, and SMXL 5, post-transcriptionally modulated by JULGI (JUL), regulate protophloem SE differentiation in a cell-autonomous manner **(Fig 2)** (Cho et al., 2018). JUL binds and directly modulates the RNA G-quadruplex in the 5′ untranslated region (UTR) of *SMXL4/5*, thus suppressing *SMXL4/5* translation and resulting in the inhibition of phloem differentiation (Cho et al., 2018). The *SMXL4/5* loss-of-function mutants show incomplete differentiation of protophloem SEs (Cho et al., 2018). Plasma membrane-associated proteins, BREVIS RADIX (BRX) and OCTOPUS (OPS), and COTYLEDON VASCULAR PATTERN2 (CVP2) and its homolog CVP2-LIKE1 (CVL1), play important roles in the asymmetric cell division (ACD) of SE precursor cells and the differentiation of protophloem SEs (Anne et al., 2015; Breda et al., 2017; Breda et al., 2019; Truernit et al., 2012). Mutants of these genes show defects in protophloem development. BRX interacts with PROTEIN KINASE ASSOCIATED WITH BRX (PAX). They are polarly co-localized with the PIN-FORMED (PIN) protein which regulates auxin transport, thereby enabling

proper development of protophloem SEs **(Fig 2)** (Marhava et al., 2018). CLAVATA3/EMBRYO SURROUNDING REGION 45 (CLE45), a small mobile peptide, is perceived by BARELY ANY MERISTEM 3 (BAM3), a leucine-rich repeat (LRR) receptor kinase. This signaling is elevated by CLAVATA2 (CLV2) and CORYNE (CRN) that promote the differentiation of protophloem SEs (Anne et al., 2018; Hazak et al., 2017). An MYB-CC TF, ALTERED PHLOEM DEVELOPMENT (APL), plays an important role in early phloem development. APL promotes differentiation of protophloem SEs by regulating NAC domain-containing TFs 45 and 86 (NAC 45 and 86) , which in turn promote protophloem SE enucleation **(Fig 2)** (Furuta et al., 2014a). In recessive *apl*, phloem development including ACD and differentiation is not well established (Bonke et al., 2003). Instead of phloem development, ectopic xylem formation is differentiated in the phloem pole (Bonke et al., 2003). Another TF, PHLOEM EARLY DOF (PEAR) serves as a short mobile signal to promote cell division in the phloem pole, which is antagonized by Class III homeodomain leucine zipper (HD-ZIP III) transcription factors (TFs) expressed in procambial cells neighboring the phloem **(Fig 2)** (Miyashima et al., 2019). Although these complicated molecular mechanisms have been reported, it is unclear how ACD is coordinated for SE and CC formation in the phloem pole.

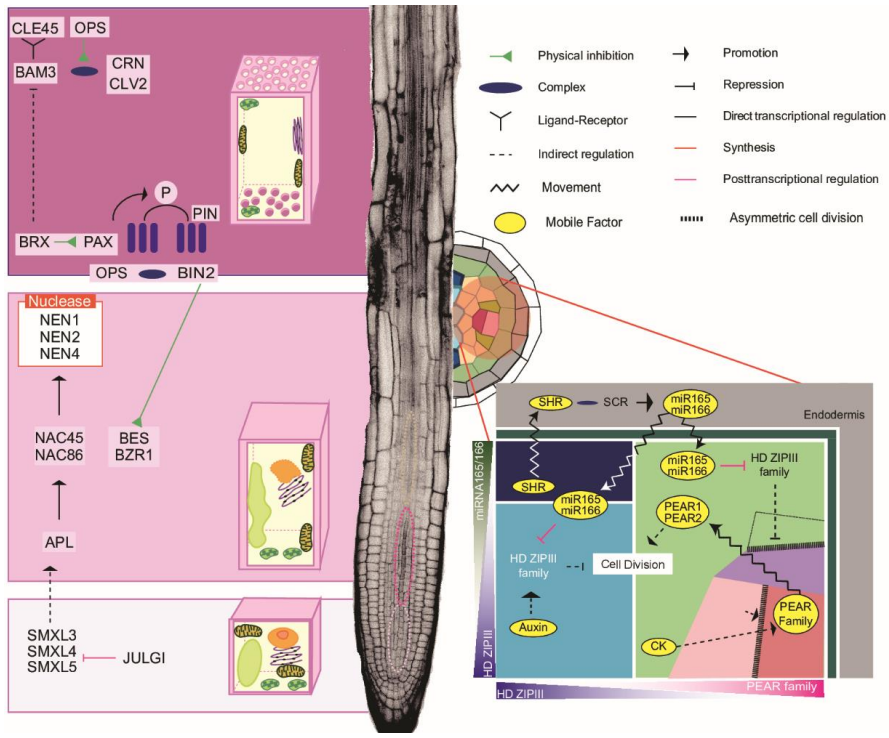

Figure 2. Genetic network mediating development of phloem sieve element. Schematic representation of genes involved in the regulation of the phloem development. This image is published in (Seo et al., 2020).

1.3. Asymmetric cell division is essential for the development of multicellular organisms.

In *Arabidopsis thaliana*, phloem development is determined by two different types of ACDs of the root meristem. The CCs are formed by ACD of the procambial cells adjoining SEs and pericycle cells. The SEs, including the proto- and metaphloem SEs are formed from two periclinal divisions of an SE-procambium precursor and an SE precursor, respectively, starting with the SE-procambium precursor cell (Heo et al., 2014a).

ACD results from two main factors in both plants and animals in general, namely, ‘intrinsic’ and ‘extrinsic’. The intrinsic factors to determine cell fate are asymmetrically segregated into two daughter cells prior to cytokinesis (Pillitteri et al., 2016). In animals, the embryo of *Caenorhabditis elegans* has been found to undergo intrinsic ACD. In the *Caenorhabditis elegans* zygote, partitioning defective protein (PAR) induces unequal segregation to determine the cell fate. The regulation of cortical actomyosin movement is promoted to the sperm-derived centrosome polarizing distribution of PAR proteins (Inaba and Yamashita, 2012). ACDs in the *Caenorhabditis elegans* zygote establish the daughter cells with

altered fate and size. The extrinsic mechanisms involve cell-to-cell communication and external microenvironmental signaling that confer distinct fates to two daughter cells asymmetrically after the cell division (Inaba and Yamashita, 2012). In *Drosophila*, germline stem cells (GSCs) physically interact with the niche and continue as a stem cell, whereas the other cells, losing direct contact with their niche, differentiate into the daughter cells (Ting, 2013).

In plants, both intrinsic and extrinsic mechanism are tightly linked with regulation of development. The stomatal development is a great model to investigate both intrinsic and extrinsic mechanisms of ACDs. The three intrinsic factors, which are involved in the stomatal lineage are transcription factors of the basic helix-loop-helix (bHLH) class, SPEECHLESS (SPCH), MUTE, and FAMA, acts as the stomatal formation starting with the ACDs and progressive cell fate specification, and finishing at the stomatal differentiation (MacAlister et al., 2007; Petricka et al., 2009). SPCH induces the initial breaking of symmetry in epidermis tissue and allows the transition to the meristemoid cell fate (Petricka et al., 2009). MUTE, the downstream gene of SPCH, regulate the ACDs and promotes the transition to the guard mother cell fate (Pillitteri et al., 2016). Furthermore, FAMA which may act downstream of SPCH and MUTE induces the transition to the guard cell fate (Pillitteri et al., 2007).

Intrinsic polarity in these cells results from the BREAKING OF ASYMMETRY IN THE STOMATAL LINEAGE (BASL) polarity module in stomatal ACD in *Arabidopsis thaliana*. The polarity complex is regulated by BASL, mitogen-activated protein kinase kinase kinase (MAPKKK), YODA (YDA), MPK3/6, and POLAR, and is inherited not in the meristemoid cell but in the stomatal lineage ground cell (SLGC) (Pillitteri et al., 2016). ACDs occur to induce the polarization of BASL via YDA and MAPK to suppress the functions of SPCH (Pillitteri et al., 2016). A subtilisin-like serine protease encoded by the STOMATAL DENSITY AND DISTRIBUTION1 (SDD1) gene, the extrinsic factor which triggers signaling cascade occur to be small proteins, lead to guard cell formation (Berger and Altmann, 2000). EPIDERMAL PATTERNING FACTOR 1 (ERF1), a small secreted peptide, is also associated with stomatal patterning (Kodama et al., 2007). Those two factors induce positional cues to inform the ACDs by the extracellular regulation similar to the animal system (Petricka et al., 2009). Furthermore, in the root apical meristem (RAM) of Arabidopsis, stem cells surrounding the quiescent center (QC) undergo ACD to specify the major tissues of the root.

1.4. SHORTROOT (SHR) is a master regulator in the vascular patterning.

The five major types of stem cells of root meristem in *Arabidopsis thaliana* that lead to the development of the root system are epidermis and lateral root cap initials, pericycle initials, cortex and endodermis initials (CEIs), distal columella initials, and stele cell initials. These stem cells surround the QC and maintain their undifferentiated status (Fukuda and Ohashi-Ito, 2019). These stem cells give rise to daughter cells through ACD and then divide further along the proximodistal axes to generate the cells with their fates determined (Fukuda and Ohashi-Ito, 2019). After the cells acquire their identities in the root meristematic zone, they start to elongate and differentiate. Finally, these cells develop into distinct cell types such as xylem vessel with the secondary cell wall deposition and programmed cell death, and enucleated phloem SEs (Seo et al., 2020).

As far as it is well known for previous researches, SHORTROOT (SHR) and SCARECROW (SCR), which are GRAS family transcription factors (TFs), were found to regulate the ACD of the CEI. These two TFs play key roles in inducing periclinal divisions of the CEI of the meristematic zone (Benfey et al., 1993; Helariutta et al., 2000; Scheres et al., 1995). SHR, a mobile TF factor expressed in

the stele cells, acts non-cell-autonomously by directly moving towards the QC, CEI, CEI daughter cells, and endodermis through the plasmodesmata (Vatén et al., 2011). SHR activates *SCR* expression and then physically interacts with SCR (Cui et al., 2007; Levesque et al., 2006). The SHR/SCR complex then promotes the expression of INDETERMINATE DOMAIN C2H2 zinc finger (BIRD) TFs like the JACKDAW (JKD), NUTCRACKER (NUC) and MAGPIE (MGP) (Welch et al., 2007). BIRD interaction with the SHR/SCR restricts SHR movement towards the stele. This interaction between BIRD protein and SHR/SCR network organizes the tissue patterns depending on the positional cues during early root growth (Moreno-Risueno et al., 2015). *CYCLIN D6;1 (CYCD6;1)*, a D-type cell cycle regulator, promotes the formative cell divisions by controlling the SHR/SCR complex as the SHR direct downstream target genes in the SCR cluster (Sozzani et al., 2010). SCR is counteracted by the phosphorylation of RETINOBLASTOMA-RELATED (RBR), a cell cycle inhibitor, by being regulated by *CYCD6;1* together with the *CDKB1;1 (CYCLIN DEPENDENT KINASE 1;1)* or *CDKB1;2* in the stem cell niche. This network restricts ACDs by forming the endodermal and cortical layer. In the endodermis, SCR directly interacts with RBR protein, which reduces the effect of SCR transcriptional regulator on spatial restriction of the division process. SCR interacts with SHR to promote together with auxin *CYCD6;1* transcription.

CYCD6;1 mediates the phosphorylation of RBR by reducing the activity of the CEI daughter cells (Wildwater et al., 2005). An auxin maximum in the CEI induces CYCD6;1 expression by promoting periclinal cell division (Cruz-Ramírez et al., 2012; Di Mambro et al., 2018). To transcriptionally regulate *CYCD6;1*, the SHR/SCR complex interacts with mediator of RNA polymerase II transcription subunit 31 (MED31), the RNA polymerase II cofactor mediator in the ground tissue of the meristematic zone (Zhang et al., 2018). Furthermore, another GRAS TF, SCARECROW-LIKE23 (SCL23) also forms the heterodimeric complex with SHR . SCL23 mediates the activity of SHR in the hypocotyl region of Arabidopsis root, reducing the accumulation of the *SHR* mRNA and SHR protein (Kim et al., 2017; Long et al., 2015). The SHR-SCR-SCL23 network has been shown to regulate endodermis development in both shoots and roots (Long et al., 2015; Yoon et al., 2016).

In the *Arabidopsis thaliana* root, the SHR/SCR complex also regulates development of the stele cells which consist of the xylem and phloem cells. The formation of the metaxylem and protoxylem is established via the dosage-dependent regulation of the Class III homeodomain leucine zipper (HD-ZIP III) gene family members. The SHR/SCR complex in the endodermis activates the

expression of microRNA 165/6 (miR165/6), that target the HD-ZIP III members. Moving out of the endodermis via the plasmodesmata, miR165/6 degrades the HD-ZIP III mRNAs at the xylem periphery. The expression of HD-ZIP III forms a gradient with the maximum in the metaxylem and minimum in the protoxylem (Carlsbecker et al., 2010). This bidirectional signaling pathway controls the biosynthesis of cytokinin by the HD-ZIP III's, which in turn mediates auxin distribution (Dello Ioio et al., 2012; Sebastian et al., 2015). SCR and its partner SHR have been largely characterized as essential effectors in the vascular patterning of the Arabidopsis initial cell layers. Taken together, the SHR protein is the most important regulator for root development which can move and function for its non-cell-autonomous activity in radial patterning of the Arabidopsis root (Nakajima et al., 2001).

1.5. SHR regulates development of both phloem SEs and CCs.

The *shr-2* mutant exhibits defects in both xylem patterning and phloem development (Carlsbecker et al., 2010). In the wild type (WT) Arabidopsis root meristems, two phloem poles, each of which consists of proto-and meta-phloem SEs, develop via aforementioned two-step ACDs. CCs develop adjacent to SEs via ACD of procambial cells adjoining SEs and pericycle. Dr. Jing Zhou who earned Ph. D under the guidance of Prof. Ji-Young Lee at Cornell University found that an *shr-2* mutant-root has only one SE-like cell in the phloem pole. Through immunostaining early SE nodulin-like protein (SE-ENOD) which specifically detects differentiating SEs (Khan et al., 2007), Dr. Zhou observed that unlike WT roots with two SEs differentiating in each phloem pole **(Fig 3A,C),** *shr-2* roots developed fewer SEs **(Fig 3B,D)**.

To examine the differentiation status of phloem SE and CC, phloem markers, *pAPL::erGFP*, which is expressed in developing protophloem SEs of the meristem **(Fig 3E)** and *pSUC2::erGFP*, which is expressed in CCs **(Fig 3G)**, were used (Bonke et al., 2003; Stadler and Sauer, 1996). In *shr-2*, *pAPL::erGFP* was expressed in the protophloem SE not of the meristem but of the elongation zone **(Fig 3F)**. In addition, *pSUC2::erGFP* was expressed in only one cell neighboring

the SEs in *shr-2* **(Fig 3H)**. These results indicated that SHR regulates ACDs associated with the formation of both CCs and SEs in phloem poles.

To check whether the SHR-SCR-miR165/6 pathway, which patterns xylem vessel types in the root, affects phloem SE development, the *pUAS*::*MIR165A; shr-2 J0571* transgenic line, which drives *miR165* expression in the ground tissue of the *shr*-2, was examined (Carlsbecker et al., 2010). The *pUAS*::*MIR165A; shr-2 J0571* transgenic line showed recovery of the stele cell numbers, unlike the SEs **(Fig 3I)**. In *shr-2 phb-6*, a double mutant of *SHR* and *PHABULOSA* (*PHB*) which encodes a member of the HD-ZIPIII family, a recovery of the procambial cell number was observed but not of the SEs **(Fig 3J)**. However, the *pUAS*::*MIR165A; shr-2 J0571* transgenic line and *shr-2 phb-6* increased the expression level of *pSUC2::erGFP*, indicating recovery of the CCs (data not shown). The *scr-4* mutant showed a decreased procambial cell number like *shr-2*, but *scr-4* was found to have two SEs **(Fig 3K)**. Furthermore, *pCRE1::PHBem:GFP*, which expressed a microRNA resistant version of *PHB* under the CRE1 promoter was developed to overexpress PHB in the whole stele (Sebastian et al., 2015). This transgenic plant was similar to the phenotype of *shr-2*, with a severe reduction in the procambium cell number.

But, the formation of phloem SEs in this transgenic plant is similar to the WT **(Fig 3L).** These results indicated that the SHR, SCR, *miR165/6*, and PHB pathways mainly control procambial cell proliferation, including the one for CC formation in the meristem but do not have a role to play in ACD for the SE development. However, it was unclear how movement of SHR promotes ACDs in the phloem pole. Here, I present that SHR moving into the phloem pole regulates phloem development via long-distance top-down signaling. SHR moving into the phloem pole seems to turn on the other transcription factors specifically in the phloem to promote ACDs for phloem development. Characterization of SHR direct downstream transcription factors led me to discover a new regulator involved in the early phloem formation of the root in *Arabidopsis thaliana*.

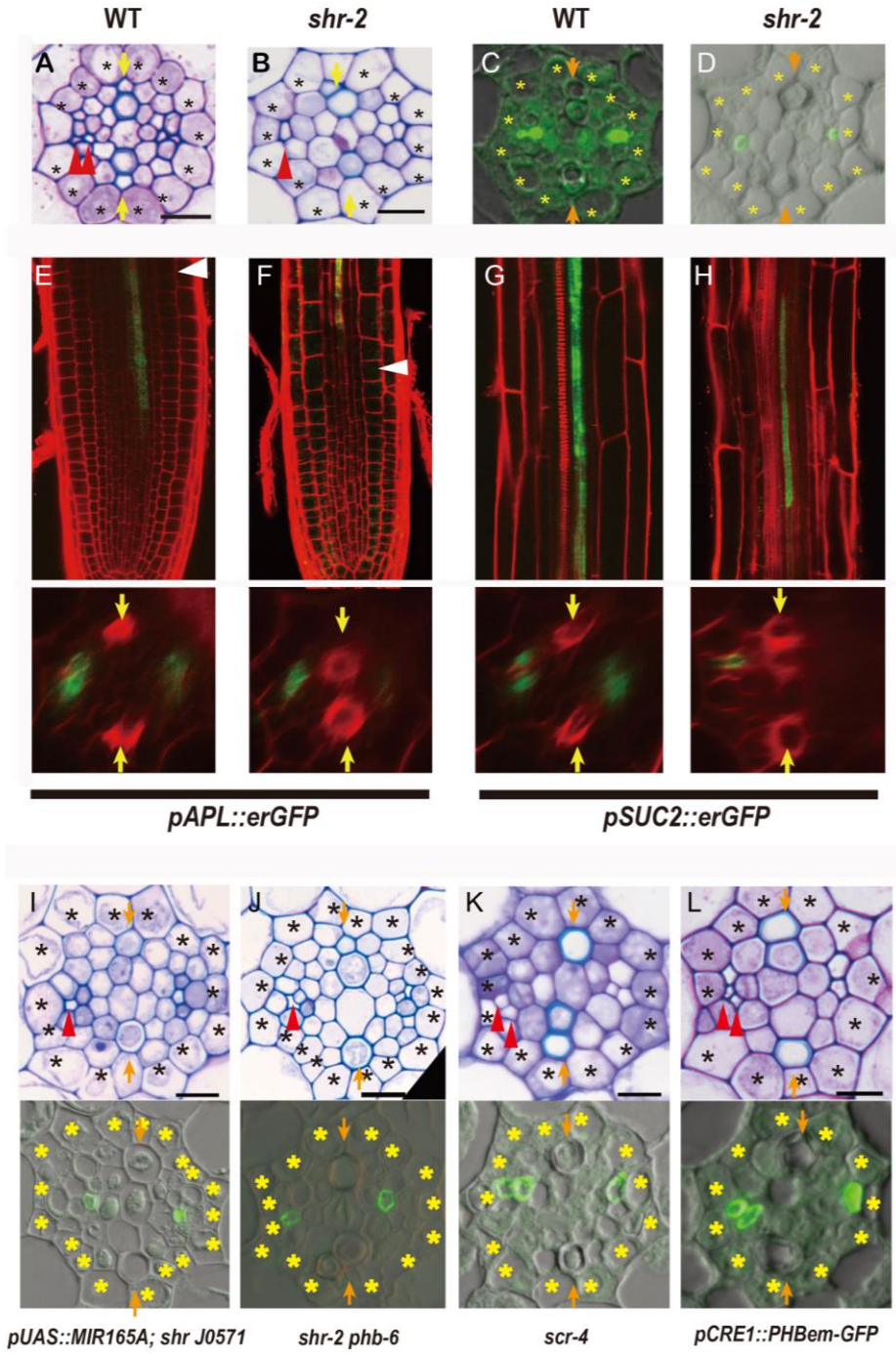
WT
shr-2
WT
shr-2
A
B
C
D
E
F
G
H
pAPL::erGFP
pSUC2::erGFP
I
J
K
L
pUAS::MIR165A; shr J0571
shr-2 phb-6
scr-4
pCRE1::PHBem-GFP

Figure 3. SHR plays the essential regulator for phloem development both phloem SEs and CCs (A-D) and PHB suppresses procambial cell divisions for CCs development (I-L). Comparison of the phloem SEs development between WT and *shr-2* through cross section stained with toluidine blue (A-B) and immunostaining SE-ENOD (C-D). (A,C) The formation of phloem SE is normal in both phloem poles of the WT roots. (B,D) In *shr-2*, the phloem SE like cell was detected in the phloem poles. (E-H) Expression of two phloem markers. The expression of *pAPL::erGFP* in the WT (E) and *shr-2* (F). The expression *pSUC2::erGFP* in the WT (G) and *shr-2* (H). Cross sections stained with toluidine blue and immunostaining SE-ENOD of *pUAS*::*MIR165A; shr-2 J0571* (I), *shr-2 phb-6* (J), *scr-4* (K) and *pCRE1::PHBem:GFP* (L) are observed. Asterisks, pericycles; Yellow and orange arrows, xylem axis; Red arrow heads, phloem SEs; White arrow heads, beginning of the transition zone of the roots; WT, wild-type. Scale bars=10μm. Data were generated by Dr. Jing Zhou and published in Kim et al. (2020) as Figure 1 and 2.

2. Material and Method

2.1. Plant Materials

Arabidopsis thaliana used in this study is ecotype Columbia (Col-0) accession. *nars1-2* (SALK_137131), *nars1-1* (SM_3_28017) and *snd2-1* (CS124048) were obtained from the Arabidopsis Biological Resources Center (ABRC). Seeds were washed surface sterilization with alcohol. After the washing, the seeds were plated on the 1x MS media which contains 4.3g/L Murashige and Skoog (MS) salts (Duchefa, M0221.0050), 1% sucrose (Duchefa, S0809), 0.5g/L MES (Sigma, M8250) hydrate (pH 5.7 with KOH) and 1% plant agar (Duchefa, P1001). Plates were grown under a 16h-light/8h-dark cycle with light intensity of 100μM m^{-2} s^{-1} at 22-23°C in a plant growth chamber for 5 to 10 days depending on the experimental condition. The following marker lines were described previously; *pNAC45:GUS-GFP* (Furuta et al., 2014a), *pAPL::erGFP* (Bonke et al., 2003), and *pSUC2::erGFP* (Stadler and Sauer, 1996).

2.2. Plasmid Construction for this study

Gateway cloning technology (Invitrogen) was used for DNA manipulations. The *NARS1* and *SND2* promoter regions were amplified from Arabidopsis Col-0 genomic DNA by PCR and inserted into pDONR P4P1R through a BP reaction according to instructions. *SND2* cDNA was amplified by RT-PCR and then cloned into pDONR221, and *NARS1* cDNA was cloned into both pDONR221 and pDONR P2RP3 by a BP reaction. Other components, in this case *GFP*, *GUS*, and *erGFP*,

were cloned into pDONR221 and pDONR P2RP3 by a BP reaction. *pSND2:SND2:GFP*, *pSND2:GUS pCRE1:SND2*, *pCRE1::SND2:GFP* were constructed into destination vector, dpGreen KanT by means of Multisite Gateway LR recombination.

pCRE1::NARS1, pCRE1::GFP:NARS1, pS29::GFP:NARS1,pNARS1::erGFP, pNARS1::GFP:NARS1, pSUC2::GFP:NARS1 and *pSUC2::XVE>>GFP:NARS1* were constructed into destination vector, dpGreen-BarT by means of Multisite Gateway LR recombination. All clones in the binary vector were transformed into Agrobacterium GV3101 with pSOUP for Arabidopsis transformation by floral dipping (Clough and Bent, 1998). PHB cDNA was cloned into pDONR221 and mutagenized to PHBm (Carlsbecker et al., 2010). SHRΔNLELDV was amplified from the plasmid containing SHRΔ NLELDV and cloned into pDONR221 (Gallagher and Benfey, 2009) GFP:nos T and nlsGFP for C terminus translational fusion were cloned into pDONR P2RP3 by means of BP recombination. *pS32::PHBm:GFP* was constructed into the dpGreen Bar by Mutisite gateway LR recombination. *pCRE1::SHRΔNLELDV:nlsGFP* and *pS32::SHRΔNLELDV:nlsGFP* were constructed into the dpGreen BarT, which is the dpGreen Bar vector with the terminator attached. . The following plasmids were described previously; S29, S32 and CRE1 promoters in pDONR P4P1R (Carlsbecker et al., 2010; Lee et al., 2006) and SUC2::XVE inducible promoter in pDONR P4P1R (Yan et al., 2019).

2.3. Microscopic observation

Seedling used in this study were collected at 5 to 6 days after transfer to the growth chamber (DAT). Only *pSUC2::XVE>>GFP:NARS1* in *nars1* transgenic plants

were observed after 8 days after transfer to the growth chamber because of visualization the signals. Longitudinal images with PI staining and vibratome sectioning images with Calcoflour staining were taken by LSM700 Laser scanning confocal microscope (Leica) with preset emission/excitation wavelengths of 488 nm/505 to 530nm for GFP or Alexa Fluor 488, and 561 nm/591 to 635 nm for propidium iodide (PI). For deep imaging to track the cell lineage with serial Z stack, Cleared samples with ClearSee solution treatment were observing using the TCS SP8 Laser confocal microscopy with preset emission/excitation wavelengths of 390nm/420nm for Calcoflour white and aniline blue staining and 488 nm/505 to 530nm for GFP or Alexa Fluor 488.

2.4. Cross-section

Roots of 6DAT seedling were fixed with 4% paraformaldehyde (PFA) dissolved in PBS buffer (10x PBS [for 1L]: add 2g KCl [27mM], 81.8g NaCl [1.4M], 11.57g $Na_2HPO_4 \bullet 2H_2O$ [65mM], and 2.04g KH_2PO_4 [15mM] in water. Prior to use, dilute to 1X and adjust pH is 7.4 with KOH.) for one day at 4℃. The fixed samples were washed in PBS three times for 30/20/10 minutes at room temperature and dehydrated in a graded series of ethanol (25, 50, 75, and 100% diluted in PBS buffer) for 1hour. After the dehydrated step, samples were continuously incubated in a series of Technovit 8100 cold-polymerizing resin (64709012, Kulzer Technique) (25 and 50% for 3hours 75 and 100% substituting twice each for 5 hours diluted in ethanol). The plastic samples were sectioned by Microtome (RM2255, Leica) with 3μm of thickness. For toluidine blue staining (T3260, Sigma), sections were stained with 0.05% Toluidine blue (pH 4.3) diluted in 1xPBS and imaged with the Eclipse Ni (Nikon) microscope.

2.5. Immunostaining SE-ENOD

Roots of 5 to 6 DAT seedlings were used in immunostaining SE-ENOD. Seedlings were fixed with 4% paraformaldehyde (PFA) dissolved in PBS buffer for one hour at room temperature. The fixed samples were washed in PBS four times for 10 minutes each at room temperature. Seedling were embedded in 4% low melting agarose (50100, Sea Plaque Agarose ™) dissolved in PBS. The samples were sectioned using a vibrating microtome (VT1000S, Leica) with 120μm thickness. Sections were collected and washed in 6 well plates containing 1X PBS. Sections were incubated in 2% BSA blocking solution (A-3912, Sigma) diluted in PBS at room temperature. Sections were transferred to the primary antibody (RS6, EIW201, Kerafast) solution, prepared by adding antibody to the blocking solution in the ratio 1:100 for overnight at 4°C. Treated samples were washed in 1X PBS 6 times for 10 min each at room temperature. After the washing, samples were applied with secondary antibody (Alexa Fluor® 488 F(ab')2 Fragment of Goat Anti-Mouse IgG, IgM (H+L), A-10680, Invitrogen) diluted 200 folds in the blocking solution. The samples were washed with 6 times in 1X PBS for 10 min each at room temperature in the dark condition. For Calcofluor white (18909, Sigma) staining, the samples were incubated in 0.1% Calcoflour white staining solution diluted in 1X PBS for 1min at room temperature with the dark condition. Signals are examined using Confocal Microscope (ZEISS, LSM700) with preset emission/excitation wavelength of 488 nm/505 to 530 nm for Alexa 488 and of 350nm/420nm for Cacoflour White 2MR.

The unpublished paper about Immuostaining SE-ENOD protocol is attached to appendix.

2.6. CFDA dye test for tracing symplastic loading pathway

Plants to monitor the CFDA symplastic movement were grown in normal MS media in growth chamber for 5 days and transfer the media included 1μM Pep1 media for 2days more under a 16h-light/8h-dark cycle with light intensity of 100μM m^{-2} s^{-1} at 22-23°C in a plant growth chamber. The symplastic tracer 5(6)-Carboxyfluorescein (Sigma, 21877) was used. The 60μg/ml CFDA fluorescent probe was loaded through the cotyledon of which the needle punched the end. To visualize the CFDA dye loading, the stereo microscope (Nikon SMZ18) detected the 450- to 490nm excitation filter and a 515nm long-pass emission filter.

2.7. ClearSee for confocal imaging

Roots for imaging were fixed with 4% PFA under the vacuum infiltration for 1 hour at room temperature. Fixed samples were washed three times in 1X PBS. Samples were incubated in ClearSee solution at room temperature for at least 4 days to clear the cellular content. ClearSee solution was prepared by diluting following components to the specified concentrations in distilled water: 10%[w/v] of Xylitol (W507930, Sigma), 15%[w/v] of Sodium deoxychlolate (D6750, Sigma), and 25% [w/v] Urea (U5378, Sigma). After the incubation, the samples were stained with 0.1% Calcoflour white 2MR staining solution diluted in 1X PBS for at least 10min at room temperature. Signals are examined using Confocal Microscope (SP8, Leica) with preset emission/excitation wavelength of 488 nm/505 to 530 nm for GFP and of 350nm/420nm for Cacoflour White 2MR.

2.8. Callose deposition assay with Aniline blue staining

Transgenic plants (*pSUC2::freeGFP*) to observe the callose deposition were germinated and grown in normal MS media in a growth chamber for 5 days, transferred to the 0.5x MS media including 1μM of Pep1 and grown for 2 days under a 16h-light/8h-dark cycle with light intensity of 100μM m^{-2} s^{-1} at 22-23°C. The peptide Atpep1 (ATKVKAKQRGKEKVSSGRPGQHN) were used in this study. Before the staining, the whole seedlings were fixed in the 4% paraformaldehyde (in 1xPBS) for 1 hour and washed three times for 10 min in 1xPBS. Seedlings were then transferred to 67mM of K_2HPO_4 (sigma, 1551128; pH was adjusted to 12 with KOH) and rinsed briefly. Seedling were further incubated in fresh 67mM of K_2HPO_4 (pH 12) for another 30min at room temperature. They were then stained in 0.01% of Aniline blue (Sigma, B8583) dissolved in 67mM of K_2HPO_4 (pH 12) for 30-60min at room temperature. The vessel with the staining solution was wrapped in the aluminum foil, because aniline blue is light sensitive. Confocal images were obtained using the TCS SP8 confocal microscope (Leica) with preset emission/excitation wavelengths of 390nm/420nm for callose detection and 488nm/530nm for GFP.

2.9. RealTime-quantitative Polymerase Chain Reaction: RT-qPCR

To identify the expression level of the *NARS1* in *nars1* mutant and *SND2* in *snd2* mutant, RT-qPCR analysis were performed using total RNAs extracted from 7DAT seedling in WT, *nars1* and *snd2* roots. Total RNA was extracted with a RNeasy plant mini prep kit (Qiagen). The reverse transcript reaction of 20μl was conducted for the first strand synthesis 1μg of total RNAs and Superscript III reverse transcriptase (Invitrogen). cDNA template was diluted 5 folds and subsequently used for qRT-PCR reacting iQ™ SYBER Green Supermix (Bio-Rad) on a BioRad CFX96 Real Time PCR machine. GADPH was used as the internal control gene for this analysis.

2.10. Statistical Analysis

The statistical analysis was used in one-way ANOVA, followed by Dunnett's multiple comparisons test (a = 0.05). And all genotypes were compared to against the WT control (Col-0). Data were expressed as mean 6 ± SEM. Statistical significance was shown as follows: ****P≤0.0001, ***P≤0.001, **P≤0.01, *P≤0.05 and nonsignificant (ns; P > 0.05). n denotes the number of samples. All analyses were done using GraphPad PRISM v.8.3.1. (Data analyzed by Dr. Nam V. Hoang, the former post doctorate researcher)

Table 1. The list of primer

Primers used in this study	Sequence (5' → 3')	Usage
SND2 promoter for	GGGGACAACTTTGTATAGAAAAGTTGCACT TGAATGACACCTTGCCG	amplifying SND2 promoter for Gateway cloning
SND2 promoter rev	GGGGACTGCTTTTTTGTACAAACTTGAGTTG TTTTGTGTCCCTAAGT	
SND2 cDNA for	GGGGACAAGTTTGTACAAAAAAGCAGGCTC CATGACTTGGTGCAATGACCG	amplifying SND2 coding regions for Gateway cloning
SND2 cDNA rev	GGGGACCACTTTGTACAAGAAAGCTGGGTC TTAAGGGATAAAAGGTTGAGAG	
SND2 RT for	CGGTAACGGTAAGAGCAACG	qRT-PCR for SND2 gene expression
SND2 RT rev	TGGTTCTGTATCCCGGTCTG	
SND2 geno for	CAATGACCGTAGCGATGTTC	genotyping *snd2-1*
SND2 geno rev	CTTGTTCCCGTCGTGTATGC	
SM specific	TACGAATAAGAGCGTCCATTTTAGAGTGA	
GAPDH for	GCATTGAGCGACAAGTTTGTG	qRT-PCR for control gene expression
GAPDH rev	AGTACGAACTCAACCACACAC	
NARS1 promoter region 1 for	GTGATGGTATTAGATGGCCAAATC	primer pair for ChIP
NARS1 promoter region 1 rev	CGTGCAATTTCAGGAAACCC	
NARS1 promoter region 2 for	AACTGGAAGATTCCAAACCAAA	primer pair for ChIP
NARS1 promoter region 2 rev	ACATAGGCCTAACTGAATCCAC	
NARS1 promoter region 3 for	GGGCGTTGAGAAGGTAACAA	primer pair for ChIP
NARS1 promoter region 3 rev	GATTCTGCTGAGACTTTGCTTTATT	
NARS1 promoter region 4 for	ACGAACAAATCGGACACTGA	primer pair for ChIP
NARS1 promoter region 4 rev	ACTACTGCGAGAATCTTATGAGC	
NARS1 promoter region 5 for	ATCAATTCAGAGTTCAGACCAAATG	primer pair for ChIP
NARS1 promoter region 5 rev	GGGTCTTTCCCGGATATAACG	
NARS1 promoter region 6 for	CAATCGTCCGATGTTTGGC	primer pair for ChIP
NARS1 promoter region 6 rev	TCCAGTGTGTGAACATTTGTAAC	
NARS1 promoter region 7 for	GTTTGAATTGCCCTGGCATC	primer pair for ChIP
NARS1 promoter region 7 rev	TGCATGCCAATCAACTAATTACC	
NARS1 promoter region 8 for	TCCAGTTGTGATTGCACGATAA	primer pair for ChIP
NARS1 promoter region 8 rev	TCTTCAACATAACGTGGGTACTG	

NARS1 promoter region 9 for NARS1 promoter region 9 rev	TGAGATTCTGAACGTCTAGCAAA CACATCCATCAGATCAAGAGACA	primer pair for ChIP
NARS1 promoter region 10 for NARS1 promoter region 10 rev	GTTACCTTCTCTGGCGATTTCT CGACACGTGTGATACCTATGG	primer pair for ChIP
NARS1 promoter region 11 for NARS1 promoter region 11 rev	TCGACATGATTAGTCAGGCTTTG CCCATATTTCAGCCGAGTTTAGT	primer pair for ChIP
NARS1 promoter region 12 for NARS1 promoter region 12 rev	ATTACGTTAATATCCGAGGGTGTAT GGAAAGGAAAGGAGTGCTGA	primer pair for ChIP
SND2 promoter region1 for SND2 promoter region1 rev	GTTAACAGGGGAGAGCAGAA CTTCACGTAGACTTCTCATGC	primer pair for ChIP
SND2 promoter region2 for SND2 promoter region2 rev	GCTCACATATGTATTCCCTC GTTGGGCTCATGGCATGTAT	primer pair for ChIP
SND2 promoter region3 for SND2 promoter region3 rev	GGCATCTCCCTCTCGTTGTT GTTCTATATACTGTATAGTGAG	primer pair for ChIP
18s for 18s rev	TACCGTCCTAGTCTCAACCA AACATCTAAGGGCATCACAG	negative control for ChIP
SCL3 for SCL3 rev	TTTTGGGAGTGAGAGGGTTC AGATGGATGGGATTGGAAAA	positive control for ChIP
NARS1 promoter for NARS1 promoter rev	GTCAGCGGCCGCGAACCATAAAGCGAATATGA TCACGCGGCCGCTGTATCCGTTGTAGAAGATA	amplifying NARS1 promoter for Gateway cloning
NARS1 cDNA for NARS1 cDNA rev	GGGGACAAGTTTGTACAAAAAAGCAGGCTCCATGGAGAGCACCGATTCTTC GGGGACCACTTTGTACAAGAAAGCTGGGTCTTAAGAAGAGTACCAATTTA	amplifying NARS1 coding region for Gateway cloning
NARS1 geno for NARS1 geno rev LB a1	TGGTACTGACTCAGTAGATCA CTATATGCATCTATACAAAC TGGTTCACGTAGTGGGCCATCG	genotyping *nars1-2*
NARS1 RT for NARS1 RT rev	GGTGTGAAGAATTTTCCGGTG CTCTAACCCCTGTGACCAATT	
nars1qRT PCR 5' nars1qRT PCR 3'	CGTCAGGTCCTATGATGATG CCTACACCGTGAAACCGTTT	NARS1 qRT-PCR

3. Results

3.1. SHORTROOT(SHR) is responsible for the phloem development.

3.1.1. SHR moving into the phloem pole controls ACD of phloem SE precursor.

The *SHR* mRNA is transcribed in the xylem, the procambium and xylem pole-pericycle cells, not in the phloem poles. The SHR proteins move to the phloem pole and the cell layer outside the stele **(Figs 4A,B).** Noticeably, SHR protein in the stele and endodermis was found not only in the root meristem but in the elongation and maturation zones.

To test whether SHR protein movement influences the process of phloem development, *pCRE1::SHRΔNLELDV:nlsGFP; shr-2*, in which *SHRΔNLELDV,* a non-mobile version of SHR, is expressed throughout the stele, was generated (Carlsbecker et al., 2010; Mähönen et al., 2000). Adding canonical nuclear localization signal to SHRΔNLELDV was found to completely inhibit the cell-to-cell movement of the SHR, but did not affect its biological functions (Gallagher and Benfey, 2009). These transgenic lines showed imperfect recovery of root growth and did not show a recovery in xylem patterning, consistent with previous

results (Carlsbecker et al., 2010). On the contrary, immunostaining SE-ENOD indicated that the number of phloem SEs increased in the *pCRE1::SHRΔNLELDV:nlsGFP* in *shr-2* transgenic plants **(Figs 5A-C**; data were provided by Dr. Jing Zhou). This result suggested that SHR in the stele induces ACDs for the formation of phloem SEs.

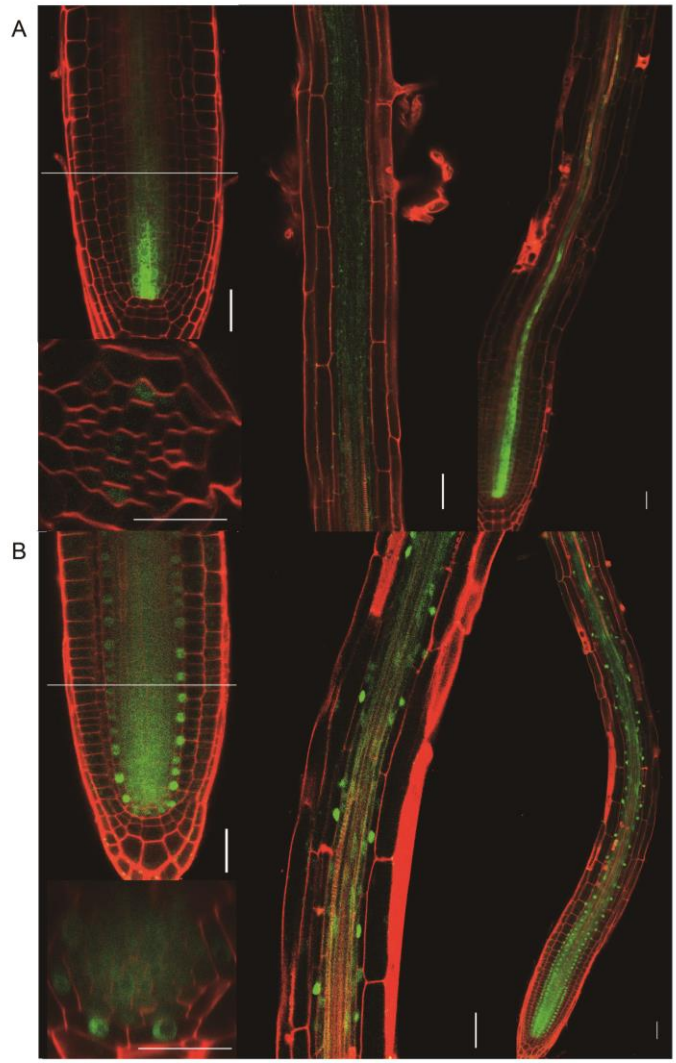

Figure 4. Expression patterns of SHR mRNA and protein. (A) Expression of *pSHR::erGFP* in meristematic zone (left) and differentiation zone (middle). (B) *pSHR::SHR:GFP* transgenic plants were expressed in the stele and endodermis. Confocal cross sections were imaged at the meristematic zone (A-B, left bottom). The expression of both *pSHR::erGFP* and *pSHR::SHR:GFP* indicate that SHR is shown to the all root developmental zones. Scale bars=20μm.

To explore whether the movement of SHR into the phloem pole is required for the ACD for SE formation, *SHRΔNLELDV* fused to nlsGFP was expressed under the *S32* promoter, which drives gene expression in early phloem SEs, was introduced to the *shr-2*(Lee et al., 2006). *pS32::SHRΔNLELDV:nlsGFP* in *shr-2* line recovered the number of SEs but did not recover the stele cell number which remained similar to the one in *shr-2* **(Figs 5D-F**; data were provided by Dr. Jing Zhou). Taken together, SHR moving into the phloem poles induces ACDs for phloem SE formation in the root meristem.

The phloem SEs are connected to CCs through the cytosolic channels, plasmodesmata. To identify if SHR should move into the phloem poles via plasmodesmata to drive the ACD for SE development, an inducible gain of function mutant of *CALLOSE SYNTHEASE3 (CAL3-M)* was expressed under the EPM (S29) promoter, which drives the transcription in the phloem SE-precursor cells with estradiol-mediated induction (Lee et al., 2006; Miyashima et al., 2019). This transgenic line showed excessive callose accumulation in the plasmodesmata when treated with estradiol. Without estradiol treatment, the SHR protein moved into phloem SE precursors **(Figs 5G,H)**, and the two phloem SEs were detected by SE-ENOD immunostaining **(Fig 5I**; data were provided by Dr. Jing Zhou).

When CAL3-M was induced with estradiol treatment, SHR was not able to move into the phloem SE precursors **(Figs 5J, K)**. In addition, only one phloem SE was formed in each phloem pole **(Fig 5L**; data were provided by Dr. Jing Zhou), consistent with other data indicating the need for SHR movement to phloem poles for the normal SE development.

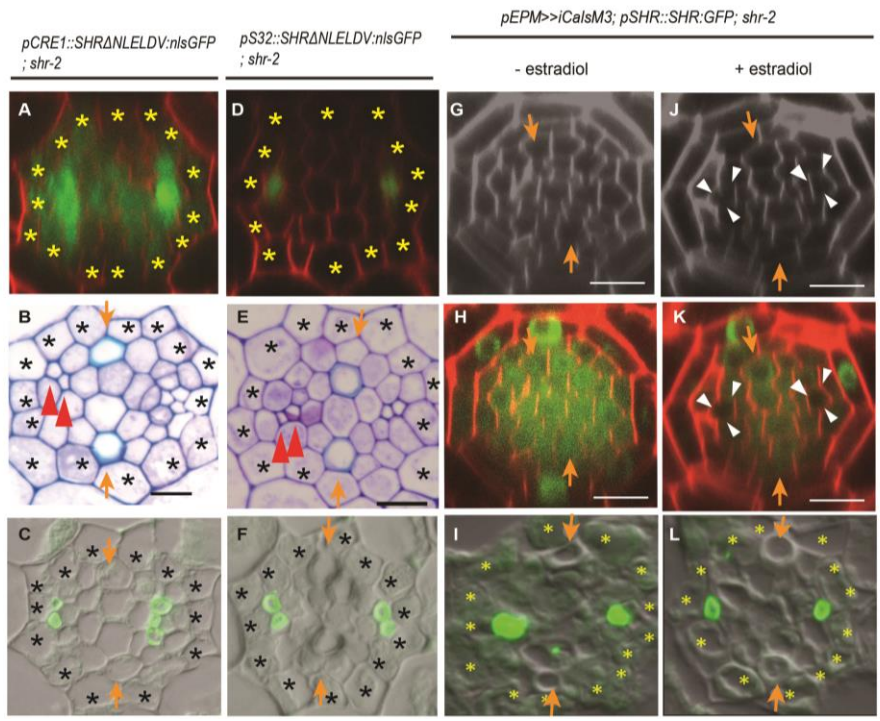

Figure 5. Movement of SHR into the phloem pole is responsible for the phloem SEs formation. (A-L) Cross sections of the root meristematic zone were imaged in *pCRE1::SHRΔNLELDV:nlsGFP* in *shr-2* with confocal (A), transverse section (B) and immunostaining SE-ENOD (C) and *pS32::SHRΔNLELDV:nlsGFP* in *shr-2* with confocal (D), transverse section (E) and immunostaining SE-ENOD (F). Confocal cross sections of the root meristematic zone (G-K) and immunostaining SE-ENOD (I-L) of *pEPM>>iCalsM3 pSHR::SHR:GFP* in *shr-2* were shown. Without the estradiol treatment, SHR moved into the phloem pole and phloem SEs were formed (G-I). With the estradiol treatment for 2days with 10μM, movement of SHR failed to the phloem pole and phloem SEs were formed abnormally. White arrow heads, phloem poles; Asterisks, pericycles; Arrows, xylem axis; Red arrows, phloem SEs; Scale bars=10μm. These data by Dr. Jing Zhou were published in Kim et al. (2020) as Figure 3.

3.1.2. Quantification and classification of phloem SE development and cell counting.

In the wild type root, the development of two phloem SEs was found in all cases. However, in the afore-mentioned genotypes, I found many deviations from such a robust wild-type SE pattern. Therefore, when studying the development of phloem SEs, I classified the observed phloem SE patterns into 6 groups and quantified their distributions in each genotype using the fast and accurate SE-ENOD immunostaining protocol which I developed **(see Appendix).** Class 1 had no SE on either of the phloem poles, exhibiting a severe defect in phloem formation. Class 2 had SEs on only one phloem pole and Class 3 had only one SE on each of the phloem poles. Class 4 had one SE on one phloem pole and more than two SEs on the other phloem pole. Class 5 had two SEs each, on each of the phloem poles. Class 6 had two SEs on one phloem pole and more than two SEs on the other phloem pole. SEs in the wild type belonged to Class 5 **(Figs 6A,B)**. Furthermore, stele cell number was also calculated for all the genotypes **(Fig 6C)**.

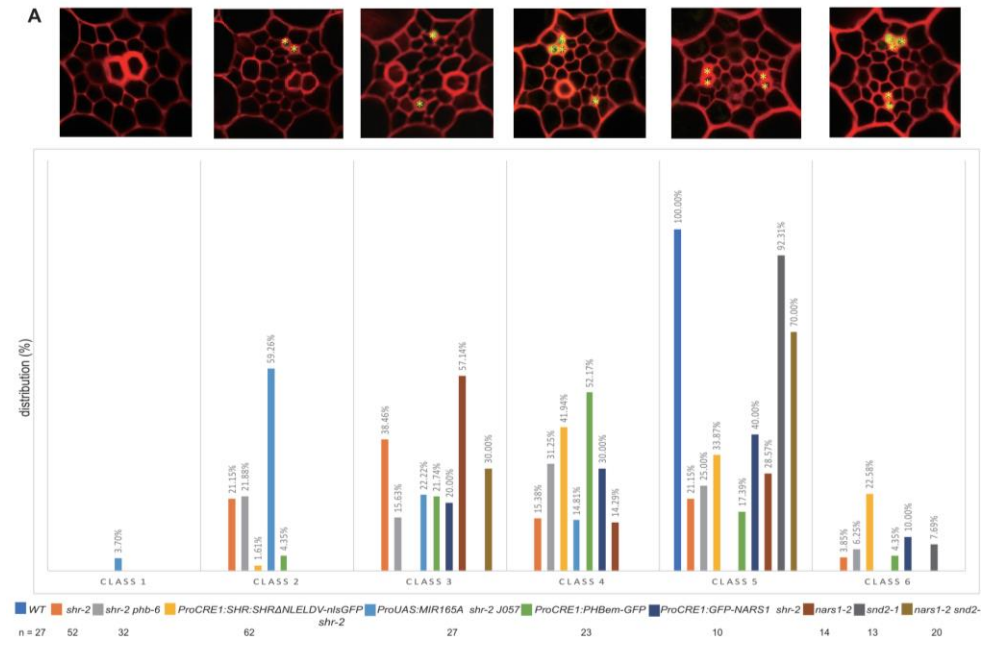
A
distribution (%)
CLASS 1
CLASS 2
CLASS 3
CLASS 4
CLASS 5
CLASS 6
WT
shr-2
shr-2 phb-6
ProCRE1:SHR:SHRΔNLELDV-nlsGFP shr-2
ProUAS:MIR165A shr-2 J057
ProCRE1:PHBem-GFP
ProCRE1:GFP-NARS1 shr-2
nars1-2
snd2-1
nars1-2 snd2-
n = 27 52 32 62 27 23 10 14 13 20

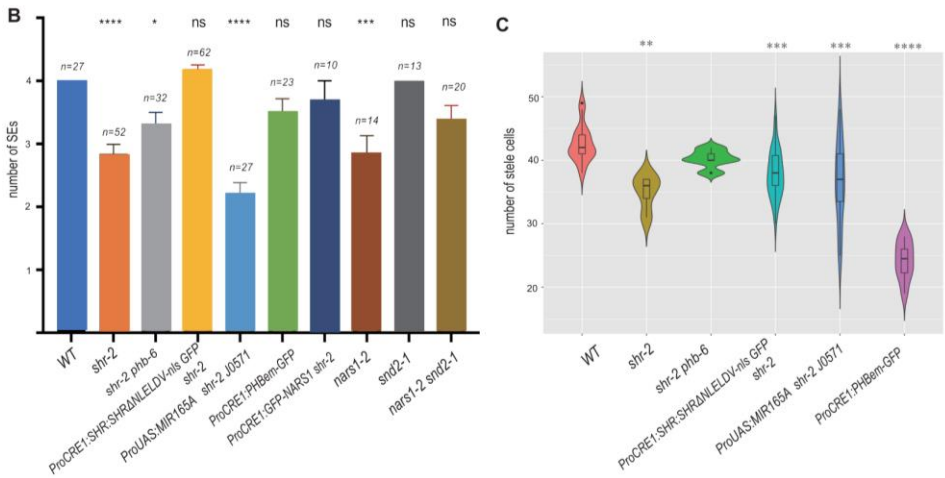
B
number of SEs
C
number of stele cells
WT
shr-2
shr-2 phb-6
ProCRE1:SHR:SHRΔNLELDV-nls GFP shr-2
ProUAS:MIR165A shr-2 J0571
ProCRE1:PHBem-GFP
ProCRE1:GFP-NARS1 shr-2
nars1-2
snd2-1
nars1-2 snd2-1

Figure 6. Classification of the phloem SEs development and cell counting with all genotypes. Quantification of the developmental patterns of phloem SEs, which were categorized into six classes. All wild-type roots develop SEs in class 5. (B) Comparison of the number of phloem SEs in the genotypes analyzed in panel (A). (C) Quantification and comparison of the stele cell numbers. (A) in the WT, *shr-2*, *pCRE1:PHBem:GFP*, *pCRE1:SHR:SHRΔNLELDV:nlsGFP* in *shr-2*, *pUAS:MIR165A* in *shr-2 J0571* and in *shr-2 phb-6* lines. The number of individuals (n) scored is identical to that in (A). The statistical analysis was performed via a one-way ANOVA, followed by Dunnett's multiple comparisons test ($\alpha = 0.05$), to compare each sample against the WT control (Col-0). Data are expressed as the mean ± SEM. Statistical significance was expressed as follows: ****$p \leq 0.0001$, ***$p \leq 0.001$, **$p \leq 0.01$, *$p \leq 0.05$ and non-significant (ns, $p > 0.05$). This is Supplemental Figure 2 in Kim et al. (2020)

3.2. Identification of *NARS1* and *SND2* as downstream targets of SHR during phloem development.

3.2.1. Genetic analysis of *NARS1* and *SND2* as downstream targets of SHR in terms of phloem development.

The SHR protein, likely turns on the expression of other TFs in the phloem pole to promote ACDs. The former lab members, Dr. Jing Zhou and Dr. Deepak Kumar, had identified SHR downstream genes using the following approaches. To find phloem-enriched genes that are up-regulated by SHR, genome-wide expression data were generated for meta-analysis of WT, *shr-2*, and the *pCRE1::SHRΔNLELDV:nlsGFP; shr-2* transgenic line using fluorescence activated cell sorting (FACS). This meta-analysis found two clusters comprising 224 phloem-enriched genes that are down-regulated in *shr-2* compared to the WT and then restored expression in *pCRE1::SHRΔNLELDV:nlsGFP* in *shr-2* transgenic plants.

To find the candidate TF genes that are direct targeted by SHR, *pSHR::SHR:GR* in *shr-2* transgenic plants induced with dexamethasone (Dex), were observed over a period of time and the expression levels in 24 candidate TFs were measured using digital droplet reverse transcription (RT)-PCR **(Fig 7B)**. Five TFs showed increased expression upon SHR-induction. These were *NARS1, AT2G03500, AT4G29100, NAC40,* and *ZIP44* **(Fig 7A)**. As the NAC domain TFs are known to be involved in vascular development, the following two genes were selected as SHR downstream candidates for the study: *NARS1* and *SND2*.

A

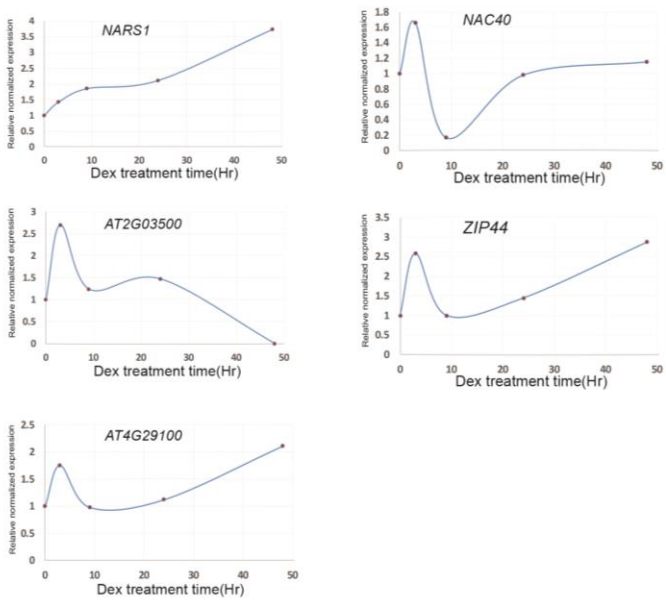

B

	Dex treatment time				
	0 hr	3 hr	9 hr	24 hr	48 hr
SCR	1	2.016	0.96	0.85	2.5
NARS1	1	1.42	1.85	2.11	3.73
SND2	1	0.885	0.31	1.29	3.05
NAC10	1	0.86	0.64	0.57	3.46
AT2G03500	1	2.7	1.24	1.47	0
OFP1	1	1.19	0.96	0.81	1.43
DOF6	1	0.515	2.42	2.02	2.73
OBP2	1	0.67	1	1.11	2.67
AT3G54390	1	0.74	0.95	1.38	2.01
AT1G76890	1	0.95	0.76	0.51	1.79
AT4G29100	1	1.75	0.98	1.12	2.11
AT5G03510	1	0.9	0.8	0.75	1.01
AT3G12730	1	1	1.16	1.67	3.23
ZFP4	1	0.82	0.43	1.37	1.675
AGL12	1	1.22	1.03	1.22	1.39
AT2G28200	1	0.86	0.798	0.68	1.13
MYR2	1	1.309	1.5	3.94	3.28
AT4G38620	1	1	0.95	1.33	4.97
CRF1	1	0.8	1.25	0.58	0.52
NAC40	1	1.66	0.17	0.98	1.152
ROXY2	1	0.51	0.717	0.833	1.05
ZIP44	1	2.58	1	1.444	2.87
AT2G40970	1	0.91	0.46	0.43	1.62

Figure 7. Expression dynamics of time course dependent on the SHR induction identify the phloem enriched transcription factors. (A) Time course experiment expressed changes of potential direct target genes of SHR in the *pSHR::SHR:GR* in *shr-2* transgenic plants in response to the Dexamethasone treatment. (B) According to the digital droplet reverse transcription (RT)-PCR results extracted from RNA samples in the root tips, expression levels of phloem enriched transcription factors dependent to the SHR induction were measured at the different time point. Expression values (copies/μl) were converted to the expression ratios via division with the expression level at 0 hour. Data were generated by Dr. Deepak Kumar and published in Kim et al. (2020) as Figure 4 and Supplemental Figure 5.

NARS1 (*NAC-REGULATED SEED MORPHOLOGY 1*; *ANAC056*; *AT3G15510*) responded early to SHR induction and *SND2* (*SECONDARY WALL-ASSOCIATED NAC DOMAIN PROTEIN2*; *ANAC073* ; *AT4G28500*) responded slower than *NARS1*, to SHR induction. To identify whether SHR-GFP directly binds to the promoters of *NARS1* and *SND2*, chromatin immunoprecipitation (ChIP) assay was performed and followed by real time qPCR using *pSHR::SHR:GFP* in *shr-2* mutant transgenic plants. Data were provided by Dr. Deepak Kumar, the former post doctorate researcher. SHR-GFP bound to ~1 kb and ~3 kb upstream regions of the *NARS1* translation start site **(Fig 8A)**, and ~1 kb upstream region of the *SND2* translation start site **(Fig 8B)**.

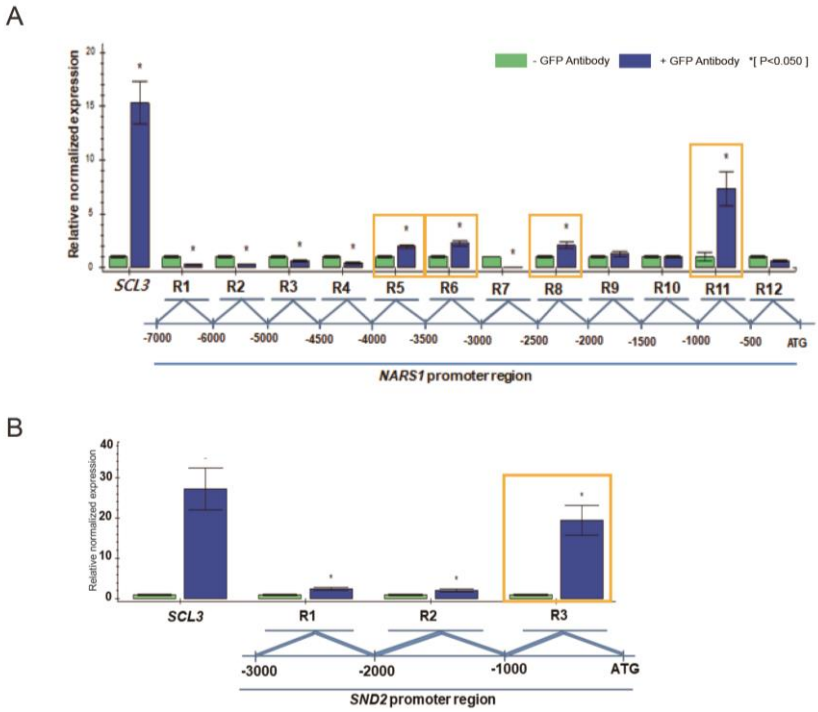

Figure 8. ChIP real-time qPCR analysis for analyzing the direct binding of SHR to the *NARS1* (A) and *SND2* (B) promoter. A ChIP was carried out in roots of 5 DAT transgenic *shr-2* plants introduced with *pSHR::SHR:GFP*. SCL3 was used in a positive control based on the previous studies (Cui et al., 2007). Data were generated by Dr. Deepak Kumar, and published in Kim et al. (2020) as Figure 5A and Supplemental Figure 12C.

3.2.2. Characteristics of NAC domain transcription factors.

NAC domain proteins (NAM, ATAF1/2, and CUC2) are plant specific TFs that are well known to play major roles in diverse plant developmental processes. NAC proteins comprise a conserved NAC domain at the N-terminus, including 160 amino acid residues (Hu et al., 2010). Amino acid residues of NAC domain TFs are divided into five sub-domains. The conserved NAC domain in the TFs is associated with nuclear localization, DNA-binding domain, and the formation of homo or hetero dimers with other NAC domain proteins in N-terminus regions, but C-terminus regions of the NAC domain TFs are divergent for transcriptional regulation (Hu et al., 2010).

According to previous studies, NARS1 was found to regulate embryogenesis by controlling the development and degeneration of ovule integuments via interaction with NARS2 (Kunieda et al., 2008). Some of the *nars1-nars2* double mutant embryos showed defects in embryogenesis by arresting at the torpedo-shaped embryo stage (Kunieda et al., 2008). In the recent study, the double mutant *nars1(anac056)* and *anac018,* shows significant reduction in the levels of cell wall ingrowth deposition in the cotyledons, which results in impaired capacity for phloem loading (Wu et al., 2018). SND2 (ANAC073) is one of the TFs associated

with the formation of secondary cell wall in fibers (Zhong et al., 2008). The dominant repression of SND2, SND3, MYB103, MYB85, MYB52, MYB54, and KNAT7, reduced secondary cell wall thickening; however, the overexpression of SND2, SND3, and MYB103 caused slight increase of the secondary cell wall thickening in fibers by inducing secondary cell wall biosynthesis genes (Zhong et al., 2008). A recent study indicated that SND2/3/4/5 regulate the expression of the downstream targets by binding with secondary cell wall NAC binding elements (SNBEs) during wood formation (Zhong et al., 2021).

3.2.3. Expression domain analysis of *NARS1* and *SND2* in WT and *shr-2.*

To characterize the expression domain of *NARS1*, *pNARS1::erGFP* was developed in the SHR heterozygote (*shr-2/+)* transgenic lines. GFP expression analysis indicated that *NARS1* mRNA was expressed in CCs of the differentiation zone in the WT **(Fig 9A, left)** roots but not in the *shr-2* roots **(Fig 9A, right).** The expression domain of *pNARS1::erGFP* is similar to that of *pSUC2::erGFP* **(Fig 9B)** (Stadler and Sauer, 1996). Unfortunately, translation of NARS1 could not been observed in the *pNARS1::GFP:NARS1*; *nars1* transgenic line. To analyze the expression pattern of *SND2*, *pSND2::GUS* was developed in *shr-2/+*. *pSND2::GUS* was expressed in the developing protophloem SEs of the meristem zone and metaxylem of the differentiation zone in the WT roots **(Fig 10A)**.

However, it was not expressed in protophloem SEs but maintained its expression in metaxylem of the *shr-2* roots **(Fig 10A)**. Consistent with the expression of transcriptional fusion lines, confocal imaging of *pSND2::SND2:GFP* transgenic lines indicated that SND2 protein is expressed in protophloem SEs of the meristem zone and metaxylem of the differentiation zone **(Fig 10B)**. In addition, in *shr-2*, SND2-GFP was not detected in protophloem SEs, but was in the metaxylem **(Fig 10B)**. These data are consistent with other data indicating that NARS1 and SND2 are upregulated by SHR in the phloem.

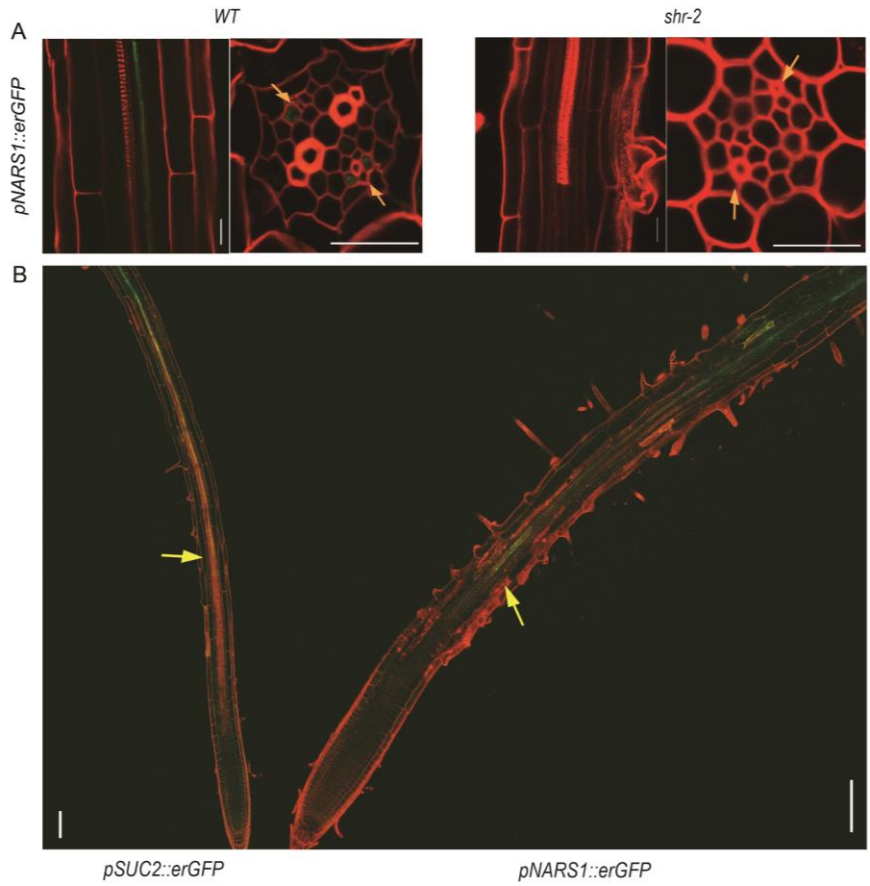

Figure 9. Expression pattern of *NARS1*. (A) NARS1 transcribed in the CCs of the differentiation zone not in *shr-2* (right) but in WT (left). (B) Expression pattern of *NARS1* mRNA (right) is similar *SUC2* expressed in CCs (left). This was published in Kim et al. (2020) as Figure 5B and Supplemental Figure 9.

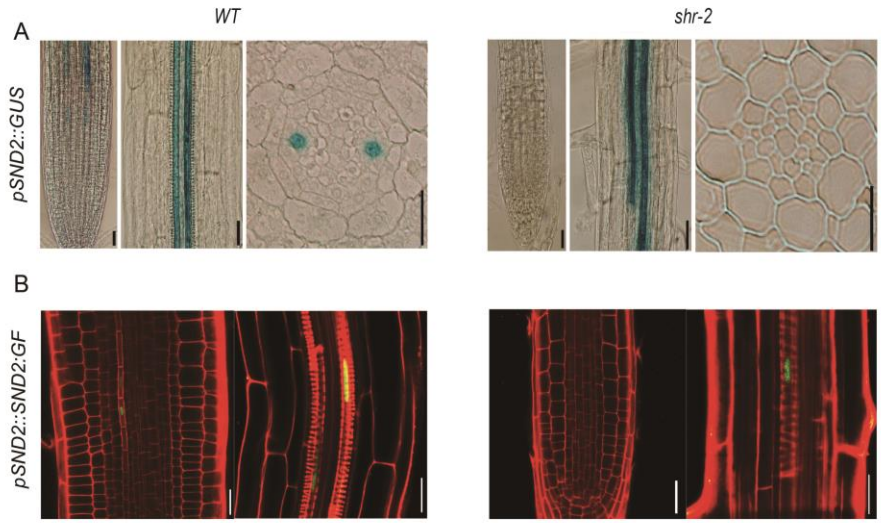

Figure 10. Expression patterns of SND2. The transcriptional expression of SND2 was shown to the proto phloem SEs and metaxylem in WT (A, left). *pSND2::GUS* in *shr-2* was not expressed in protophloem SEs but still remain the metaxylem (A, right). Consistent with expression of *pSND2::GUS*, translational GFP fusion transgenic plants were visualized identically (B). Scale bars=20μm. This is published in Kim et al. (2020) as Figure 5C.

3.2.4. Characterization of *nars1* and *snd2* mutant phenotype.

To determine the biological function underpinning phloem development, a T-DNA insertion line, *nars1*, (*SALK_137131*; *nars1-2)* which had a T-DNA inserted at the 3′ UTR **(Fig 11A)**, and an Spm transposable element insertion line, s*nd2-1* (CS124048, *snd2-1)* mutant, which had an Spm transposable element inserted at the second exon of the coding region **(Fig 11C)**, were used in this study. The expression level of NARS1 showed reduction in the roots of the *nars1* mutant compared with that of the WT, according to the result of the RT-PCR **(Fig 11B)**. In addition, the expression level of SND2 showed reduction in the roots of the *snd2* mutant compared with that of the WT, according to the result of the RT-PCR **(Fig 11D)**. The rate of primary root growth was significantly reduced in the *nars1* mutant **(Figs 12A-C)**. Sucrose, an important mobile form of carbon, is produced in photosynthesizing tissues transporting the phloem SEs in the plants. When *nars1* mutant seedlings were grown on MS media without sucrose, the rate of primary root growth was reduced more significantly than when grown in the normal 1% sucrose media **(Fig 12A).** Furthermore, the root lengths of *snd2* mutants were slightly reduced compared to those of the WT **(Figs 12B, C)**.

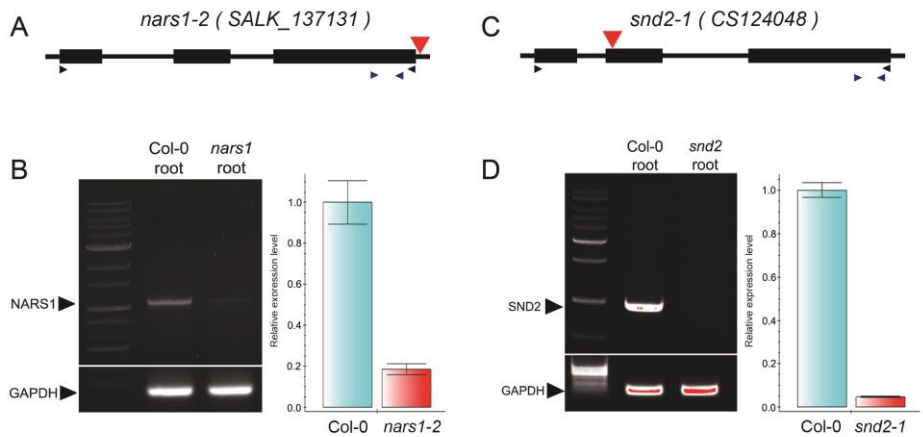

Figure 11. Characterization of *nars1* and *snd2*. (A,C) A schematic diagram of the genome structure of *NARS1* locus in the *nars1-2* (A) and *SND2* locus in the *snd2-1* (C). (B,D) PCR results of reverse transcription indicated *NARS1* expression levels (1095bp) both Col-0 (WT) and *nars1* (B) and *SND2* expression levels (918bp) both Col-0 (WT) and *snd2* (D). Marked primers (A,C arrowheads) were used in PCR. GADPH was used for positive control. This is published in Kim et al. (2020) as Supplemental Figure 6.

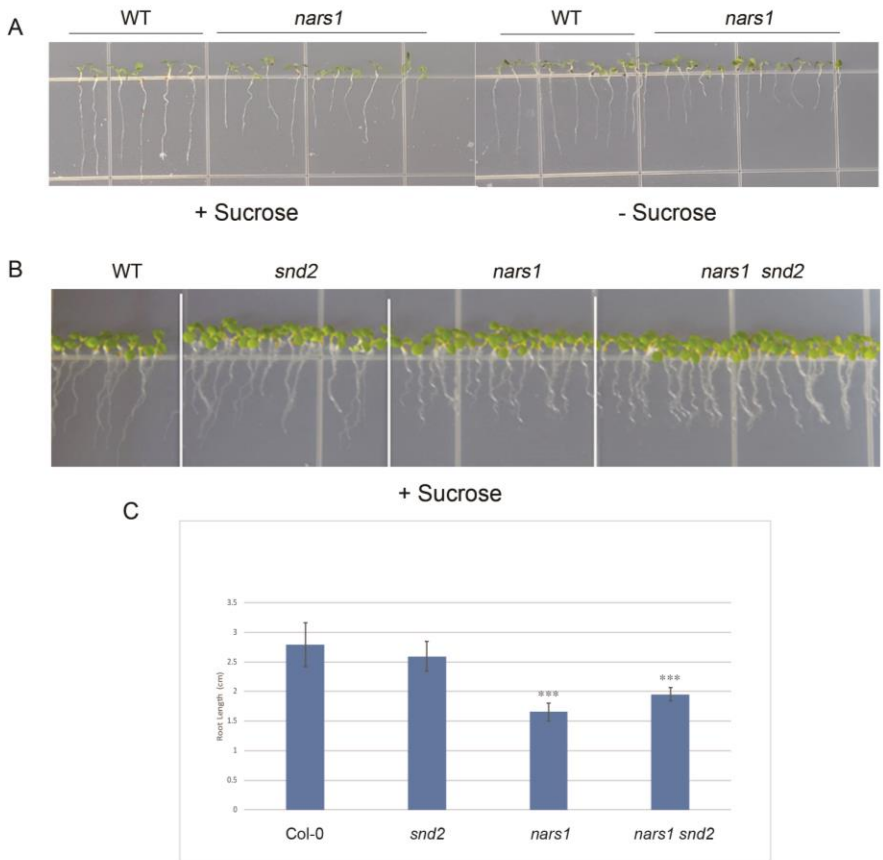

Figure 12. Comparison to the root growth in WT, *nars1*, *snd2* and *nars1 snd2*.

(A) Root lengths of 5DAT seedlings were compared between WT and *nars1* with or without sucrose media. (B) Root lengths of 5DAT seedlings were compared between WT, *nars1*, *snd2* and *nars1 snd2* with sucrose media. (C) Root lengths of 5DAT seedlings were measured in WT, *snd2*, *nars1* and *nars1 snd2*. Error bars indicate the standard error. N=8 for the WT, 7 for *snd2-1*, 8 for *nars1-2*, and 9 for *nars1-2 snd2-1*; ***, P<0.001 for Student's *t*-test against Col-0 wild type. Panel C is published in Kim et al. (2020) as Supplemental Figure 6E.

3.2.5. Marker analysis in the *nars1* and *snd2* mutants.

To better interpret the roles of both NARS1 and SND2 in phloem development, expression analysis of several phloem markers was conducted. For the analysis of protophloem SEs and CCs, *pAPL::erGFP* was introduced into the WT, *nars1*, and *snd2* genotypes (Bonke et al., 2003). The developing protophloem SEs were continuously expressed in both WT, *snd2* and *nars1* **(Figs 13A-C, top)** Also, the expression of CCs was normal in both phloem poles adjoining with phloem SEs in all genotypes **(Figs 13A-C, bottom).** The expression of *GUS:GFP* driven by the promoter of NAC45, which regulates phloem enucleation, showed no difference in the WT, *nars1*, and *snd2* **(Figs 14A-C)** (Furuta et al., 2014b). As enucleation is a normal process, *nars1* and *snd2* did not have undifferentiated cells in the protophloem SEs. Based on the analysis of the phloem differentiation marker using propidium iodide (PI) staining, protophloem differentiation was observed to be normal in all the three genotypes **(Figs 15A-C)**.

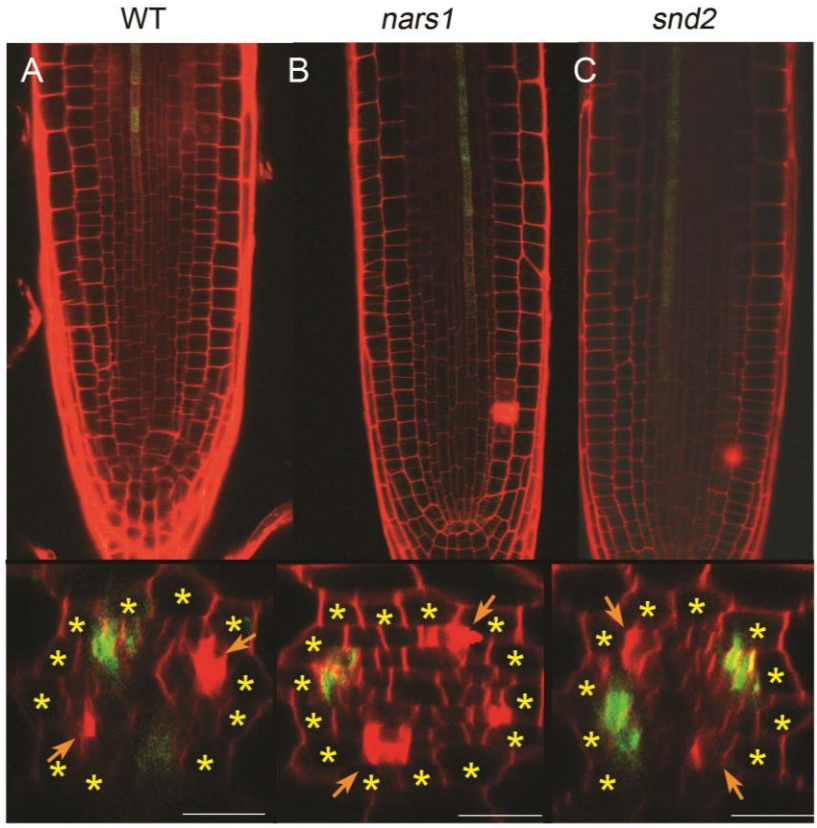

Figure 13. Expression patterns of *pAPL::erGFP* in WT, *nars1* and *snd2*. (A-C, top) The expression of *pAPL::erGFP* in WT(A), *nars1* (B) and *snd2* (C) was visualized normal in protophloem SEs of the root meristematic zone. (A-C, bottom) The confocal cross sections of *pAPL::erGFP* in WT(A), *nars1* (B) and *snd2* (C) was expressed in the CCs both phloem poles in the maturation zone. Scale bars=20μm. This is published in Kim et al. (2020) as Supplemental Figure 7.

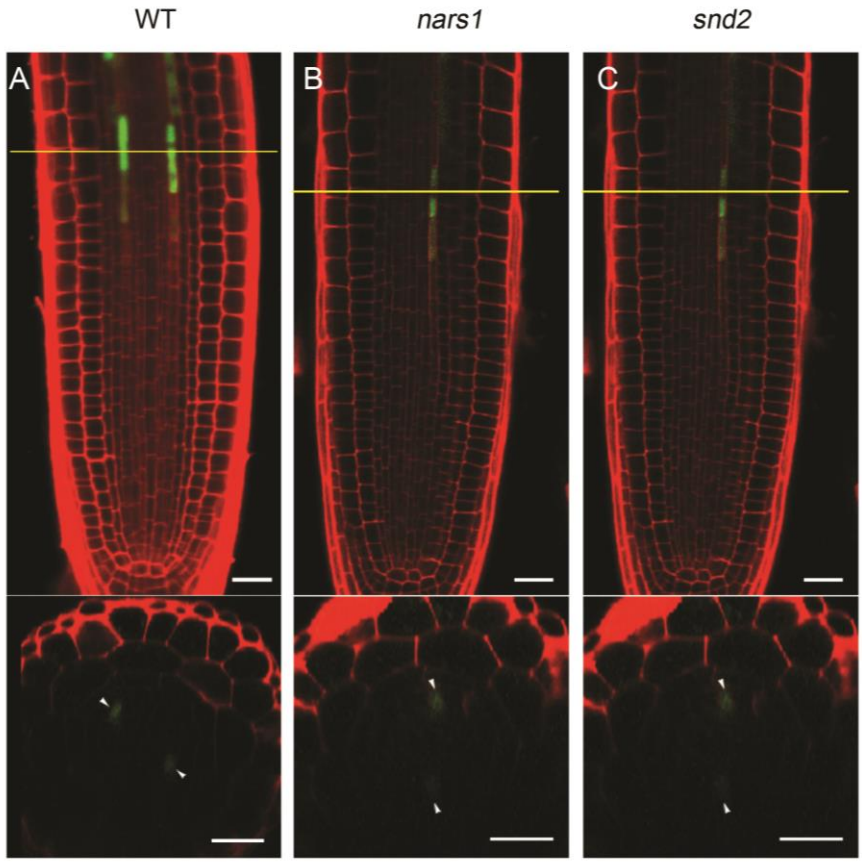

Figure 14. Expression patterns of *pNAC45::GUS-GFP* in WT, *nars1* and *snd2*.

(A-C, top) The expression of *pNAC45::GUS-GFP* in WT(A), *nars1* (B) and *snd2* (C) was visualized in differentiating protophloem SEs of the root meristematic zone. (A-C, bottom) The confocal cross sections of *pNAC45::GUS-GFP* in WT(A), *nars1* (B) and *snd2* (C) was expressed in the protophloem SEs both phloem poles of the root meristematic zone. Scale bars=20μm. This is published in Kim et al. (2020) as Supplemental Figure 7B-I.

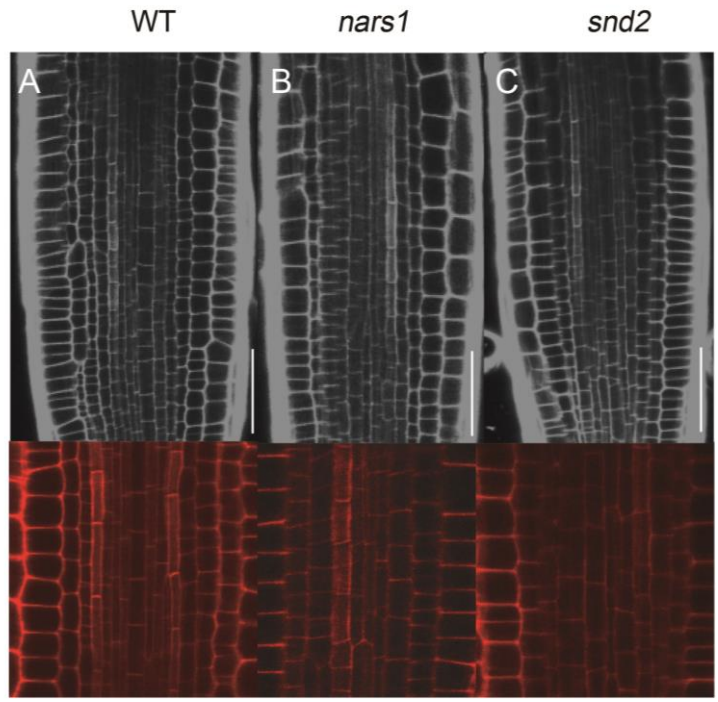

Figure 15. Analysis of protophloem cell lineage and differentiation. (A-C) Differentiation of protophloem SE was visualized with propidium iodide (PI) staining of WT (A), *nars1* (B) and *snd2* (C). No differences of protophloem SEs between all genotypes were observed. Scale bars=20μm. This is published in Kim et al. (2020) as Figure 6A-C.

3.2.6. Abnormal formation of phloem SEs in the *nars1* mutant.

pAT5G48060::H2B:YFP, expressed in differentiating protophloem SE stably because of H2B, was observed as an interesting point in *nars1*. Unlike WT **(Fig 16A)** and *snd2* **(Fig 16C)**, the *nars1* introducing *pAT5G48060::H2B:YFP* showed H2B-YFP in adjacent cells of the phloem SEs as well as the protophloem SEs **(Fig 16B)** (Furuta et al., 2014b). Consistent with this result, H2B:GFP under the *S32* promoter which drives expression H2B-YFP in procambial cells of the QC region and in the phloem precursor and protophloem SE of meristem zone, showed expression broadly in neighboring cells of phloem SEs as well as protophloem SEs in *nars1* **(Fig 17E)**, which was strikingly different from the WT **(Fig 17D)** and *snd2* **(Fig 17F).** In contrast, the expression of *pS32::erGFP* in *nars1* **(Fig. 17B)** did not show any difference from the one in WT **(Fig 17A)** and *snd2* **(Fig 17C)**. The spreading and broadening expression of the stable H2B-YFP in *nars1* indicated that the division pattern of procambial cells in the meristematic zone might have changed in the phloem pole.

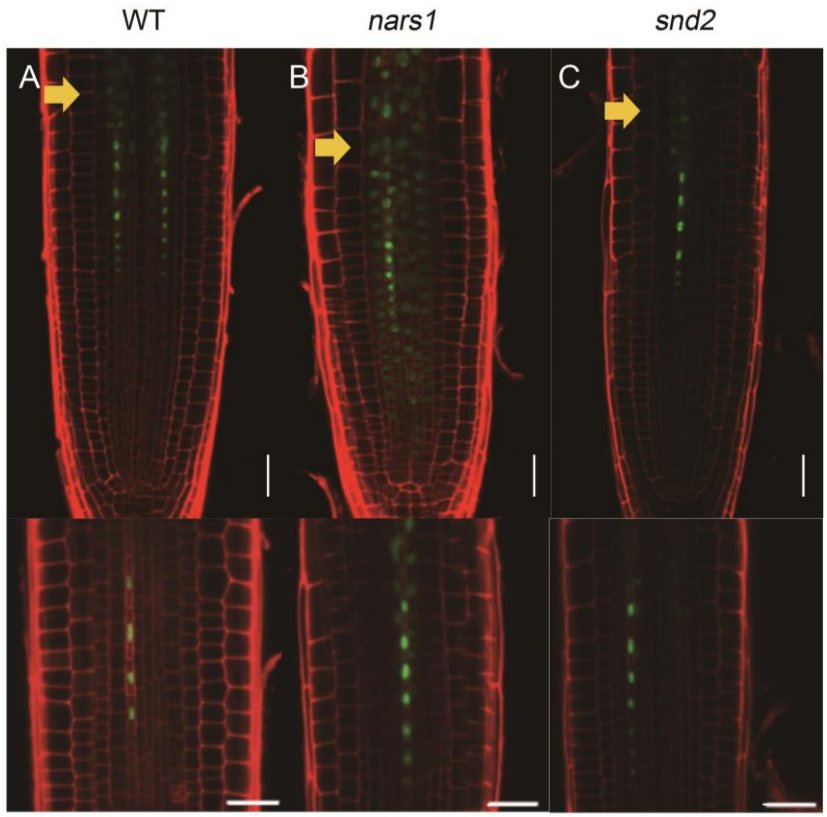

Figure 16. Expression patterns of *pAT5G48060::H2B:YFP* in WT , *nars1* and *snd2*. (A-C, top) The expression of *pAT5G48060::H2B:YFP* in WT(A), *nars1* (B) and *snd2* (C) was visualized in differentiating protophloem SEs of the root meristematic zone. (A-C, bottom) The nucleus morphologies of *pAT5G48060::H2B:YFP* in WT(A), *nars1* (B) and *snd2* (C) was expressed in protophloem SEs cell files of the root meristematic zone. In *nars1* (B), the expression of H2B-YFP was broader than both WT (A) and *snd2* (C). The elongating protophloem SEs undergoing enucleation process was marked by the yellow arrow. Scale bars=20μm. This is published in Kim et al. (2020) as Figure 6D-F.

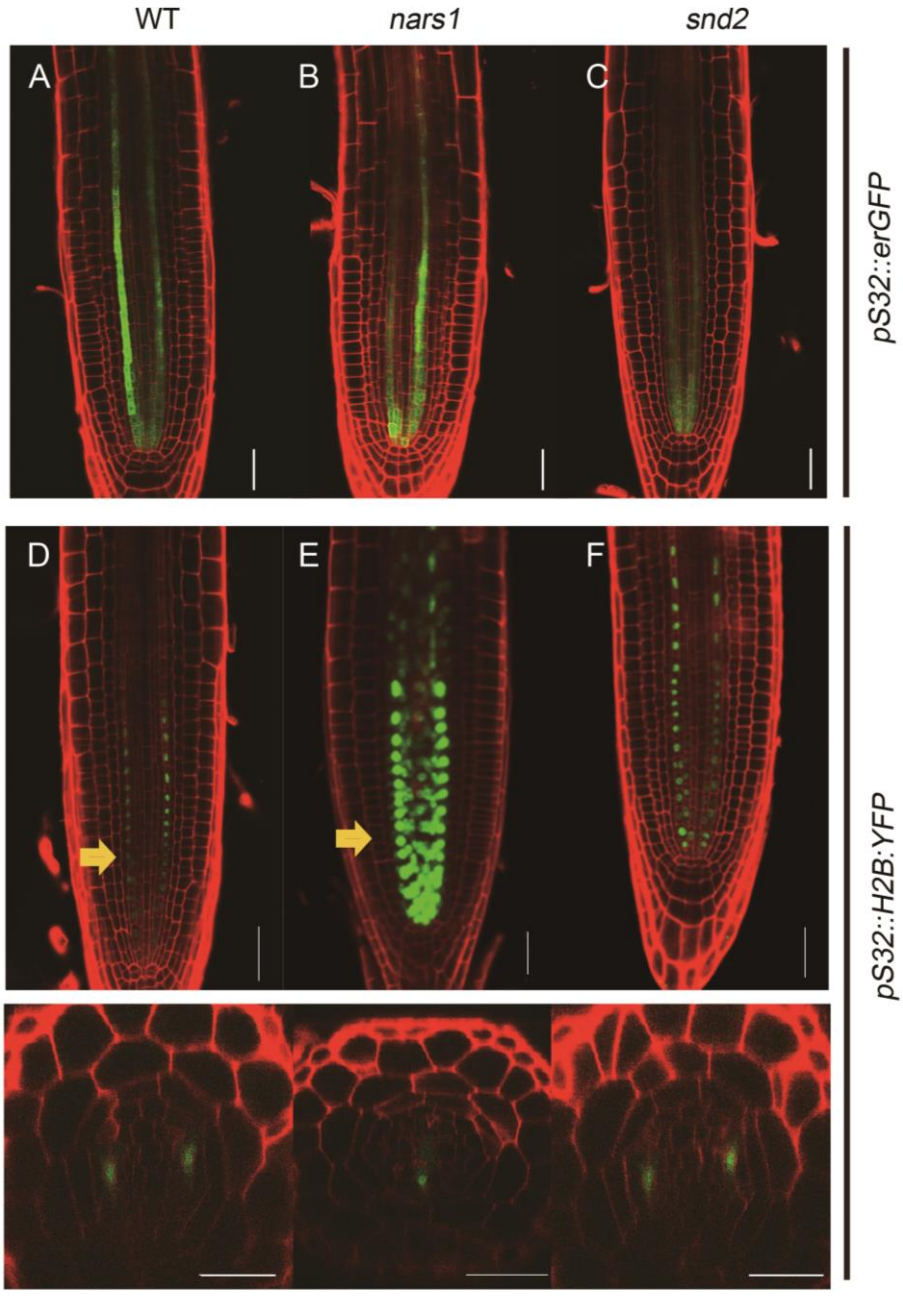
WT
nars1
snd2
A
B
C
pS32::erGFP
D
E
F
pS32::H2B:YFP

Figure 17. Expression patterns of *pS32::erGFP* and *pS32::H2B:YFP* in WT , *nars1* and *snd2.* (A-C) The expression of *pS32::erGFP* in WT(A), *nars1* (B) and *snd2* (C) was visualized from phloem initial cells to protophloem SEs of the root meristematic zone. No differences were observed in pS32::erGFP in WT, *nars1* and *snd2*. (D-E, bottom) The nucleus morphologies of *pS32::H2B:YFP* in WT(D), *nars1* (E) and *snd2* (F) was expressed in protophloem SEs cell files and phloem initial cells of the root meristematic zone. In *nars1* (E), the expression of H2B-YFP was broader than both WT (D) and *snd2* (F). H2B-YFP was expressed broadly in the meristem zone of nars1 both under *S32* and *AT5G48060* promoter. These results indicated that the division pattern of the phloem initials is changed in *nars1*. The elongating protophloem SEs undergoing enucleation process was marked by the yellow arrow. Scale bars=20μm. This is published in Kim et al. (2020) as Figure 6G-L.

3.3. NARS1 regulates the ACD of the phloem SE as the potential long-distance top-down signal.

3.3.1. NARS1 is a key regulator of ACD of the phloem SE precursor.

To perform cell lineage analysis, the cells were tracked through serial cross sections of the root meristem in the WT, *snd2*, *nars1*, and *nars1-snd2* double mutants. In WT and *snd2*, the phloem SE precursor cells divided into proto- and meta-phloem SEs via ACD of phloem SE precursor cells **(Figs 18A,B,D,E)**. Also, immunostaining SE-ENOD indicated that phloem SEs are fully differentiated in both WT **(Fig 18C)** and *snd2* **(Fig 18F).** However, in *nars1* and *nars1-snd2* double mutant, ACD of phloem SE precursor cells did not occur **(Figs 18G,H,J,K)**. Instead of the normal division, the inner procambial cell contacting the phloem precursor cell divided into the phloem SE-like cell. Consistent with this abnormal division, phloem SEs did not fully differentiated in *nars1* and *nars1 snd2* when I examined them using SE-ENOD immunostaining **(Fig 18I,L).**

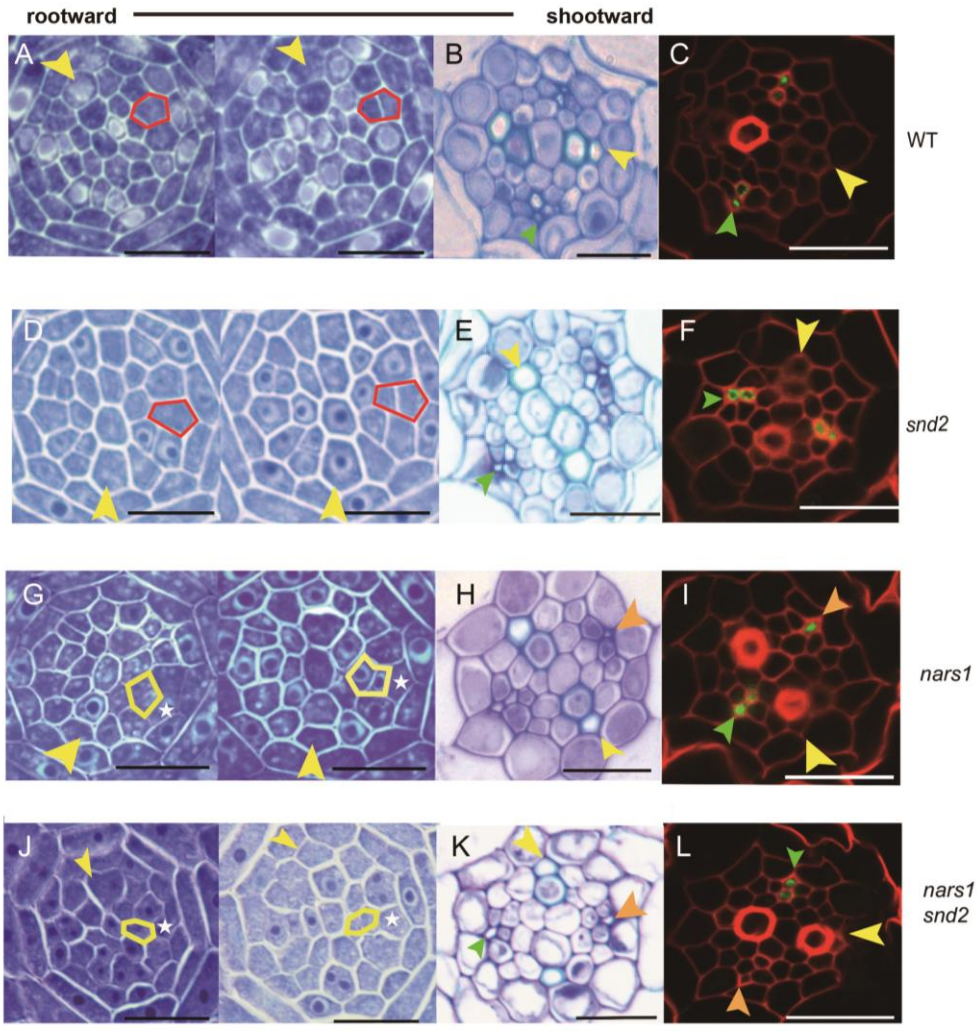
rootward
shootward
A
B
C
WT
D
E
F
snd2
G
H
I
nars1
J
K
L
nars1
snd2

Figure 18. Examination of the asymmetric cell division patterns for phloem SEs formation in the WT, *nars1*, *snd2* and *nars1 snd2*. (A-L) Analysis of division patterns of phloem SE precursors in the roots of the WT (A,C), *nars1* (G-I), *snd2* (D-F) and the *nars1 snd2* double mutant (J-L) using cross section stained toluidine blue and immunostaining SE-ENOD. Analysis of cell division patterns using consecutive cross-sections in the WT (A), *nars1* (G), *snd2* (D) and *snd2 nars1* double mutant (J) and resulting cell organization in the root differentiation zone (B,E,H,K). The immunostaining SE-ENOD were observed with two differentiated phloem SEs in the WT (C) and *snd2* (F) but only one in *nars1* (I, Orange arrow head) and *nars1 snd2* (L, Orange arrow head). Yellow arrowhead, xylem axis; green arrowhead, pole with two phloem SEs; orange arrowhead, pole with one phloem SE; Scale bar, 20μm. This is published in Kim et al. (2020) as Figure 7A-P.

The ACDs on the phloem SE lineage are detected as divided cells shaping like flipped ‘T’, when the PI-stained roots are observed in a longitudinal axis under confocal microscope. Consistent with the data already presented, *nars1* showed defects in the division of phloem SE precursors, showing only one ‘T’ shape division. not two found in the WT **(Figs 19A-C)**. Both WT and *snd2* were established with sequential ACDs of the phloem SE procambium- precursor cells and phloem SE precursor cells **(Figs 19A,C)**. On the other hand, in *nars1*, ACD of phloem SE precursor cells was not observed **(Figs 19B)**. *pS32::erGFP* in WT, *nars1* and *snd2* transgenic plants, viewed under a confocal microscope further supported these ACD patterns **(Figs 19D,E)**.

In addition, another mutant allele of *nars1*, SM-3-28017 (*nars1-1*), showed defects in phloem SE formation consistent with the results of *nars1-2* (SALK_137131) **(Figs 20A,B)**. Both *nars1-2* and *nars1-1* did not show ACD of the phloem SE precursor cells **(Figs 19B, 20A)** and the only one SE-like cell detected via SE-ENOD **(Figs 18C, 20B).** *nars1-2* and *snd2-1* were used in the study without mention of allele numbers. These results indicated that NARS1 is one of the key regulators of SE development, acting as the direct downstream of SHR**.**

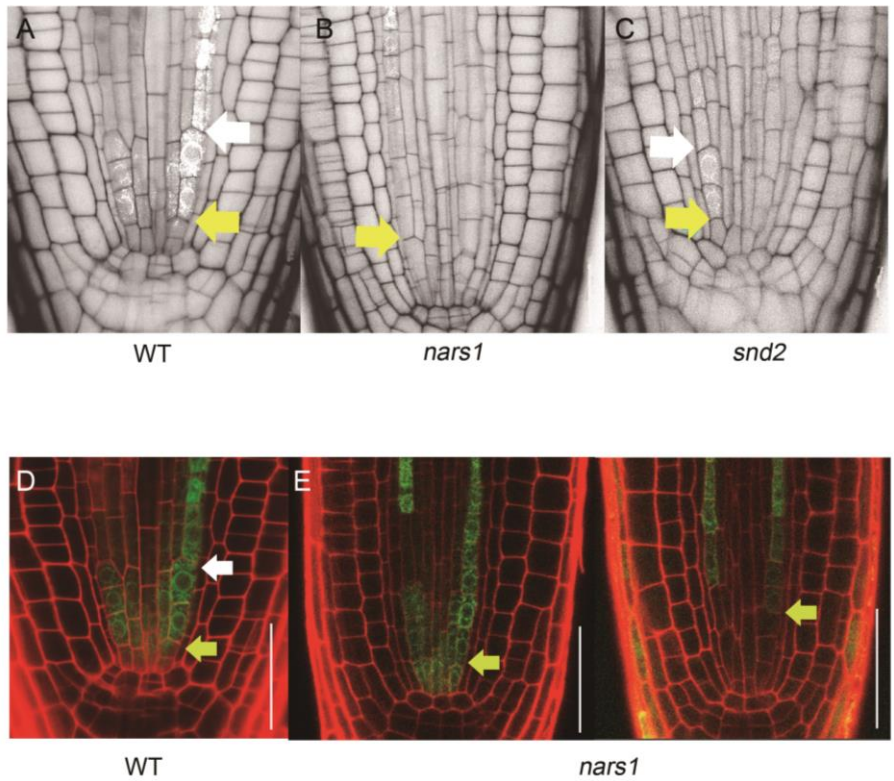

Figure 19. Analysis of asymmetric cell division in the WT, *nars1* and *snd2*. (A-C) Confocal images of the WT (A), *nars1* (B), and *snd2* (C) in the meristem zone were used for analyzing cell lineage. Phloem precursor cells in the WT(A) and *snd2* (C) divide twice, whereas that in *nars1* (B) divides only once. The expression of *pS32::erGFP* was visualized with starting phloem SE precursors both WT (D) and nars1 (E). In nars1, the ACD of phloem SE precursor was missing (E). Yellow arrow, ACD of the phloem SEs procambium precursor; White arrow, ACD of the phloem SE precursor; Scale bar=20μm. This is published in Kim et al. (2020) as Figure 7Q-S.

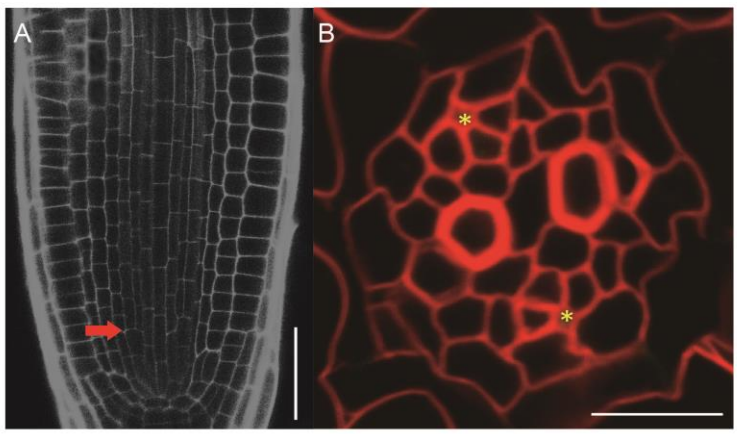

Figure 20. Analysis of phloem SEs in another *nars1* mutant allele. (A-B) The *nars1-1* (SM_3_28017), another *nars1* mutant allele, revealed defects in ACD of the phloem SE precursor (A) and differentiation (B). ACD occurs once as marked with a red arrow. Asterisks, phloem SEs; Scale bars=20μm. This is published in Kim et al. (2020) as Supplemental Figure 6F.

3.3.2. Analysis of phloem unloading in the root meristem.

Sucrose molecules synthesized in the leaves move into the CC via sucrose-proton symporters and then get loaded to the SEs through the plasmodesmata to be distributed to sink organs (Stadler and Sauer, 2019). In the sink, sucrose is unloaded via a process reverse to what happens in the source. To better understand whether abnormal ACD of the phloem precursor cells in *nars1* affected the functions of SEs in transportation and symplastic unloading, the symplastic tracer 5(6)-carboxyfluorescein diacetate (CFDA) was used **(Fig 21)**. The CFDA loaded to phloem was shown to rapidly translocate from the shoot to the root via longitudinal veins (Haupt et al., 2001). When CFDA was injected in the punctured cotyledon of the 6DAT seedlings, the fluorescent dye was observed to move down to the root within three minutes. Compared with the WT, *nars1* and *snd2* showed no changes in the symplastic unloading system and did not show discontinuous connection with phloem SEs **(Fig 21A)**. In addition, to better identify the molecular level of expression, *pSUC2::GFP*, which synthesizes free GFP in the CCs and travels from the phloem through the plasmodesmata into all cells of the root meristem, was developed into WT, *nars1*, and *snd2* (Imlau et al., 1999; Stadler and Sauer, 2019). Consistent with CFDA results, WT, *nars1*, and *snd2* had no problem with GFP unloading in the root meristem **(Fig 21B)**.

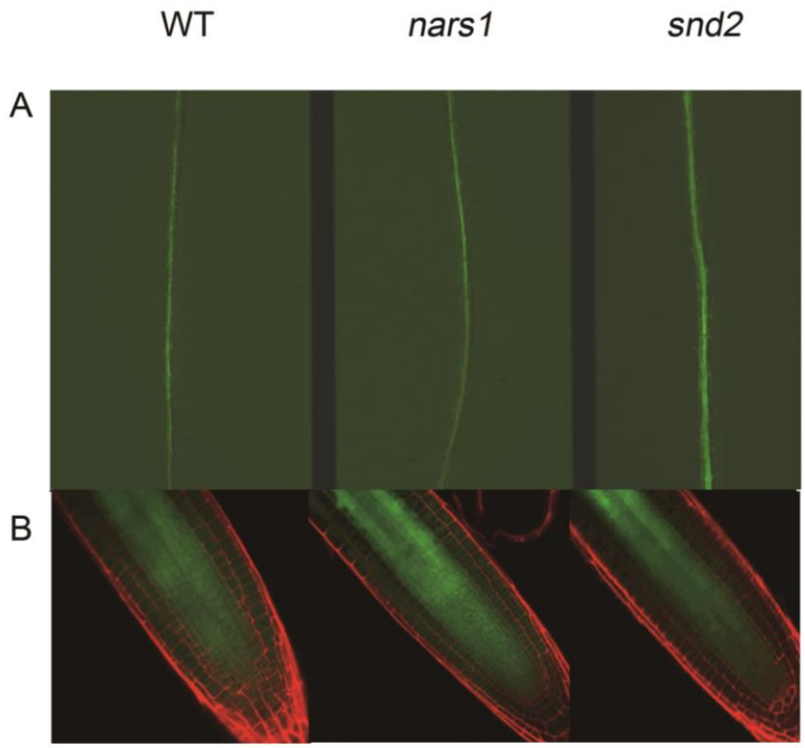

Figure 21. Analysis of symplastic phloem unloading in WT, *nars1* and *snd2*.

The symplastic unloading experiment using CFDA dye was performed in WT, *nars1* and *snd2* (A). To deeply monitor the transport activity, *pSUC2::freeGFP* in WT, *nars1* and *snd2* transgenic plants were observed in meristem zone (B). No differences with WT, *nars1* and *snd2* were identified.

3.3.3. NARS1 acts as a potential long-distance top-down signal to regulate ACD in phloem SEs.

NARS1 expressed in the CCs of the root differentiation zone regulates ACDs of phloem SE precursor cells of the root meristematic zone, but SND2 expressed in the developing protophloem SEs of the root meristematic zone does not affect ACDs for phloem development. To further investigate the relationship between NARS1 and SND2, *pNARS1::erGFP* was introduced into the *snd2* mutant and *pSND2::GUS* was introduced into the *nars1* mutant. *pSND2::GUS* showed reduced expression in *nars1* **(Figs 22E-H),** whereas *pNARS1::erGFP* expression in *snd2* did not show considerable difference, as compared to that in the WT **(Figs 22A-D)**. This indicated that *NARS1* promotes *SND2* expression in protophloem SEs. The immunostaining SE-ENOD result did not show the addictive effect in the *nars1 snd2* double mutant, consistent with the relationship between NARS1 and SND2 (Quantification: 6 out of 20 individuals).

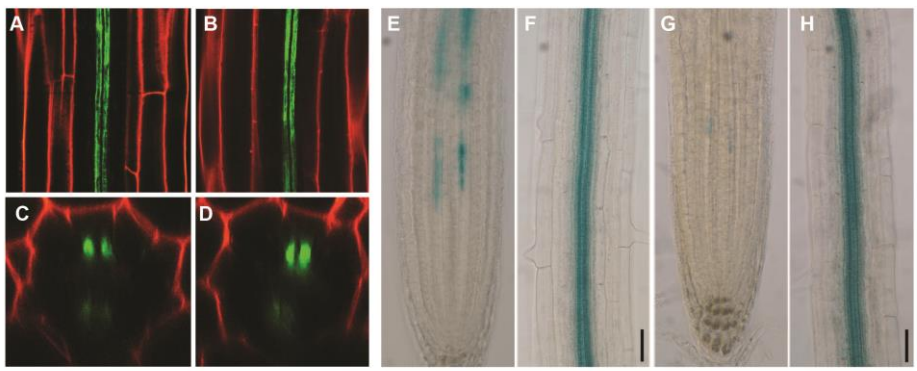

Figure 22. Relationship between *NARS1* and *SND2*. (A-H) Expression patterns of *pNARS1::erGFP* in the WT (A,C) and *snd2* (B,D). *NARS1* was equally expressed in CCs both WT (A,C) and *snd2* (B,D). However, the expression of *pSND2::GUS* in *nars1* (G) was reduced in the protophloem SEs of the roots meristematic zone compare with *pSND2::GUS* in WT (E). The *SND* expression of metaxylem was not affected in both WT (F) and *nars1* (H). Scale bars=10μm. This is published in Kim et al. (2020) as Supplemental Figure 8.

NARS1 expressed in the CCs of the differentiation zone (*pSUC2::GFP:NARS1*) recovered ACD of the phloem SE precursor of the root meristematic zone **(Figs 23B,E)**. The *pSUC2::erGFP* transgenic lines showed similar expression pattern of the *NARS1* mRNA. However, no signals of the *pSUC2::GFP:NARS1* in *nars1* transgenic plants were expressed in the root meristematic zone and CCs of the root differentiation zone, but expression of the GFP signal seemed spread out **(Fig 23C;** Data was provided by Dr.Chulmin Park, current post doctorate researcher.). To find out whether *NARS1* is locally involved in ACD in the meristematic zone, GFP-NARS1 under the S29 (*PEAR1*, *AT2G37590*) promoter driving expression in the phloem precursor cells of the meristematic zone, was introduced into the *nars1* mutant. The expression of *pS29::GFP:NARS1* in the *nars1* transgenic line was detected in the phloem precursor cells and ACDs of the phloem SE precursor recovered **(Fig 23A)**. Both *pSUC2::GFP:NARS1* and *pS29::GFP:NARS1* in *nars1* transgenic plants recovered the rate of primary root growth and ACD of the phloem SE precursor divisions in the meristem **(Figs 23D, E)**. (Quantification: 14 observed for *pS29:GFP-NARS1* in *nars1*; 21 observed for *pSUC2:GFP-NARS1* in *nars1*)

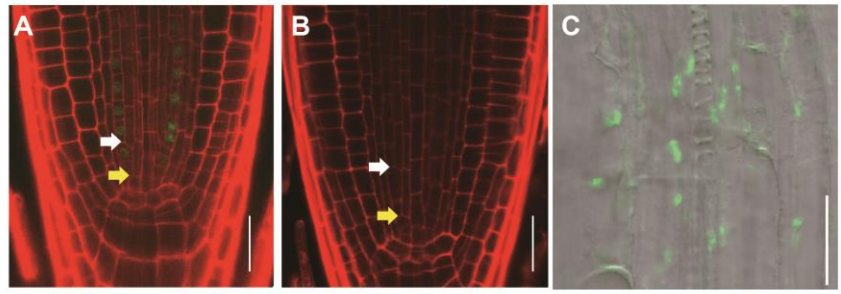
A
B
C

D

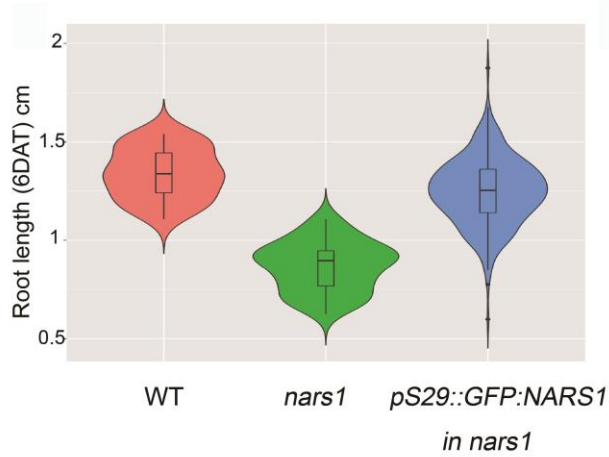
Root length (6DAT) cm
2
1.5
1
0.5
WT
nars1
pS29::GFP:NARS1
in nars1

E

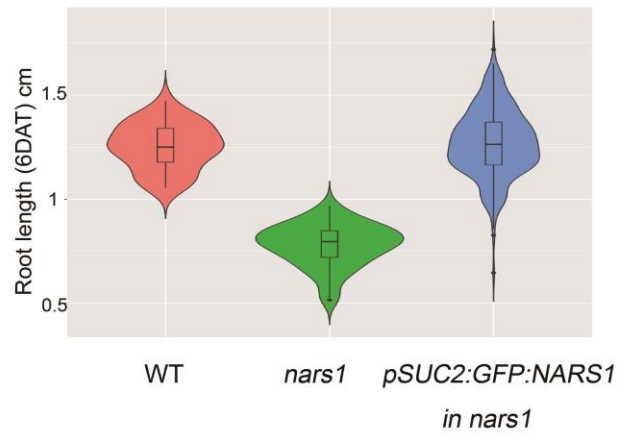
Root length (6DAT) cm
1.5
1
0.5
WT
nars1
pSUC2:GFP:NARS1
in nars1

Figure 23. Complementation of functional NARS1 for phloem development. (A-E) Analysis of the division of phloem SEs and root length recovery in *pS29::GFP:NARS1* and *pSUC2::GFP:NARS1* in *nars1* transgenic plants. The ACDs of sequential phloem SE were recovered both *pS29::GFP:NARS1* and *pSUC2::GFP:NARS1* in *nars1* transgenic plants (A,B). The expression of *pS29::GFP:NARS1* in *nars1* transgenic plants was visualized in the phloem initial cells (A) and the expression of *pSUC2::GFP:NARS1* in nars1 transgenic plants was punctuated in differentiation zone (C). (D,E) Measurement of the root length recovery process of *pS29::GFP:NARS1* in *nars1* [three independent homozygous T3 lines (n=263), wild type (WT; n=32) and nars1 (n=50); (D)] and *pSUC2::GFP:NARS1* in *nars1* (three independent homozygous T3 lines [n=256], WT [n=35] and nars1 [n=50]; (E) (D,E; Data were provided by Dr.Nam.V. Hoang) Scale bars=20μm. Panel C was provided by Dr. Chulmin Park. The figure is published in Kim et al. (2020) as Figure 8A-E.

3.3.4. Ectopic expression of *NARS1* and *SND2* promote the extra phloem SE formation

To investigate whether NARS1 promotes ACD for phloem formation, the *pCRE1::GFP:NARS1* was introduced into the WT and *shr-2*. Both *shr-2* and WT transgenic plants expressing *pCRE1::GFP:NARS1* showed more than two phloem SEs in the phloem pole **(Figs 24A-C; WT, G-H; *shr-2*).** Even though *pCRE1::GFP:NARS1* in *shr-2* recovered two phloem SEs in phloem pole, it did not recover the stele cell number **(Figs 24G,H).**

Then, *pCRE1::SND2:GFP* was introduced into the WT plants. These transgenic plants showed more phloem SE cell numbers than non-transgenic WT **(Figs 24D,E).** Consistent with the results of immunostaining SE-ENOD and cross section data, the expression of *pAPL::erGFP* was broader than that of the WT **(Figs 25A-D)** in both *pCRE::SND2* **(Figs 25E-H)** and *pCRE::NARS1* **(Fig 25I-L)** transgenic plants. In contrast, *pSUC2::erGFP* domain did not show any change in both *pCRE1::SND2* **(Fig 26B,E)** and *pCRE1::NARS1* **(Fig 26C,F)**, compared to the WT **(Figs 26A,D).** These data collectively suggest that NARS1 might serve as a long-distance signal molecule that moves from the differentiation zone to the meristem to locally promote ACD of the phloem SE precursors.

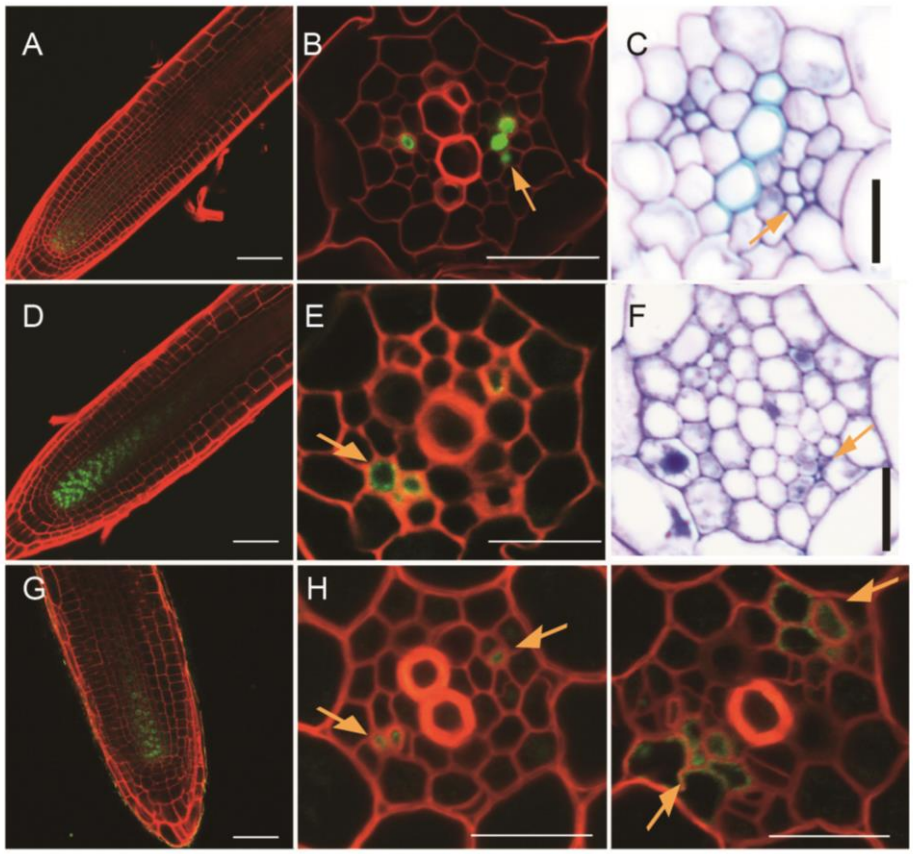

Figure 24. Analysis of ectopic expression of phloem SEs under CRE1 promoter. Expression patterns of *pCRE1::SND2:GFP* in WT (D-F), *pCRE1::GFP:NARS1* in WT (A-C), *pCRE1::GFP:NARS1* in *shr-2* (G-H). (B,E,H) Inducing the additional cell divisions in *pCRE1::SND2:GFP* in WT (E) , *pCRE1::GFP:NARS1* in WT(B) and *pCRE1::GFP:NARS1* in *shr-2* (H) are detected in the phloem pole through immunostaining SE-ENOD. Consistent with immunostaining results, transverse sections stained with toluidine blue were observed ectopic phloem SEs in *pCRE1::SND2:GFP* in WT (F) , *pCRE1::GFP:NARS1* in WT (C). Orange arrows, ectopic phloem SEs; Scale bars=20μm. The figure is published in Kim et al. (2020) as Figure 8F-M.

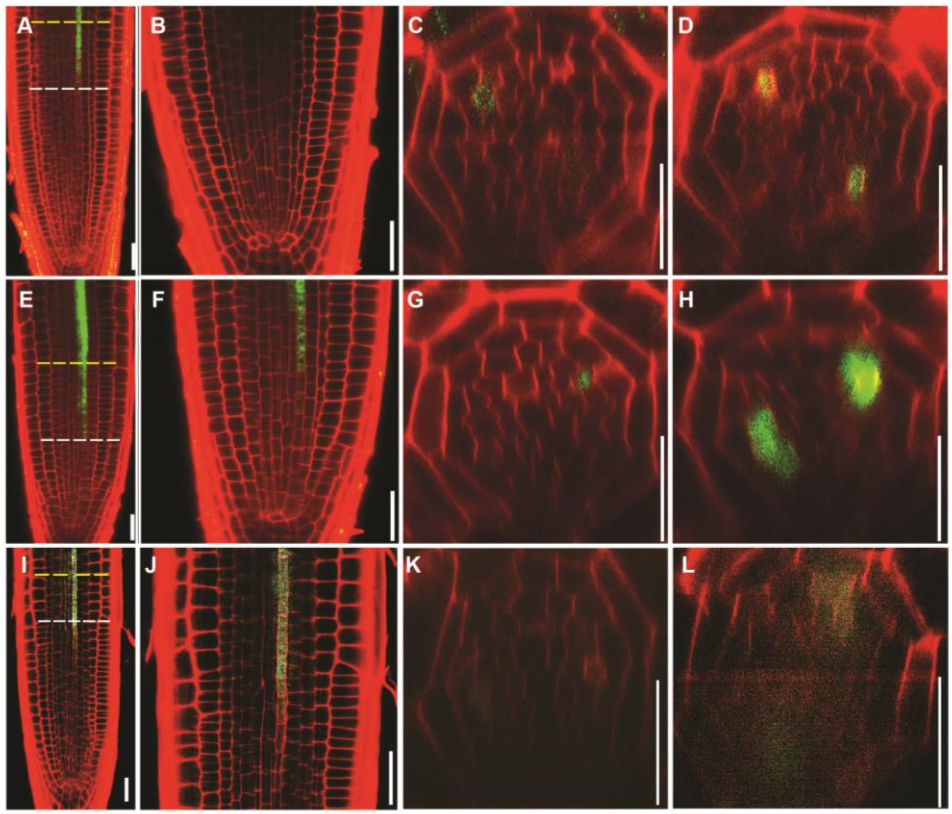

Figure 25. Facilitating of expression for phloem SEs by NARS1 and SND2. (A-L) Expression patterns of *pAPL::erGFP* in *pCRE1::SND2* and *pCRE1::NARS1* transgenic plants. Longitudinal confocal images and cross sections of *pAPL::erGFP* were broadly expressed in *pCRE1::SND2* (E-H) and *pCRE1::NARS1* (I-L) compare to the WT (A-D). Cross sections were imaged of the region marked by the white dotted lines (C,G,K) and by the yellow dotted lines (D,H,L). Scale bars=20μm. The figure is published in Kim et al. (2020) as Supplemental Figure 10.

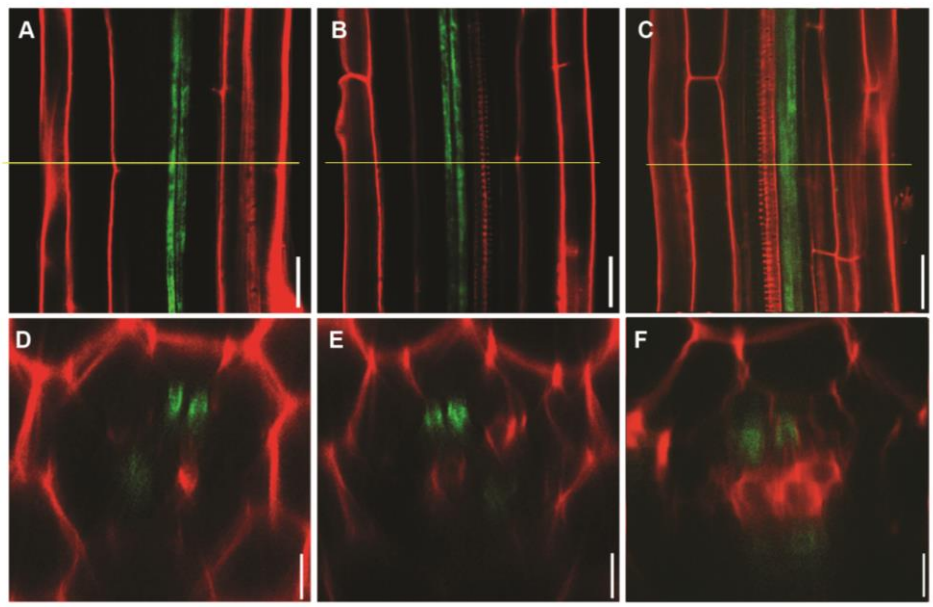

Figure 26. Expression patterns of *pSUC::erGFP* introduced into the *pCRE1::SND2* and *pCRE1::NARS1* transgenic plants. To monitor the aspects of CCs development in ectopically expressing NARS1 and SND2 transgenic plants under the CRE1 promoter, *pSUC::erGFP* was introduced in the *pCRE1::SND2* (B,E) and *pCRE1::NARS1* transgenic plants (C,F). Development of CCs were no differences in the *pCRE1::SND2* (B,E) and *pCRE1::NARS1* transgenic plants (C,F) compare to the WT (A,D). Cross sections (D,E,F) were imaged by position marked yellow lines (A,B,C). Scale bars=20μm. The figure is published in Kim et al. (2020) as Supplemental Figure 11.

3.3.5. Observation of NARS1 proteins using an estradiol-mediated transactivation system.

To investigate how NARS1 works in the meristematic zone despite its expression in CCs of the differentiation zone, NARS1 was introduced into the *nars1* mutant under the inducible system using the XVE trans-activator promoter. An inducible system is frequently used in developmental research as it allows for a spatial and temporal control of gene expression. It uses the XVE transcription factor that involves three modules: the bacterial transcriptional-repressor *LexA* as a DNA-binding domain, the transcription-activating domain of virus transcription factor VP16, and the estrogen receptor (Machin et al., 2019). With estradiol treatment, the entry of the XVE factor into the nucleus and binding to the LexA operator sequence allows the gene of interest to be transcribed (Machin et al., 2019). This enhances the expression level of the target molecule by controlling the induction time point.

pSUC2-XVE>>GFP:NARS1 inducible system was transformed into the *nars1* plants (Brand et al., 2006; Yan et al., 2019). When the transgenic seeds were germinated in presence of estradiol media (5 μM), the XVE transcription factor bound to *LexA* operator and allowed for the expression of GFP-NARS1 in CCs of

the differentiation zone **(Fig 27A).** The expression of *pSUC2-XVE>>GFP:NARS1* in *nars1* transgenic plants treated with estradiol, was not detected until 5 days after germination, though plants expressing *pSUC2::erGFP* showed GFP expression regardless of growth stages of seedlings **(Fig 27B).** Interestingly, when estradiol treatment was applied for 8 days, *pSUC2-XVE>>GFP:NARS1* in *nars1* transgenic plants was expressed in the CCs of the late differentiation zone **(Fig 28A).**

To clearly identify cell type where NARS1 is expressed, an imaging technique using ClearSee was used. This approach allowed for visualizing GFP and cell types in the differentiation zone of the roots (Kurihara et al., 2015). The expression of NARS1 was enhanced in the lateral root primordia region **(Fig 28B).** Furthermore, in the late stage of differentiation, the GFP-NARS1 was expressed not only in the CCs but also in the procambium cells **(Fig 28C).** In addition, the transgenic lines recovered ACD in phloem SEs of the meristematic zone of the roots **(Fig 29)**. Collectively, these data suggest that accumulation of the NARS1 in the differentiation zone might be promoted in the old seedling roots. Although the expression of NARS1 was not visualized in the meristem of the root, NARS1 may trigger the ACDs and thereby play a pivotal role in the formation of phloem SEs.

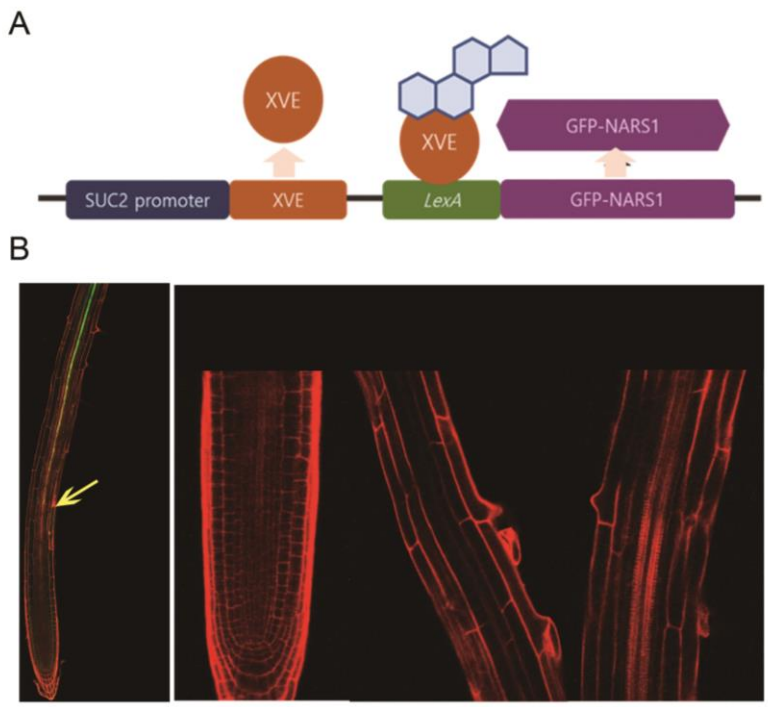

Figure 27. An estrogen receptor based trans-activator inducible XVE system. A schematic diagram explain the XVE system how *pSUC2-XVE>>GFP:NARS1* in *nars1* works (A). The expression pattern of *pSUC2::erGFP* in WT transgenic plant as the control (B, left). No expression in *pSUC2-XVE>>GFP:NARS1* in *nars1* for 5DAT seedling (B, right)

A

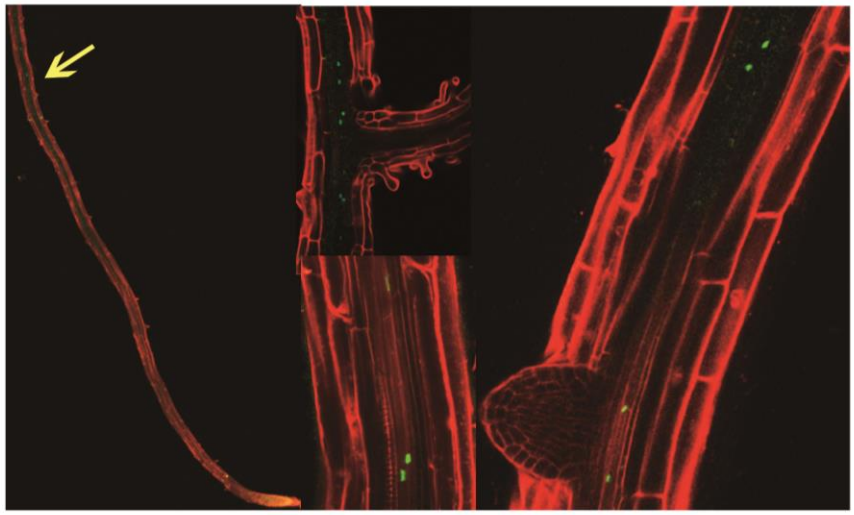

B

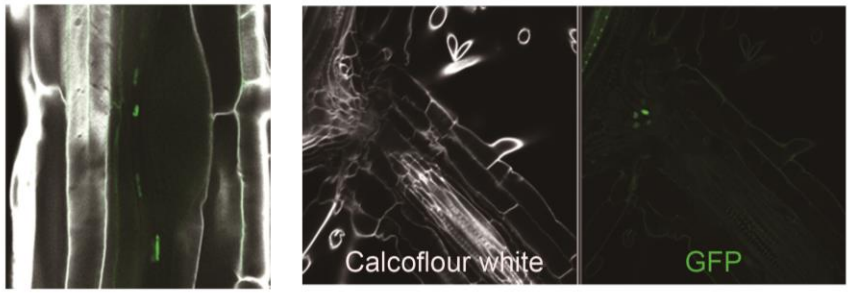

C

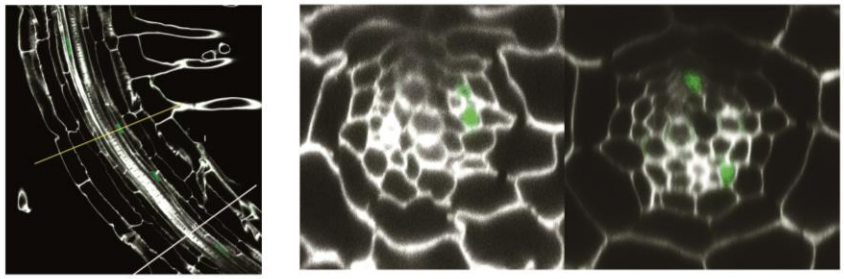

Figure 28. Analysis of expression patterns in *pSUC2-XVE>>GFP:NARS1* introduced into the *nars1*. The expression of *pSUC2-XVE>>GFP:NARS1* in *nars1* was visualized after 8DAT seedling in late differentiation zone of the root (A). To clearly check the expression, 8DAT seedling samples with incubation in ClearSee solution was observed (B,C). The signals of GFP-NARS1 were increased in the lateral root primordia region of the maturation zone (B). Cross sections were imaged of the region marked by the white lines and by the yellow dotted lines. Scale bars=20μm.

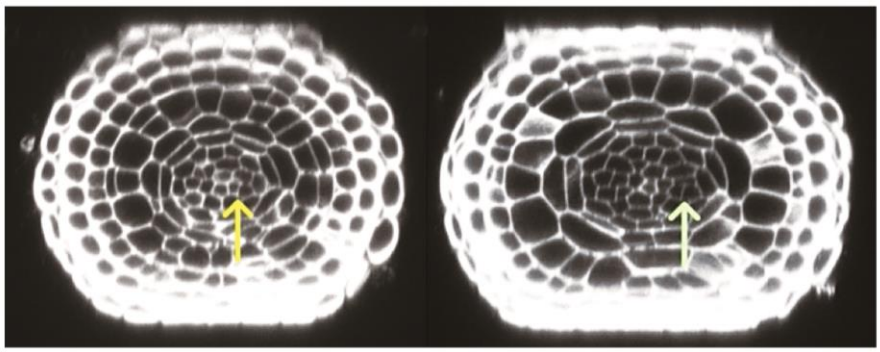

Figure 29. Recovery of cell divisions for phloem SE precursors in *pSUC2-XVE>>GFP:NARS1* introduced into the *nars1-2*. Confocal sequential cross sections were imaged and tracked to the cell division process. *pSUC2-XVE>>GFP:NARS1* in *nars1* transgenic plant was complemented with the ACD of the phloem precursor (green arrow). Yellow arrow, a division plane of phloem SEs procambium precursor.

3.3.6. Artificial restriction of phloem unloading using PEP1 treatment as a way to monitor NARS1.

The innate immune system in plant roots have specialized plasma membrane-localized pattern recognition receptors (PRRs) to perceive pathogen or microbe associated molecular patterns (PAMPs, MAMPs) (Boller and Felix, 2009; Jing et al., 2019; Ryan et al., 2007). In *Arabidopsis thaliana*, PEPs, the Plant Elicitor Peptides derived from endogenous precursor proteins, activate danger- or damage-associated molecular patterns (DAMPs) as a part of immune responses. PEPs were isolated from *Arabidopsis thaliana* and found to represent a 23 amino acid peptide (Huffaker et al., 2006). PEPs are perceived by the receptor-like kinases, PEPR1 and PEPR2 at the plasma membrane to defend the pathogen (Huffaker et al., 2006). The PEPs trigger the inhibition of plant growth by inducing root hair formation and swelling of the epidermis and cortex cells in the transition zone of the root (Jing et al., 2019). Furthermore, callose deposition at the plasma membrane is increased in the presence of the plant pathogen (Luna et al., 2011). The receptors of PEPR1 and PEPR2 perceive various PEPs having different affinities (Yamaguchi et al., 2010). The eight PEPs originated from the precursor proteins PROPEP1 to PROPEP8 are found in *Arabidopsis thaliana* (Bartels et al., 2013).

PEP1 and 2 are recognized by PEPR2, whereas PEPR1 perceives PEP1 to 8. The perception of pathogens activates a variety of defense mechanisms in the plant roots. Callose deposition takes place at the plasma membrane to block the penetration of pathogens (Voigt, 2014). The presence of 1μM Pep1 induced callose (β-1,3-glucan) deposition in the SEs (Yan et al., 2019). Consistent with these findings, GFP unloading out of the phloem in *pSUC2::GFP* plants was blocked when Pep1 was treated for 2 days after germinating and growing *pSUC2::GFP* plants on the normal MS media **(Fig 30A)**. Aniline blue staining indicated the increase in callose deposition in Pep1 treated plants **(Fig 30B).**

Based on this observation, *pSUC2-XVE>>GFP:NARS1* in *nars1* transgenic plants were germinated and grown for 5 days on Pep1-containing media. The pattern of NARS1 expression was found to be continuous in the CCs of early phloem differentiation zone regardless of the time point **(Fig. 30C)**. These results indicated that the possibility of NARS1 movement is inhibited when the plasmodesmata is blocked as a result of callose accumulation.

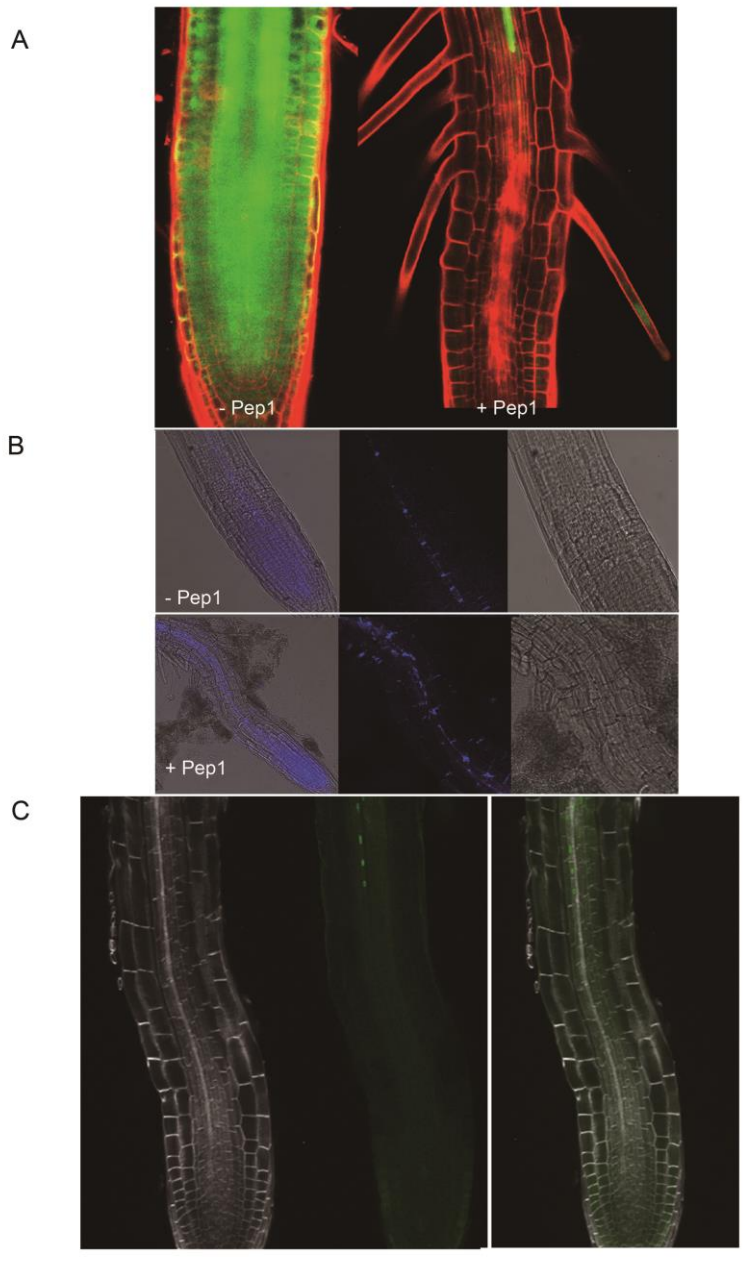
A
- Pep1
+ Pep1
B
- Pep1
+ Pep1
C

Figure 30. Limitation of NARS1 movement to block the plasmodesmata with Pep1 treatment. (A-B) Restriction of symplastic unloading transport due to callose deposition with Pep1 treatment. (A) Presence in Pep1 prevent the symplastic unloading transport from deposition of callose, inhibiting the movement of freeGFP in *pSUC2::freeGFP* transgenic plants. (B) Callose deposition assay with aniline blue staining with or without Pep1 treatment. (C) When *pSUC2-XVE>>GFP:NARS1* in *nars1* transgenic plants were germinated in estradiol and Pep1 containing media, expression of NARS1 was observed regardless of the timing because of blocking the plasmodesmata to inhibit the NARS1 movement.

4. Discussion

In multicellular organisms, asymmetric cell divisions (ACDs) and positional signaling determine cell fate specification and patterning (Abrash and Bergmann, 2009). Especially for the root development, stem cells surrounding in the QC produce the cells that plants need to survive via ACDs. In the *Arabidopsis thaliana* roots, there are two different types of ACDs for formation of CCs and SEs. The protophloem SEs and metaphloem SEs are originated from two periclinal ACDs of the phloem SE procambium precursors and the phloem SE precursors respectively. On the other hand, CCs are generated from two procambium cells adjoining both the SE precursor cells and the pericycle cells through ACDs. The orientation of SEs and CCs are different, but they are functionally correlated. In this process, movement of SHR fine-tunes the ACDs of the phloem initials for both CCs and phloem SEs.

According to the diverse molecular approaches such as genome-wide expression of stele in the roots, time-course induction and ChIP assay, downstream targets of SHR regulating the phloem SEs were identified (Kim et al., 2020). The time-course induction experiment using *pSHR::SHR:GR* transgenic plants indicated that *NARS1* was induced after 3 hours, which is faster than *SND2*. *SND2* was induced after 24

hours by SHR-GR activated with dexamethasone. This phenomenon is expected to involve other factors between *NARS1* and *SND2* for phloem development. Nevertheless, ChIP assay revealed that SHR-GFP directly binds to the promoter regions of *NARS1* and *SND2*.

Between the *NARS1* and *SND2*, *NARS1* might play a role as a primary regulator of ACDs for phloem SE formation. Both SE-ENOD immunostaining and the cell lineage analyses using cross sections and confocal microscopy revealed that *nars1* has a defect in the phloem SE formation and the ACD of phloem SE precursor cells. Furthermore, the ectopic expression of *NARS1* in the stele using *pCRE1::GFP:NARS1* transgenic plants increased the number of phloem SEs in both *nars1* and *shr-2*. That result further supported the idea that *NARS1* is a key factor of ACD for phloem SE precursor cells. Interestingly, ectopic expression of SND2 also increased the number of phloem SEs. We found that this transgenic line showes the upregulation of *NARS1* expression (data not shown). Considering SHR also directly regulates SND2 expression and NARS1 does too, we think that the phloem formation is regulated by formation of positive feedforward loop between SHR, NARS1 and SND2.

Based on several lines of experimental data, NARS1 seems to be associated with temporal dynamics of gene regulation for phloem formation in the root meristem. *NARS1* is transcribed in the CCs of the differentiation zone and activates not only SND2 expression in the protophloem SE of the meristematic zone also potentially other phloem enriched TFs. NARS1 functions as the regulator of ACDs of the phloem SE precursors of the root meristematic zone, but *NARS1* expressed in CCs of the differentiation zone. *pS29::GFP:NARS1* in *nars1* transgenic plants that NARS1 is artificially expressed phloem precursors rescues the ACDs of the phloem SE precursor and formation of phloem SEs. In addition, *pSUC2::GFP:NARS1* in *nars1* transgenic plants, which *NARS1* mRNA expressed in CCs of the differentiation zone complemented the primary root length and ACDs in the meristem zone but NARS1 protein didn't visualize. Putting these results together, we think NARS1 might be potentially function as the mobile long-distance top-down signal to cause the ACDs of the phloem SEs.

A new approach to visualize the expression of NARS1 via an inducible system using *pSUC2-XVE>>GFP:NARS1* in *nars1* transgenic plants was successful and could to be used to investigate the NARS1 mobility from differentiation zone to meristem zone of the root. In the presence of continuous estradiol induction,

NARS1 was expressed when the meristem activity was subdued. Furthermore, the ACD of the phloem precursors was recovered *pSUC2-XVE>>GFP:NARS1* in *nars1* transgenic plants. But, direct NARS1 movement was not visible in the meristem of the root. Thus, additional investigation is required whether *NARS1* locally or remotely regulates the ACDs of the phloem SE precursors.

The SHR, the master regulator, coordinates two ACDs for phloem formation via temporal and spatial gene networking. Essentially, the *NARS1* expression is amplified by *SND2* by forming a positive feedforward loop in this process **(Fig 31)**. Further studies of the direct function of NARS1 will reveal what is the actual genetic mechanism which controls ACDs of the phloem SE precursors. NARS1 protein expression has been finally detected using estradiol inducible transactivation system, which has opened the possibility of further research identifying the long-distance top-down signaling for the phloem development in *Arabidopsis thaliana*.

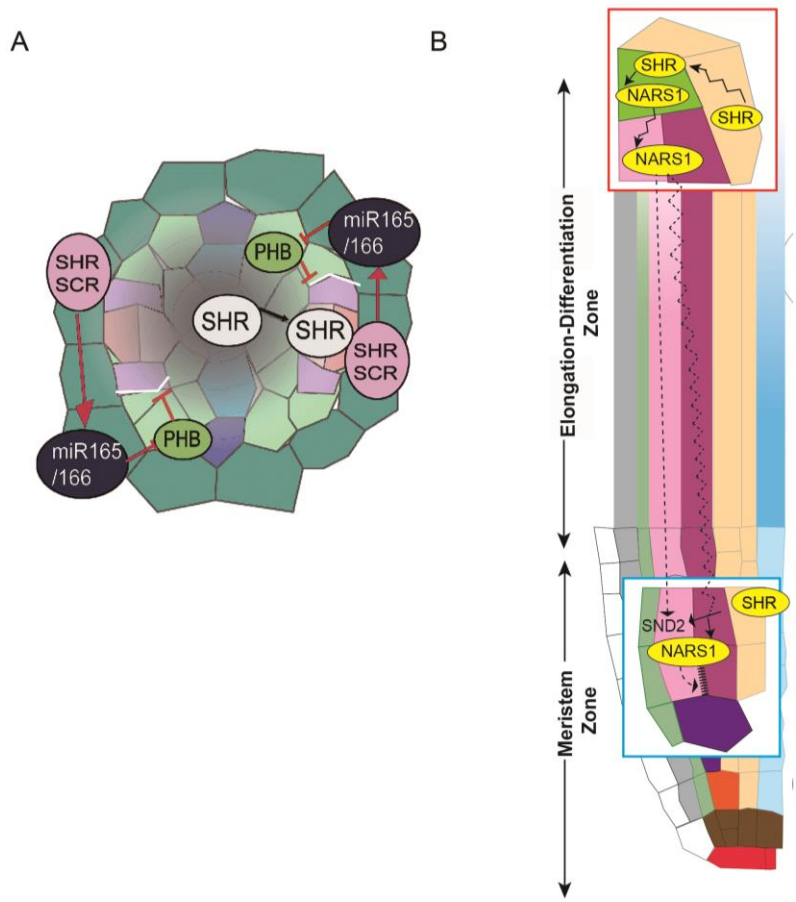

Figure 31. NARS1 is a potential long-distance top-down signal for ACDs of phloem SEs. The regulator mechanism shown on the cross-section diagram, the repression of *NARS1* by *PHB* is shown (A). The longitudinal diagram explained the positive feedforward regulatory loop associated with *SHR*, *NARS1* and *SND2*. NARS1 and SND2 also mediated the positive feedback regulation (B).

5. Reference

Abrash, E.B., and Bergmann, D.C. (2009). Asymmetric Cell Divisions: A View from Plant Development. Developmental Cell *16*, 783-796.

Anne, P., Amiguet-Vercher, A., Brandt, B., Kalmbach, L., Geldner, N., Hothorn, M., and Hardtke, C.S. (2018). CLERK is a novel receptor kinase required for sensing of root-active CLE peptides in *Arabidopsis*. Development *145*, dev162354.

Anne, P., Azzopardi, M., Gissot, L., Beaubiat, S., Hématy, K., and Palauqui, J.C. (2015). OCTOPUS Negatively Regulates BIN2 to Control Phloem Differentiation in Arabidopsis thaliana. Curr Biol *25*, 2584-2590.

Anne, P., and Hardtke, C.S. (2018). Phloem function and development-biophysics meets genetics. Curr Opin Plant Biol *43*, 22-28.

Atkinson, J.A., and Wells, D.M. (2017). An Updated Protocol for High Throughput Plant Tissue Sectioning. Front Plant Sci *8*, 1721.

Bartels, S., Lori, M., Mbengue, M., van Verk, M., Klauser, D., Hander, T., Böni, R., Robatzek, S., and Boller, T. (2013). The family of Peps and their precursors in Arabidopsis: differential expression and localization but similar induction of pattern-triggered immune responses. Journal of Experimental Botany *64*, 5309-5321.

Benfey, P.N., Linstead, P.J., Roberts, K., Schiefelbein, J.W., Hauser, M.T., and Aeschbacher, R.A. (1993). Root development in Arabidopsis: four mutants with dramatically altered root morphogenesis. Development *119*, 57-70.

Berger, D., and Altmann, T. (2000). A subtilisin-like serine protease involved in the regulation of stomatal density and distribution in Arabidopsis thaliana. Genes Dev *14*, 1119-1131.

Blob, B., Heo, J.-O., and Helariutta, Y. (2018). Phloem differentiation: an integrative model for cell specification. Journal of plant research *131*, 31-36.

Boller, T., and Felix, G. (2009). A renaissance of elicitors: perception of microbe-associated molecular patterns and danger signals by pattern-recognition receptors. Annu Rev Plant Biol *60*, 379-406.

Bonke, M., Thitamadee, S., Mähönen, A.P., Hauser, M.-T., and Helariutta, Y. (2003). APL regulates vascular tissue identity in Arabidopsis. Nature *426*, 181-186.

Borner, G.H., Lilley, K.S., Stevens, T.J., and Dupree, P. (2003). Identification of glycosylphosphatidylinositol-anchored proteins in Arabidopsis. A proteomic and genomic analysis. Plant Physiol *132*, 568-577.

Brand, L., Hörler, M., Nüesch, E., Vassalli, S., Barrell, P., Yang, W., Jefferson, R.A., Grossniklaus, U., and Curtis, M.D. (2006). A versatile and reliable two-component system for tissue-specific gene induction in Arabidopsis. Plant Physiol *141*, 1194-1204.

Breda, A.S., Hazak, O., and Hardtke, C.S. (2017). Phosphosite charge rather than shootward localization determines OCTOPUS activity in root protophloem. Proceedings of the National Academy of Sciences *114*, E5721-E5730.

Breda, A.S., Hazak, O., Schultz, P., Anne, P., Graeff, M., Simon, R., and Hardtke, C.S. (2019). A Cellular Insulator against CLE45 Peptide Signaling. Current Biology *29*, 2501-2508.e2503.

Carlsbecker, A., Lee, J.-Y., Roberts, C.J., Dettmer, J., Lehesranta, S., Zhou, J., Lindgren, O., Moreno-Risueno, M.A., Vatén, A., Thitamadee, S., *et al.* (2010). Cell signalling by microRNA165/6 directs gene dose-dependent root cell fate. Nature *465*, 316-321.

Chen, Q., Payyavula, R.S., Chen, L., Zhang, J., Zhang, C., and Turgeon, R. (2018). *FLOWERING LOCUS T* mRNA is synthesized in specialized companion cells in *Arabidopsis* and Maryland Mammoth tobacco leaf veins. Proceedings of the National Academy of Sciences *115*, 2830-2835.

Cho, H., Cho, H.S., Nam, H., Jo, H., Yoon, J., Park, C., Dang, T.V.T., Kim, E., Jeong, J., Park, S., *et al.* (2018). Translational control of phloem development by RNA G-quadruplex–JULGI determines plant sink strength. Nature Plants *4*, 376-390.

Clough, S.J., and Bent, A.F. (1998). Floral dip: a simplified method for Agrobacterium -mediated transformation of Arabidopsis thaliana. The Plant Journal *16*, 735-743.

Cruz-Ramírez, A., Díaz-Triviño, S., Blilou, I., Grieneisen, Verônica A., Sozzani, R., Zamioudis, C., Miskolczi, P., Nieuwland, J., Benjamins, R., Dhonukshe, P., *et al.* (2012). A Bistable Circuit Involving SCARECROW-RETINOBLASTOMA Integrates Cues to Inform Asymmetric Stem Cell Division. Cell *150*, 1002-1015.

Cui, H., Levesque, M.P., Vernoux, T., Jung, J.W., Paquette, A.J., Gallagher, K.L., Wang, J.Y., Blilou, I., Scheres, B., and Benfey, P.N. (2007). An evolutionarily conserved mechanism delimiting SHR movement defines a single layer of endodermis in plants. Science *316*, 421-425.

Dello Ioio, R., Galinha, C., Fletcher, A.G., Grigg, S.P., Molnar, A., Willemsen, V., Scheres, B., Sabatini, S., Baulcombe, D., Maini, P.K., *et al.* (2012). A PHABULOSA/cytokinin feedback loop controls root growth in Arabidopsis. Curr Biol *22*, 1699-1704.

Di Mambro, R., Sabatini, S., and Dello Ioio, R. (2018). Patterning the Axes: A Lesson from the Root. Plants (Basel) *8*, 8.

Fukuda, H., and Ohashi-Ito, K. (2019). Vascular tissue development in plants. Curr Top Dev Biol *131*, 141-160.

Furuta, K.M., Yadav, S.R., Lehesranta, S., Belevich, I., Miyashima, S., Heo, J.-o., Vatén, A., Lindgren, O., De Rybel, B., Van Isterdael, G., *et al*. (2014a). Arabidopsis NAC45/86 direct sieve element morphogenesis culminating in enucleation. Science *345*, 933.

Furuta, K.M., Yadav, S.R., Lehesranta, S., Belevich, I., Miyashima, S., Heo, J.-o., Vatén, A., Lindgren, O., De Rybel, B., Van Isterdael, G., *et al.* (2014b). *Arabidopsis* NAC45/86 direct sieve element morphogenesis culminating in enucleation. Science *345*, 933-937.

Gallagher, K.L., and Benfey, P.N. (2009). Both the conserved GRAS domain and nuclear localization are required for SHORT-ROOT movement. The Plant Journal *57*, 785-797.

Geldner, N. (2014). Making phloem—a near-death experience. Science *345*, 875-876.

Haupt, S., Duncan, G.H., Holzberg, S., and Oparka, K.J. (2001). Evidence for Symplastic Phloem Unloading in Sink Leaves of Barley. Plant Physiology *125*, 209-218.

Hazak, O., Brandt, B., Cattaneo, P., Santiago, J., Rodriguez-Villalon, A., Hothorn, M., and Hardtke, C.S. (2017). Perception of root-active CLE peptides requires CORYNE function in the phloem vasculature. EMBO Rep *18*, 1367-1381.

Helariutta, Y., Fukaki, H., Wysocka-Diller, J., Nakajima, K., Jung, J., Sena, G., Hauser, M.-T., and Benfey, P.N. (2000). The SHORT-ROOT Gene Controls Radial Patterning of the Arabidopsis Root through Radial Signaling. Cell *101*, 555-567.

Heo, J.-o., Roszak, P., Furuta, K.M., and Helariutta, Y. (2014). Phloem development: Current knowledge and future perspectives. American Journal of

Botany *101*, 1393-1402.

Hu, R., Qi, G., Kong, Y., Kong, D., Gao, Q., and Zhou, G. (2010). Comprehensive Analysis of NAC Domain Transcription Factor Gene Family in Populus trichocarpa. BMC Plant Biology *10*, 145.

Huffaker, A., Pearce, G., and Ryan, C.A. (2006). An endogenous peptide signal in *Arabidopsis* activates components of the innate immune response. Proceedings of the National Academy of Sciences *103*, 10098-10103.

Imlau, A., Truernit, E., and Sauer, N. (1999). Cell-to-Cell and Long-Distance Trafficking of the Green Fluorescent Protein in the Phloem and Symplastic Unloading of the Protein into Sink Tissues. The Plant Cell *11*, 309-322.

Inaba, M., and Yamashita, Yukiko M. (2012). Asymmetric Stem Cell Division: Precision for Robustness. Cell Stem Cell *11*, 461-469.

Jing, Y., Zheng, X., Zhang, D., Shen, N., Wang, Y., Yang, L., Fu, A., Shi, J., Zhao, F., Lan, W., *et al.* (2019). Danger-Associated Peptides Interact with PIN-Dependent Local Auxin Distribution to Inhibit Root Growth in Arabidopsis. The Plant Cell *31*, 1767-1787.

Kallarackal, J., and Milburn, J. (1983). Studies on the Phloem Sealing Mechanism in *Ricinus* Fruit Stalks. Functional Plant Biology *10*, 561-568.

Khan, J.A., Wang, Q., Sjölund, R.D., Schulz, A., and Thompson, G.A. (2007). An Early Nodulin-Like Protein Accumulates in the Sieve Element Plasma Membrane of Arabidopsis. Plant Physiology *143*, 1576-1589.

Kim, H., Zhou, J., Kumar, D., Jang, G., Ryu, K.H., Sebastian, J., Miyashima, S., Helariutta, Y., and Lee, J.-Y. (2020). SHORTROOT-Mediated Intercellular Signals Coordinate Phloem Development in Arabidopsis Roots. The Plant Cell *32*, 1519-1535.

Kodama, H., Ito, K., and Nakamura, Y. (2007). The role of N-terminal domain of translational release factor eRF3 for the control of functionality and stability in S. cerevisiae. Genes to Cells *12*, 639-650.

Kunieda, T., Mitsuda, N., Ohme-Takagi, M., Takeda, S., Aida, M., Tasaka, M., Kondo, M., Nishimura, M., and Hara-Nishimura, I. (2008). NAC Family Proteins NARS1/NAC2 and NARS2/NAM in the Outer Integument Regulate Embryogenesis in *Arabidopsis*. The Plant Cell *20*, 2631-2642.

Kurihara, D., Mizuta, Y., Sato, Y., and Higashiyama, T. (2015). ClearSee: a rapid optical clearing reagent for whole-plant fluorescence imaging. Development *142*, 4168-4179.

Lee, J.-Y., Colinas, J., Wang, J.Y., Mace, D., Ohler, U., and Benfey, P.N. (2006). Transcriptional and posttranscriptional regulation of transcription factor expression in *Arabidopsi*s roots. Proceedings of the National Academy of Sciences *103*, 6055-6060.

Lentini, Z., Tabares, E., and Buitrago, M.E. (2020). Vibratome Sectioning and Clearing for Easing Studies of Cassava Embryo Formation. Frontiers in Plant Science *11*.

Levesque, M.P., Vernoux, T., Busch, W., Cui, H., Wang, J.Y., Blilou, I., Hassan, H., Nakajima, K., Matsumoto, N., Lohmann, J.U., *et al.* (2006). Whole-Genome Analysis of the SHORT-ROOT Developmental Pathway in Arabidopsis. PLOS Biology *4*, e143.

Long, Y., Goedhart, J., Schneijderberg, M., Terpstra, I., Shimotohno, A., Bouchet, B.P., Akhmanova, A., Gadella Jr, T.W.J., Heidstra, R., Scheres, B., *et al.* (2015). SCARECROW-LIKE23 and SCARECROW jointly specify endodermal cell fate but distinctly control SHORT-ROOT movement. The Plant Journal *84*, 773-784.

López-Salmerón, V., Cho, H., Tonn, N., and Greb, T. (2019). The Phloem as a Mediator of Plant Growth Plasticity. Current Biology *29*, R173-R181.

Luna, E., Pastor, V., Robert, J., Flors, V., Mauch-Mani, B., and Ton, J. (2011). Callose deposition: a multifaceted plant defense response. Mol Plant Microbe Interact *24*, 183-193.

MacAlister, C.A., Ohashi-Ito, K., and Bergmann, D.C. (2007). Transcription factor control of asymmetric cell divisions that establish the stomatal lineage. Nature *445*, 537-540.

Machin, F.Q., Beckers, M., Tian, X., Fairnie, A., Cheng, T., Scheible, W.-R., and Doerner, P. (2019). Inducible reporter/driver lines for the Arabidopsis root with intrinsic reporting of activity state. The Plant Journal *98*, 153-164.

Mähönen, A.P., Bonke, M., Kauppinen, L., Riikonen, M., Benfey, P.N., and Helariutta, Y. (2000). A novel two-component hybrid molecule regulates vascular morphogenesis of the Arabidopsis root. Genes Dev *14*, 2938-2943.

Marhava, P., Bassukas, A.E.L., Zourelidou, M., Kolb, M., Moret, B., Fastner, A., Schulze, W.X., Cattaneo, P., Hammes, U.Z., Schwechheimer, C., *et al.* (2018). A molecular rheostat adjusts auxin flux to promote root protophloem differentiation. Nature *558*, 297-300.

Miyashima, S., Roszak, P., Sevilem, I., Toyokura, K., Blob, B., Heo, J.O., Mellor, N., Help-Rinta-Rahko, H., Otero, S., Smet, W., *et al.* (2019). Mobile PEAR transcription factors integrate positional cues to prime cambial growth. Nature *565*, 490-494.

Moreno-Risueno, M.A., Sozzani, R., Yardımcı, G.G., Petricka, J.J., Vernoux, T., Blilou, I., Alonso, J., Winter, C.M., Ohler, U., Scheres, B., *et al.* (2015). Transcriptional control of tissue formation throughout root development. Science *350*, 426-430.

Nakajima, K., Sena, G., Nawy, T., and Benfey, P.N. (2001). Intercellular movement of the putative transcription factor SHR in root patterning. Nature *413*, 307-311.

Ohtani, M., Akiyoshi, N., Takenaka, Y., Sano, R., and Demura, T. (2016). Evolution of plant conducting cells: perspectives from key regulators of vascular cell differentiation. Journal of Experimental Botany *68*, 17-26.

Olsen, A.N., Ernst, H.A., Leggio, L.L., and Skriver, K. (2005). NAC transcription factors: structurally distinct, functionally diverse. Trends in Plant Science *10*, 79-87.

Petricka, J.J., Van Norman, J.M., and Benfey, P.N. (2009). Symmetry breaking in plants: molecular mechanisms regulating asymmetric cell divisions in Arabidopsis. Cold Spring Harb Perspect Biol *1*, a000497-a000497.

Pillitteri, L.J., Guo, X., and Dong, J. (2016). Asymmetric cell division in plants: mechanisms of symmetry breaking and cell fate determination. Cellular and molecular life sciences : CMLS *73*, 4213-4229.

Pillitteri, L.J., Sloan, D.B., Bogenschutz, N.L., and Torii, K.U. (2007). Termination of asymmetric cell division and differentiation of stomata. Nature *445*, 501-505.

Roberts, A.G. (2005). Plasmodesmal Structure and Development. In Plasmodesmata, pp. 1-32.

Ryan, C.A., Huffaker, A., and Yamaguchi, Y. (2007). New insights into innate immunity in Arabidopsis. Cell Microbiol *9*, 1902-1908.

Sauer, N. (2007). Molecular physiology of higher plant sucrose transporters. FEBS Letters *581*, 2309-2317.

Scheres, B., Di Laurenzio, L., Willemsen, V., Hauser, M.T., Janmaat, K., Weisbeek, P., and Benfey, P.N. (1995). Mutations affecting the radial organisation of the Arabidopsis root display specific defects throughout the embryonic axis.

Development *121*, 53-62.

Schulz, A. (2005). Role of Plasmodesmata in Solute Loading and Unloading. In Plasmodesmata, pp. 135-161.

Sebastian, J., Ryu, K.H., Zhou, J., Tarkowská, D., Tarkowski, P., Cho, Y.H., Yoo, S.D., Kim, E.S., and Lee, J.Y. (2015). PHABULOSA controls the quiescent center-independent root meristem activities in Arabidopsis thaliana. PLoS Genet *11*, e1004973.

Seo, M., Kim, H., and Lee, J.-Y. (2020). Information on the move: vascular tissue development in space and time during postembryonic root growth. Current Opinion in Plant Biology *57*, 110-117.

Sjolund, R.D. (1997). The Phloem Sieve Element: A River Runs through It. The Plant Cell *9*, 1137.

Sozzani, R., Cui, H., Moreno-Risueno, M.A., Busch, W., Van Norman, J.M., Vernoux, T., Brady, S.M., Dewitte, W., Murray, J.A., and Benfey, P.N. (2010). Spatiotemporal regulation of cell-cycle genes by SHORTROOT links patterning and growth. Nature *466*, 128-132.

Stadler, R., and Sauer, N. (1996). The Arabidopsis thaliana AtSUC2 Gene is Specifically Expressed in Companion Cells. Botanica Acta *109*, 299-306.

Stadler, R., and Sauer, N. (2019). The AtSUC2 Promoter: A Powerful Tool to Study Phloem Physiology and Development. In Phloem: Methods and Protocols, J. **Liesche, ed.** (New York, NY: Springer New York), pp. 267-287.

Tamaki, T., Oya, S., Naito, M., Ozawa, Y., Furuya, T., Saito, M., Sato, M., Wakazaki, M., Toyooka, K., Fukuda, H., *et al.* (2020). VISUAL-CC system uncovers the role of GSK3 as an orchestrator of vascular cell type ratio in plants. Communications Biology *3*, 184.

Ting, X. (2013). Control of germline stem cell self-renewal and differentiation in the Drosophila ovary: concerted actions of niche signals and intrinsic factors. WIREs Developmental Biology *2*, 261-273.

Torode, T.A., O'Neill, R., Marcus, S.E., Cornuault, V., Pose, S., Lauder, R.P., Kračun, S.K., Rydahl, M.G., Andersen, M.C.F., Willats, W.G.T., *et al.* (2018). Branched Pectic Galactan in Phloem-Sieve-Element Cell Walls: Implications for Cell Mechanics. Plant Physiology *176*, 1547-1558.

Truernit, E., Bauby, H., Belcram, K., Barthélémy, J., and Palauqui, J.-C. (2012). OCTOPUS, a polarly localised membrane-associated protein, regulates phloem differentiation entry in *Arabidopsis thaliana*. Development *139*, 1306-1315.

Vatén, A., Dettmer, J., Wu, S., Stierhof, Y.-D., Miyashima, S., Yadav, Shri R., Roberts, Christina J., Campilho, A., Bulone, V., Lichtenberger, R., *et al.* (2011). Callose Biosynthesis Regulates Symplastic Trafficking during Root Development. Developmental Cell *21*, 1144-1155.

Voigt, C.A. (2014). Callose-mediated resistance to pathogenic intruders in plant defense-related papillae. Frontiers in plant science *5*, 168-168.

Welch, D., Hassan, H., Blilou, I., Immink, R., Heidstra, R., and Scheres, B. (2007). Arabidopsis JACKDAW and MAGPIE zinc finger proteins delimit asymmetric cell division and stabilize tissue boundaries by restricting SHORT-ROOT action. Genes & development *21*, 2196-2204.

Wildwater, M., Campilho, A., Perez-Perez, J.M., Heidstra, R., Blilou, I., Korthout, H., Chatterjee, J., Mariconti, L., Gruissem, W., and Scheres, B. (2005). The RETINOBLASTOMA-RELATED gene regulates stem cell maintenance in Arabidopsis roots. Cell *123*, 1337-1349.

Wu, Y., Hou, J., Yu, F., Nguyen, S.T.T., and McCurdy, D.W. (2018). Transcript Profiling Identifies NAC-Domain Genes Involved in Regulating Wall Ingrowth Deposition in Phloem Parenchyma Transfer Cells of Arabidopsis thaliana. Frontiers in plant science *9*, 341-341.

Yamaguchi, Y., Huffaker, A., Bryan, A.C., Tax, F.E., and Ryan, C.A. (2010). PEPR2 Is a Second Receptor for the Pep1 and Pep2 Peptides and Contributes to Defense Responses in Arabidopsis The Plant Cell *22*, 508-522.

Yan, D., Yadav, S.R., Paterlini, A., Nicolas, W.J., Petit, J.D., Brocard, L., Belevich, I., Grison, M.S., Vaten, A., Karami, L., *et al.* (2019). Sphingolipid biosynthesis modulates plasmodesmal ultrastructure and phloem unloading. Nature Plants *5*, 604-615.

Yoon, E.K., Dhar, S., Lee, M.-H., Song, J.H., Lee, S.A., Kim, G., Jang, S., Choi, J.W., Choe, J.-E., Kim, J.H., *et al.* (2016). Conservation and Diversification of the SHR-SCR-SCL23 Regulatory Network in the Development of the Functional

Endodermis in Arabidopsis Shoots. Molecular Plant *9*, 1197-1209.

Zhang, X., Zhou, W., Chen, Q., Fang, M., Zheng, S., Scheres, B., and Li, C. (2018). Mediator subunit MED31 is required for radial patterning of *Arabidopsis* roots. Proceedings of the National Academy of Sciences *115*, E5624-E5633.

Zhong, R., Lee, C., Haghighat, M., and Ye, Z.-H. (2021). Xylem vessel-specific SND5 and its homologs regulate secondary wall biosynthesis through activating secondary wall NAC binding elements. New Phytologist.

Zhong, R., Lee, C., Zhou, J., McCarthy, R.L., and Ye, Z.-H. (2008). A Battery of Transcription Factors Involved in the Regulation of Secondary Cell Wall Biosynthesis in Arabidopsis. The Plant Cell *20*, 2763-2782.

6. Abstract in Korean

국문초록

식물의 뿌리는 정단분열조직에서 일어나는 세포 분열을 통하여 길이 성장을 한다. 지속적인 길이 성장을 위해서는 분열능이 왕성한 세포를 공급하는 미분화 상태의 줄기세포(stem cell)들이 정단분열조직에서 유지하고 있다. 특히, 애기장대 뿌리분열조직에서는 분열지연중심부를 에워싼 줄기세포의 정렬된 비대칭분열을 통하여 뿌리 중심주에 무기양분을 수송하는 물관부가 일렬로 형성되고, 양분과 포도당 및 다양한 형태의 신호전달 물질을 수송하는 두 개 축의 체관부가 물관부의 수직 방향으로 형성된다. 이 때, 체관세포는 식물이 성장하는 데 필수 영양소와 신호 전달 분자의 운반을 중재하는 중요한 역할을 한다. 이러한 기능을 가지는 체관세포는 두 가지 주요 비대칭 세포 분열을 통해 반세포(Companion cells, CCs)와 phloem sieve elements (phloem SEs)로 발달된다. 애기장대 뿌리 분열조직에서는 반세포는 phloem SEs를 마주하는 procambial 세포와 내피(pericycle)의 비대칭분열을 통해 생성되며, 이와 다르게 proto phloem SE와 metaphloem SE로 구성된 체관 SE는 두 번의 연속적인 체관 전구세포의 비대칭분열로 발달하게 된다.

실험실의 이전 연구에서 GRAS 계열 전사 인자인 SHORTROOT (SHR)가 뿌리의 체관 발달과정에서 sieve element(SE)와 반세포를 형성하기 위한 비대칭분열에 주요한 역할을 한다는 것을 밝혔다. SHR의 전사체는 뿌리에서 체관세포를 제외한 물관, procambium 세포층에서 발현되지만, SHR의

단백질은 체관부로 이동하여 체관 SE 형성에 필요한 비대칭분열을 유도한다. 이미 endodermis 및 분열지연중심부 (Quiescent center, QC)에서 SHR은 SCRACOW (SCR)의 발현을 활성화하고 SCR과 상호 작용한다는 것은 알려져 있다. 이 둘의 단백질 복합체는 *microRNA165/6* (*miR165/6*)의 발현을 유발시키고 이들은 뿌리 중심부로 이동하여 Class III homeodomain leucine zipper (HD-ZIPIII) mRNA를 분해하여 HD-ZIPIII의 농도 구배를 형성한다. 이러한 농도 구배는 protoxylem과 metaxylem을 형성하여 물관부를 조직화한다. 이전 코넬대학교에서 이지영 교수님께 지도를 받았던 박사과정 학생, Dr. Jing Zhou는 체관부로의 SHR 이동이 체관세포 비대칭 세포 분열을 촉진하여 체관세포 발달에 주요한 역할을 한다는 것을 관찰하였다. 그러나, 뿌리중심부의 SHR의 이동이 phloem SEs 및 CCs 형성을 위한 비대칭분열을 어떻게 조절하는지에 관한 구체적인 과정은 여전히 불분명했다. 따라서 본 연구는 SHR와 그 하위 유전자들이 어떻게 체관세포 발달에 기여하는지 알아내는 것을 목표로 삼았다. 이를 밝히기 위해, SHR 하위 유전자로서의 NARS1, SND2가 체관세포 형성을 위해 어떠한 기능을 하는지 분석하였고 이들의 관계를 밝히고자 하였다.

본 연구를 통해 SHR와 그의 직접적인 하위 전사 인자인 *NAC-REGULATED SEED MORPHOLOGY 1 (NARS1)*과 *SECONDARY WALL-ASSOCIATED NAC DOMAIN PROTEIN 2 (SND2)*가 positive feedforward loop를 형성하며 체관세포 발달에 관여한다는 사실을 밝힐 수

있었다. 특히, NARS1이 'Top-down long distance signal'을 통한 전사 조절인자로 체관 SE 전구(precursor)세포의 비대칭 분열을 조절할 것이라는 잠재적 가능성을 제시하였다. 흥미롭게도, *NARS1*의 전사체는 뿌리의 분열조직(meristem)이 아닌 세포들의 비대칭분열이 끝나고 성장하는 분화대(differentiation zone)의 반세포에서 발현이 된다. 그러나 *nars1*의 돌연변이체는 체관 전구세포의 비대칭분열이 비정상적으로 일어난다. 이는 NARS1의 위쪽 반세포에서의 발현이 아래 분열조직에서의 비대칭분열을 조절한다는 'Long distance top-down signaling' 의 가능성을 제시한다. 게다가 SND2는 NARS1을 통해 뿌리의 분열조직인 protophloem SE에서 발현되며 NARS1의 발현을 활성화하여 positive feedback loop를 형성하는 데 뒷받침된다. 이러한 결과들을 종합해볼 때, 본 연구는 NARS1이 phloem SE의 비대칭분열을 위해 'Long distance top-down signaling' 을 통해 조절하며, 이는 분화된 phloem 세포들이 아직 분화되지 않은 전구세포를 규제할 수 있게 한다는 가능성을 제시한다. 이러한 연구를 통해 다이나믹한 식물 성장 과정 중 관다발 조직 시스템의 세포 유형 패턴 형성과 세포 분화에 대한 새로운 통찰력을 제공할 것이라 기대한다.

주요어: Phloem sieve element, 비대칭세포분열, 애기장대, Long-distance signaling, SHORTROOT, NARS1

학번 : 2014-25012

7. Appendix

A method for a rapid and accurate detection of phloem sieve element development; its application and scalability

Hyoujin Kim[1], Ji-Young Lee[1,2]

[1]School of Biological Sciences, College of Natural Science, Seoul National University, Seoul, Korea

[2]Plant Genomics and Breeding Institute, Seoul National University, Seoul, Korea

Corresponding author: Lee, Ji-Young (jl924@snu.ac.kr)

ABSTRACT

Vascular system plays an important role for the plant growth and survival under dynamic environmental conditions. As part of vascular tissues, a phloem consists of phloem sieve elements (SEs) and companion cells (CCs). In the root apical meristem of *Arabidopsis thaliana*, CCs are generated by the asymmetric cell divisions (ACDs) of procambial cells adjoining SEs and pericycle cells. The proto- and metaphloem SEs are originated from sequential ACDs of a SE-procambium precursor and a SE precursor. To study the development of vascular tissues, researchers have mainly relied on histological methods that take days with multiple steps. While investigating molecular mechanisms underlying phloem SE development, we developed a rapid and reliable method that allows for the

detection of differentiating phloem SEs. This protocol employs monoclonal antibody RS6, which was selected from hybridomas raised against SEs isolated from tissue cultures of California shield leaf, *Streptanthus tortuosus* (Khan et al., 2007). RS6 is known to recognize a SE-specific early nodulin-like protein, SE-ENOD, which is specifically localized to the plasma membrane of differentiating and mature SEs. This protocol enables quantitative assessment of phloem SEs in a large scale for a broad range of species beyond *Arabidopsis thaliana*.

Keywords. *Arabidopsis thaliana.* Immunostaining of SE-ENOD. RS6 antibody. Phloem sieve element. 3D printing. Vibratome.

INTRODUCTION

The vascular system is a key innovation in the evolutionary history of plants, which enabled plant bodies to grow far above the ground without undergoing dehydration. The vascular system is composed of the following three major tissues: xylem that mainly transports water and dissolved minerals from the root to the shoot, phloem which conveys the nutrients, and (pro)cambium serving as a reservoir of stem cells for xylem and phloem. Phloem, a major tissue that transports photo-assimilates and mediates long-distance signaling molecules such as small RNAs, hormones, or proteins from a source to a sink (Chen et al., 2018), consists of sieve elements (SE) and companion cells (CC). These two cell types together form a functional unit of the phloem. Phloem SEs make a conduit for transportation of substances such as carbohydrates, amino acids and minerals. For this, phloem SEs undergo a special differentiation process involving enucleation, the breakdown of nuclei. Though the nuclei are lost, phloem-specific proteins (p-proteins), mitochondria and plastids remain functional in SEs (Blob et al., 2018). SEs are symplastically connected to the CCs through plasmodesmata, thereby enabling the unloading of macromolecules in the CCs to the SEs (Anne and Hardtke, 2018).

In the root of *Arabidopsis thaliana*, hereafter Arabidopsis, CCs and SEs develop from precursors of different origins. The CCs are generated by the asymmetric cell divisions (ACD) of procambial cells adjoining SEs and pericycle cells. The proto- and metaphloem

SEs are originated from two periclinal ACDs of a SE procambium precursor and a SE precursor (Heo et al., 2014; Kim et al., 2020). We recently reported that the ACDs for generating CCs and SEs are coordinated by SHORTROOT (SHR), a GRAS family transcription factor (Kim et al., 2020). SHR moving into the phloem pole promotes ACDs for SEs while SHR moving into the endodermis promotes ACDs for CCs. Direct downstream genes of SHR, encoding two transcription factors, NAC-REGULATED SEED MORPHOLOGY 1 (NARS1) and SECONDARY WALL-ASSOCIATED NAC DOMAIN PROTEIN 2 (SND2), are associated with the SE development via long distance top-down signaling. Especially, NARS1 functions as a important regulator of ACDs of phloem SE precursors in the root meristem (Kim et al., 2020).

450 million years ago, land plants had developed vascular tissues. Early land plants before then (i.e.. bryophytes) had developed water-conducting cells with smooth cell walls called hydroids, and the protophloem-sieve-element(SE)-like cell called leptoid (Thomas et al., 1988). Phloem sieve cells, equivalent to sieve (tube) elements in angiosperms, develop in seedless vascular plants and gymnosperms (Esau et al., 1953). ALTERED PHLOEM DEVELOPMENT (APL), a MYB coiled-coil transcription factor family member, is the first key regulator of phloem development discovered in Arabidopsis (Bonke et al., 2003). APL controls the phloem SE differentiation including the enucleation process by turning on NAC domain transcription factors, NAC45/86 (Furuta et al., 2014). These together with our recent finding (Kim et al., 2020) indicate that several NAC domain transcription factors serve for the phloem SE development. Understanding their regulation in the evolutionary context would be very interesting, however difficult to pursue due to the lack of proper markers that can distinguish phloem SEs in evolutionarily divergent species.

RS6 is a monoclonal antibody selected from hybridomas raised against SEs from tissue cultures of California shield leaf, *Streptanthus tortuosus*. In Arabidopsis, RS6 was found to specifically recognize SE-ENOD, encoded by *AT3G20570* (Khan et al., 2007). SE-ENOD is composed of four domains: phytocyanins which have a similar domain structure of an amino-terminal signal peptide, plastocyanin-like copper-binding domain, proline/serine-rich domain, and carboxy-terminal hydrophobic domain. N-terminal signal

peptide is recognized by a secretory pathway. Two proline/serine-rich domains (PAPAP and PAPTP) are arabinoglycan glycosylation recognition sites. SE-ENOD also has a glycosylphosphatidylinositol (GPI) anchor that allows for the covalent attachment of mature SE-ENOD on the SE plasma membrane (Khan et al., 2007). The post-translationally processed SE-ENOD seems exposed outside the plasma membrane of phloem SEs, which makes the recognition by RS6 feasible. Several studies including ours employed RS6 antibody to detected phloem SEs in Arabidopsis (Absmanner et al., 2013; Hoth et al., 2005; Hoth et al., 2008; Khan et al., 2007; Meyer et al., 2004; Wippel and Sauer, 2011), however no report is yet available beyond Arabidopsis.

In a recent study, we performed RS6 based immunostaining to localize phloem SEs (Kim et al., 2020). Two approaches for tissue preparation were used in the immunostaining. First, wax-embedding and tissue sectioning were utilized as described on previous studies (Paciorek et al., 2006; Sauer and Friml, 2010) The other was proceeded using an agar-embedding and vibratome sectioning. The first method takes about seven days, while the second method carries out only two days for immunostaining. In addition, the degree of detection through the immunostaining using wax-embedded sections varied depending on the condition of the tissue preparation. Therefore, the second protocol using the vibratome section for immunostaining was further optimized to be used in a broad range of research. This paper presents our optimized protocol step-by step, and the results of experiments performed in a large scale and in plant species beyond Arabidopsis.

MATERIALS

Chemicals

MES hydrate (Sigma, M8250)

Murashige & Skoog medium (MS salt; Duchefa, M0221.0050)

Sucrose (Duchefa, S0809)

Plant Agar (Duchefa, P1001)

Agarose LE (Seakem agarose, Lonza 50004)

Low melting agarose (Sea Plaque Agarose ™ 50100)

BSA fraction V (Sigma, A-3912)

Alexa Fluor® 488 F(ab')2 Fragment of Goat Anti-Mouse IgG, IgM (H+L) (Invitrogen A-10680)

RS6 antibody (Kerafast, EIW201)

Calcofluor white 2MR (Sigma, 18909)

Paraformaldehyde (Sigma, 158127)

KCl (Sigma, P9541)

NaCl (Sigma, S7653)

$Na_2HPO_4 \bullet 2H_2O$ (Sigma, 71643)

KH_2PO_4 (Sigma, P9791)

KOH (Sigma, P1767)

HCl (Sigma, 320331)

Equipment and Consumables

A laminar flow hood

Autoclave

Vibrating blade microtome (Leica VT1000S)

Confocal laser scanning microscope (ZEISS, LSM700)

Stirring hot plate (Corning PC-420d)

Mini shaker (VWR shaker 12620-938)

Multi six-well plate (Sigma CLS3335)

3D printed embedding molds and strainer

Square dish (SPL,11125)

Forceps (Dumont 11295-10)

Double edge razor blade (Feather)

Cyanoacrylate adhesive (Loctite, 401)

Nail polish

Reagent preparation

Plant Growth Media. To prepare 1L, 4.3g of Murashige and Skoog (MS) salts (1X) , 10g of sucrose (1%) and 0.5g of MES hydrate were added and dissolved in 850ml of deionized water. After dissolving solution completely, deionized water was added up to 1 liter and the pH was adjusted to 5.7 by adding drops of 1M of KOH. The solution was combined and stirred with 10g of plant agar (1%), and then sterilized for 15 min at 121°C. 90-100ml of media was poured into square plates in a sterile laminar flow hood.

PBS (pH 7.4). To prepare 1L of 10X PBS, 2g of KCl (27mM), 81.8 g of NaCl (1.4M), 11.57g of $Na_2HPO_4 \bullet 2H_2O$ (65mM), and 2.04g of KH_2PO_4 (15mM) were dissolved in deionized water. The solution can be autoclaved for 15 min at 121°C and stored for many months. Prior to use, dilute to 1x and check if pH is 7.4. If not, adjust with KOH or HCl.

PFA. To prepare 100ml of 4% PFA solution, 4g of Paraformaldehyde (PFA, 4g) powder (in the fume hood and wearing gloves because PFA is highly toxic and the powder is very fine) was measured and dissolved in 1x PBS. Some KOH pellets were added to facilitate dissolving. After PFA powder was completely dissolved, pH was adjusted to 7.4 with drops of HCl in the fume hood. The PFA fixative solution is best when freshly prepared, but it can be also aliquoted and stored at –20°C for a few months.

PROCEDURE

Growing Arabidopsis seedlings

1. Sterilize the surface of the seeds and plant them in a row on plant growth media.

2. Germinate and grow the seedlings vertically, under a 16-h-light/8-h-dark cycle with light intensity of 100 μmol m^{-2} s^{-1} at 22-23°C in a plant growth chamber**.**

Tissue fixation (Fig 1)

3. Collect 5 day-old seedlings.

4. Transfer whole seedlings to a six-well plate containing 4% PFA solution and fix seedlings by placing the plate on a rotary mini shaker at room temperature for 1 hour.

5. Wash the plant material 4 times in 1X PBS for 10 min each.

   Option. Perform vacuum infiltration and incubate overnight in 4% PFA at 4°C depending on your sample.

Embedding seedling roots (Fig 1)

6. Melt 4% of low melting agarose (Sea Plaque Agarose) in 1X PBS at 80°C on a stirring hot plate (Corning PC-420d).

Caution. Be careful not to lump the agarose because of high concentration.

7. Align 4 or 5 seedlings in a custom designed (Supplemental Fig. S1A) mold and add 4% of low melting agarose.

8. Solidify the agarose block at 4°C for at least 1 hour until the block is completely hardened.

Sectioning (Fig 1)

9. Detach the agar block from the mold and place it on the vibrating microtome mounting disc as described in steps 10-12.

10. A vibrating microtome is set to cut sections at 80 - 250μm of thickness. For observing the meristem zone of Arabidopsis roots, thickness should be set to 90 - 120μm.

11. Set the vibrating speed at 90 and frequency at 10 and adjust depending on the types of specimens.

12. Locate the agar block in the middle of mounting disk and glue it with cyanoacrylate adhesive.

13. Wait for about 2 min, to fully attach the block on the mounting disc.

14. After the adhesive curing time, fill up the disk container with 1X PBS.

15. Trim the sections carefully not to cut off the specimen. Collect the target sections using a custom designed strainer (Supplemental Fig. S1B).

16. Keep the sections in multi six well plates containing the 1X PBS.

Immunostaining (Fig 1)

17. Wash the sections in 1X PBS for 10 min at room temperature.

18. Incubate the sections in each well containing the 4 ml of blocking solution (2% BSA in the 1X PBS should be prepared fresh) for 1 hour at room temperature with gentle shaking.

19. Transfer the sections to the primary antibody (RS6) solution, which is prepared by adding antibody to the blocking solution at the ratio 1:100.

20. Seal the multi-well plate with parafilm and incubate the samples for 3 hours at 37°C, or overnight at 4°C with gentle shaking.

21. Wash the sections in 1X PBS for 10 min at room temperature.
22. Repeat step 21 five more times.
23. Apply the sections with the secondary antibody (Alexa Fluor® 488 F(ab')2 Fragment of Goat Anti-Mouse IgG, IgM (H+L)) which is diluted 200 folds in the blocking solution.
24. Incubate the sections in the dark for 1 hour at room temperature with gentle shaking.
25. Wash the sections 1X PBS for 10 min each at room temperature in the dark.
26. Repeat step 25 five more times in the same condition.

Staining the cell wall for microscopy (Fig 1)

27. Stain the sections in Calcofluor white 2MR (0.3 mg/ml of 1X PBS) for 1 min at room temperature in the dark.
28. Place the specimens on the microscope slide glass, mount them with antifadent AF1 (Citifluor Ltd), and seal the edge of the cover slip with nail polish.
29. Signals are examined using Confocal Microscope (ZEISS, LSM700) with the emission/excitation wavelength of 488 nm/505 to 530 nm for alexa488 and 390nm/420nm for Calcoflour white.

RESULTS AND DISCUSSION

A modified RS6 antibody-based immunostaining method enables a large-scale analysis of phloem sieve element development

Following the protocol presented in this study, we performed the immunostaining using RS6 antibody against the root sections of 5 day-old Arabidopsis seedlings. Fluorescence signals for RS6 antibodies were specifically found in the proto– and metaphloem SEs in the wild type **(Fig. 2B).** We recently reported that SHR and NARS1 play major roles in the ACDs for the development of phloem SEs (Kim et al., 2020). In *shr-2*, the number of SEs was reduced but in a varied manner: 1) two SEs on one phloem pole and no SE in the other **(Fig. 2D)**, 2) one SE on each of two phloem poles **(Fig. 2E)**, 3) two SEs on one and one SE on the other side of phloem poles **(Fig. 2F)**, and 4) two SEs on each pole **(Fig. 2G)**. Such a variation in SE numbers in one genotype indicates the importance of quantitative assessments in the study of phloem SE development. NARS1 is directly regulated by SHR to promote the ACD of the phloem SE precursor. In *nars1* mutant, we found three SE types: 1) one SE on each of two phloem poles **(Fig. 2H)**, 2) two SEs on one and one SE on the other side of phloem poles **(Fig. 2I)**, and 3) two SEs on each pole **(Fig. 2J)**. Consistent with the role of NARS1 as the one promoting SE formation, the transgenic line expressing *pCRE1::GFP:NARS1,* in which NARS1 was expressed throughout the stele, displayed more than two phloem SEs **(Fig. 2K)**.

RS6 antibody can detect phloem sieve elements in a broad range of eudicot species

To find out the applicability of our RS6 antibody based phloem SE detection method in evolutionarily divergent species, we conducted immunostaining in the roots of selected monocot and eudicot species. We chose *Spirodela polyrhiza, Brachypodium distachyon* and *Sorhgum bicolor* among monocots. From the eudicots, *Brassica oleracea capitata* (khorabi) and *Brassica rapa* (turnip, bok choy) were selected as representatives of the Brassicaceae family. As species more distantly related to Arabidopsis, we selected *Solanum lycopersicum* (tomato), *Cucurbita moschata Duch* (pumpkin) and *Glycine max* (soybean).

In our extended analyses, we found that RS6 antibody robustly detects the phloem

SEs in the roots of khorabi (**Fig. 3A-D)**, turnip (**Fig. 3E-H**) and bok choy **(Fig. 3I-L**). Furthermore, weak but reproducible RS6 bound signals were found in phloem SE positions in the roots of tomato (**Fig. 4A-D**), pumpkin (**Fig. 4E-H**) and soybean (**Fig. 4I-L**). However, none of the selected monocot species such as *Spirodela polyrhiza* **(Fig. 5A),** *Brachypodium distachyon* **(Fig. 5B)** and *Sorhgum bicolor* **(Fig. 5C)** showed a binding signal of RS6 antibody**.** These data collectively indicate that our immunolocalization method using RS6 antibody can be applied for detecting phloem SEs in a broad range of eudicot species.

Conservation of SE-ENOD proteins

A BLAST query (https://phytozome-next.jgi.doe.gov/) using the amino acid sequence of Arabidopsis SE-ENOD protein (AT3G20570) was performed to identify potential orthologues in species selected for immunolocalization. The genome sequence of *Cucurbita moschata* was not available in phytozome data, therefore the genome of *Cucumis sativus*, a closely related species to *Cucurbita moschata*, was included in the query. Potential orthologues of SE-ENOD were found except for *Spirodela polyrhiza*. The sequences aligned with Mega X is shown in **Fig. 6** (Madeira et al., 2019).

Arabidopsis SE-ENOD is predicted to be glycosylphosphatidylinositol (GPI) anchored (Borner et al., 2003). It has an attachment sites for the GPI membrane anchor near the C-terminal hydrophobic domain. Arabidopsis SE-ENOD also has two proline-serine rich domains, PAPAP (145 amino acid) and PAPTP (167 amino acid), which are related to arabinoglycan glycosylation recognition (Khan et al., 2007). Based on the data of sequence alignment, the attachment site for the GPI anchor seems conserved in all the SE-ENOD seuences. The first proline-serine rich domain (PAPAP) is conserved only in the eudicots, not in the monocot. The second domain (PAPTP) is highly variable even among SE-ENOD in other eudicots species. Amino acid alignment collectively indicates that key features of SE-ENOD are conserved in eudicots, which might be related to our finding that RS6 antibody can detect phloem SEs in a broad spectrum of eudicots species.

CONCLUSION

The immunostaining of SE-ENOD using RS6 antibody is a useful technique to analyze phloem tissue identification. Unlike other immunochemistry experiments, our modified method does not need steps required for the embedding in paraffin or Steedman wax. Combining the shortened steps with imaging using confocal microscopy, we could reduce the time for experiments and increase throughputs.

This protocol based on RS6 antibody can be applied in eudicot species such as *Solanum lycopersicum* and *Glycine max*, beyond the Brassicaceae. Comparing tissue morphologies of the phloem SEs is more difficult than comparing that of the xylem vessels. The cell wall of the xylem is lignified and thickened, so it is easy to be detected by simple staining. However, it is not easy to clearly distinguish the phloem SEs from other cells like (pro)cambium cells or companion cells. In that context, our exploration of SE detection could help phloem research in a diverse plant species.

ACKNOWLEDGEMENTS

We thank the members of the Lee lab for assisting in the experiments at various stages, and Ms. Hannah Oh (University of Washington, Seattle, WA, United States) for instructing and providing 3-D designs. This work was supported by Plant Immunity Research Center (NRF-2018R1A5A1023599) and Basic Research Program (NRF-2021R1A2C3006061) funded by National Research Foundation of Korea to J-YL. HK was supported by WooDuk Foundation.

CONFLICT OF INTEREST

The authors declare that the research was conducted in the absence of any commercial or financial relationships that could be construed as a potential conflict of interest.

References

Absmanner, B, Stadler, R, Hammes, UZ (2013) Phloem development in nematode-induced feeding sites: the implications of auxin and cytokinin. Front Plant Sci 4: 241.

Anne, P, Hardtke, CS (2018) Phloem function and development-biophysics meets genetics. Curr Opin Plant Biol 43: 22-28.

Blob, B, Heo, J-O, Helariutta, Y (2018) Phloem differentiation: an integrative model for cell specification. J Plant Res 131: 31-36.

Bonke, M, Thitamadee, S, Mähönen, AP, Hauser, M-T, Helariutta, Y (2003) APL regulates vascular tissue identity in Arabidopsis. Nature 426: 181-186.

Borner, GH, Lilley, KS, Stevens, TJ, Dupree, P (2003) Identification of glycosylphosphatidylinositol-anchored proteins in Arabidopsis. A proteomic and genomic analysis. Plant Physiol 132: 568-577.

Chen, Q, Payyavula, RS, Chen, L, Zhang, J, Zhang, C, Turgeon, R (2018) *FLOWERING LOCUS T* mRNA is synthesized in specialized companion cells in *Arabidopsis* and Maryland Mammoth tobacco leaf veins. Proc Natl Acad Sci 115: 2830-2835.

Esau, K, Cheadle, VI, Gifford Jr., EM (1953) Comparative structure and possible trends of specialization of the phloem. Am J Bot 40: 9-19.

Furuta, KM, Yadav, SR, Lehesranta, S, Belevich, I, Miyashima, S, Heo, J-o, Vatén, A, Lindgren, O, De Rybel, B, Van Isterdael, G, Somervuo, P, Lichtenberger, R, Rocha, R, Thitamadee, S, Tähtiharju, S, Auvinen, P, Beeckman, T, Jokitalo, E, Helariutta, Y (2014) *Arabidopsis* NAC45/86 direct sieve element morphogenesis culminating in enucleation. Science 345: 933-937.

Heo, JO, Roszak, P, Furuta, KM, Helariutta, Y (2014) Phloem development: current knowledge and future perspectives. Am J Bot 101: 1393-1402.

Hoth, S, Schneidereit, A, Lauterbach, C, Scholz-Starke, J, Sauer, N (2005) Nematode infection triggers the de novo formation of unloading phloem that allows macromolecular trafficking of green fluorescent protein into syncytia. Plant Physiol 138: 383-392.

Hoth, S, Stadler, R, Sauer, N, Hammes, UZ (2008) Differential vascularization of nematode-induced feeding sites. Proc Natl Acad Sci 105: 12617-12622.

Khan, JA, Wang, Q, Sjölund, RD, Schulz, A, Thompson, GA (2007) An Early Nodulin-Like Protein Accumulates in the Sieve Element Plasma Membrane of Arabidopsis. Plant Physiol 143: 1576.

Kim, H, Zhou, J, Kumar, D, Jang, G, Ryu, KH, Sebastian, J, Miyashima, S, Helariutta, Y, Lee, J-Y (2020) SHORTROOT-Mediated Intercellular Signals Coordinate Phloem Development in Arabidopsis Roots. Plant Cell 32: 1519-1535.

Madeira, F, Park, Ym, Lee, J, Buso, N, Gur, T, Madhusoodanan, N, Basutkar, P, Tivey, ARN, Potter, SC, Finn, RD, Lopez, R (2019) The EMBL-EBI search and sequence analysis tools APIs in 2019. Nucleic Acids Res 47: 636-641.

Meyer, S, Lauterbach, C, Niedermeier, M, Barth, I, Sjolund, RD, Sauer, N (2004) Wounding Enhances Expression of AtSUC3, a Sucrose Transporter from Arabidopsis Sieve Elements and Sink Tissues. Plant Physiology 134: 684-693.

Paciorek, T, Sauer, M, Balla, J, Wiśniewska, J, Friml, J (2006) Immunocytochemical technique for protein localization in sections of plant tissues. Nat Protoc 1: 104-107.

Sauer, M, Friml, J (2010) Immunolocalization of Proteins in Plants. In Plant Developmental Biology: Methods and Protocols, L. Hennig,C. Köhler, eds. Totowa, NJ: Humana Press, pp. 253-263.

Thomas, R, Schiele, EM, Scheirer, DC (1988) TRANSLOCATION IN POLYTRICHUM COMMUNE (BRYOPHYTA) I. CONDUCTION AND ALLOCATION OF PHOTOASSIMILATES. Am J Bot 75: 275-281.

Wippel, K, Sauer, N (2011) Arabidopsis SUC1 loads the phloem in *suc2* mutants when expressed from the SUC2 promoter. J Exp Bot 63: 669-679.

Figure Caption

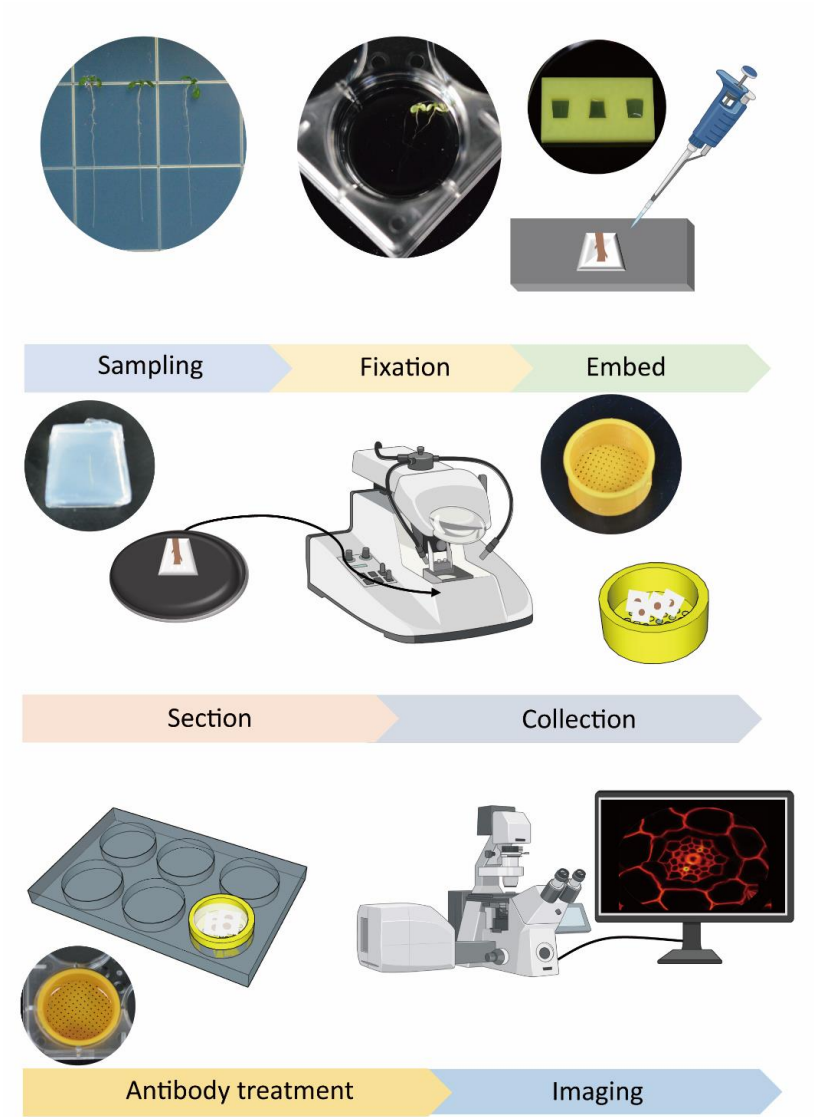

Fig 1. The experimental scheme of immunostaining process for detecting phloem SEs. The graphical description and images to introduce the whole process of SE-ENOD immunostaining from tissue preparation to signal detection via confocal microscopy.

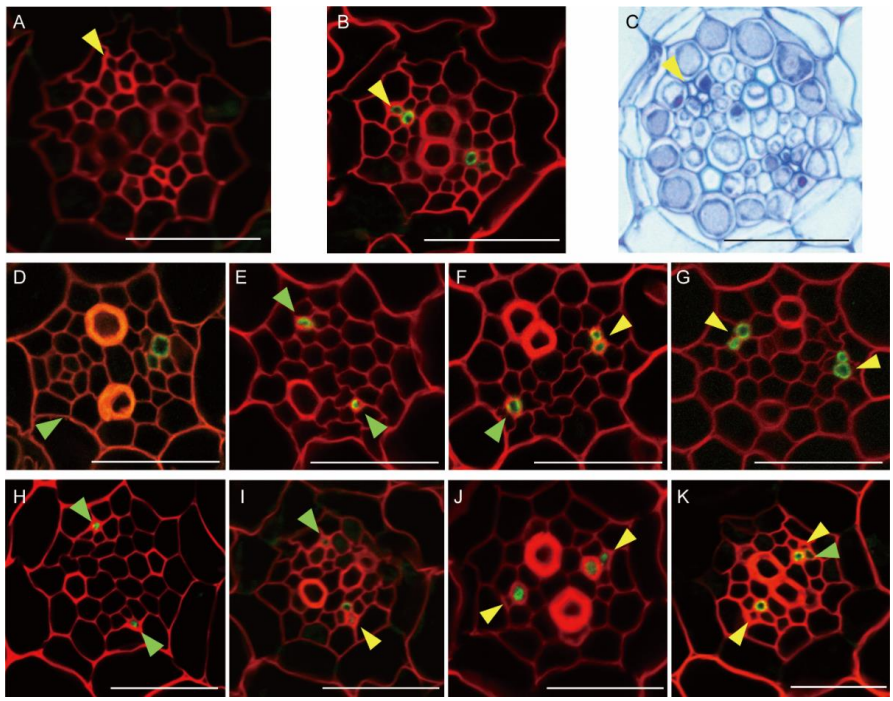

Fig 2. RS6 antibody immunostaining and cross-sections of roots in *Arabidopsis thaliana.*

A-K The cross sections were proceeded using differentiation zone of the 5-6 day old Arabidopsis seedling roots. **A** Negative control (no RS6 antibody) was used in SE-ENOD immunostaining. **B** SE-ENOD immunostaining detected in both proto- and metaphloem SEs in the differentiation zone of the wild type (Col-0) root. **C** Transverse section stained with Toluidine-blue to compare to the SE-ENOD immunostaining. **D-G** Classification of phloem SE development in *shr-2* (n=50). Class 1 had two SEs on one phloem pole and no SE in the other **(D**; n=11**)**. Class 2 had one SE on each of two phloem poles **(E**; n=20**)** and class 3 had two SEs on one and one SE on the other side of phloem poles **(F**; n=8**)**. Class 4 had two SEs on each pole but laterally arranged **(G**; n=11**)**. **H-J** Classification of phloem SE development in *nars1* (SALK_137131; n=14). Class 1 had one SE on each of two phloem poles **(H**; n=8**)**. Class 2 had two SEs on one and one SE on the other side of phloem poles **(I**; n=2**).** Class 3 had two SEs on each pole similar to the WT **(J**; n=4**). K** Transgenic roots expressing *pCRE1::GFP:NARS1* with more than two phloem SEs in SE-ENOD immunostaining. Yellow arrows indicate the phloem SEs. Green arrows indicate the abnormal phloem SEs. Scale bars, 20μm.

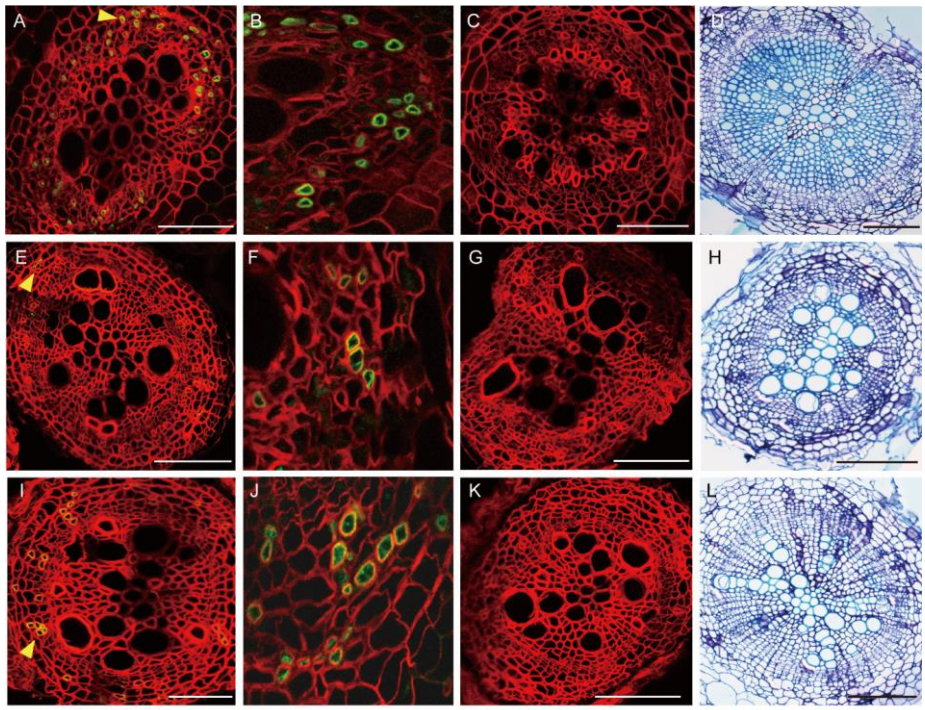

Fig 3. RS6 antibody immunostaining and cross-sections of roots in selected Brassicaceae species. A-C, E-G, I-K Immunostaining of SE-ENOD using RS6 antibody in roots of *Brassica oleracea* **(**khorabi, **A-C**), *Brassica rapa* **(**turnip, **E-G**) and *Brassica rapa* **(**bok choy**, I-K**). **D,H,L** Toluidine blue staining of cross sections of roots in *Brassica oleracea* (khorabi**, D**), *Brassica rapa* (turnip, **H**) and *Brassica rapa* (bok choy**, L**). **B, F, J** Images magnified the regions marked with yellow arrow head where the RS6 antibodies (signals) were detected in panels **A, E, I**. **C, G, K** Negative controls (no RS6 antibody) used in SE-ENOD immunostaining for *Brassica oleracea* **(**khorabi, **C**), *Brassica rapa* **(**turnip, **G**) and *Brassica rapa* **(**Bok choy, **K**). Yellow arrows indicate the areas of magnification. Scale bars, 100㎛.

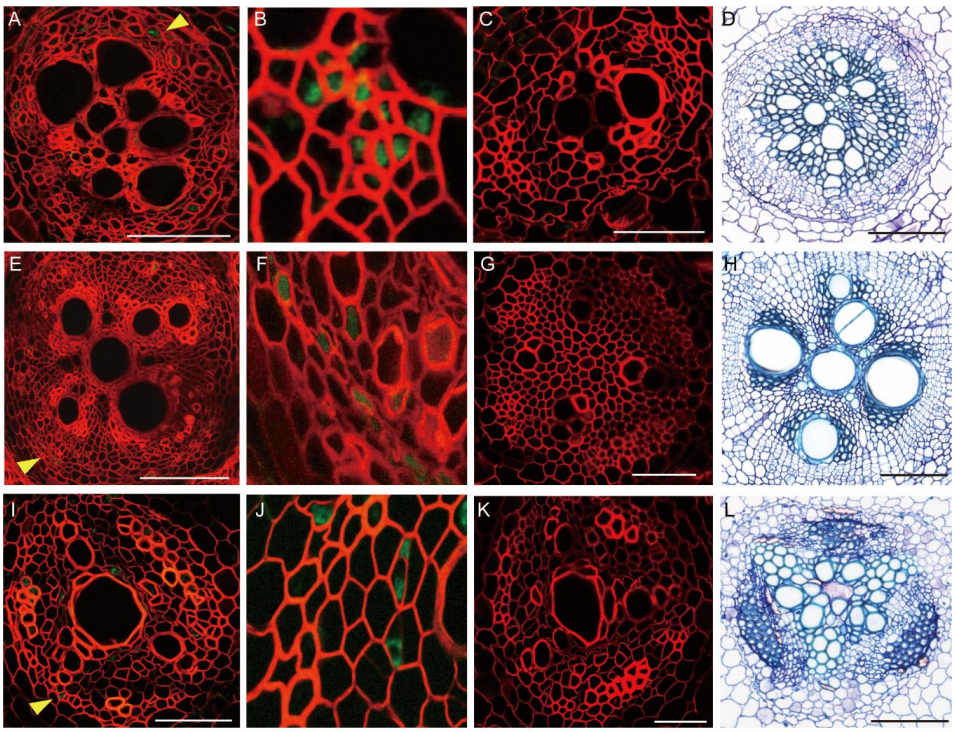

Fig 4. Immunostaining and cross-section of seedling roots for selected eudicot species. **A-C, E-G, I-K** Immunostaining of SE-ENOD detected phloem SE in *Solanum lycopersicum* **(**tomato, **A-C**), *Cucurbita moschata* **(**pumpkin, **E-G**) and *Glycine max* **(**soybean, **I-K**). **D, H, L** Histological analysis of cross sections of seedling roots in *Solanum lycopersicum* **(**tomato**, D**), *Cucurbita moschata* **(**pumpkin**, H**) and *Glycine max* **(**soybean, **L**). **B, F, J** Images magnified for the regions marked with yellow arrow head where the RS6 antibody signals were detected. **C, G, K** Negative controls (no RS6 antibody) used in SE-ENOD immunostaining *Solanum lycopersicum* **(**tomato, **C)**, *Cucurbita moschata* **(**pumpkin, **G**) and *Glycine max* **(**soybean, **K**). Yellow arrows indicate the areas of magnification. Scale bars, 100μm.

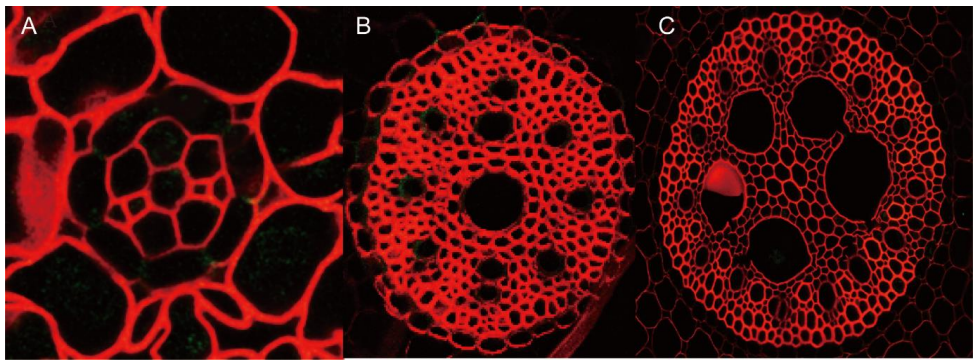

Fig 5. Immunostaining in the seedling roots of selected monocots. A-C No RS6 antibody binding signal was detected in the *Spirodela polyrhiza* **(A)**, *Brachypodium distachyon* **(B)**, *a*nd *Sorhgum bicolor* **(C)**.

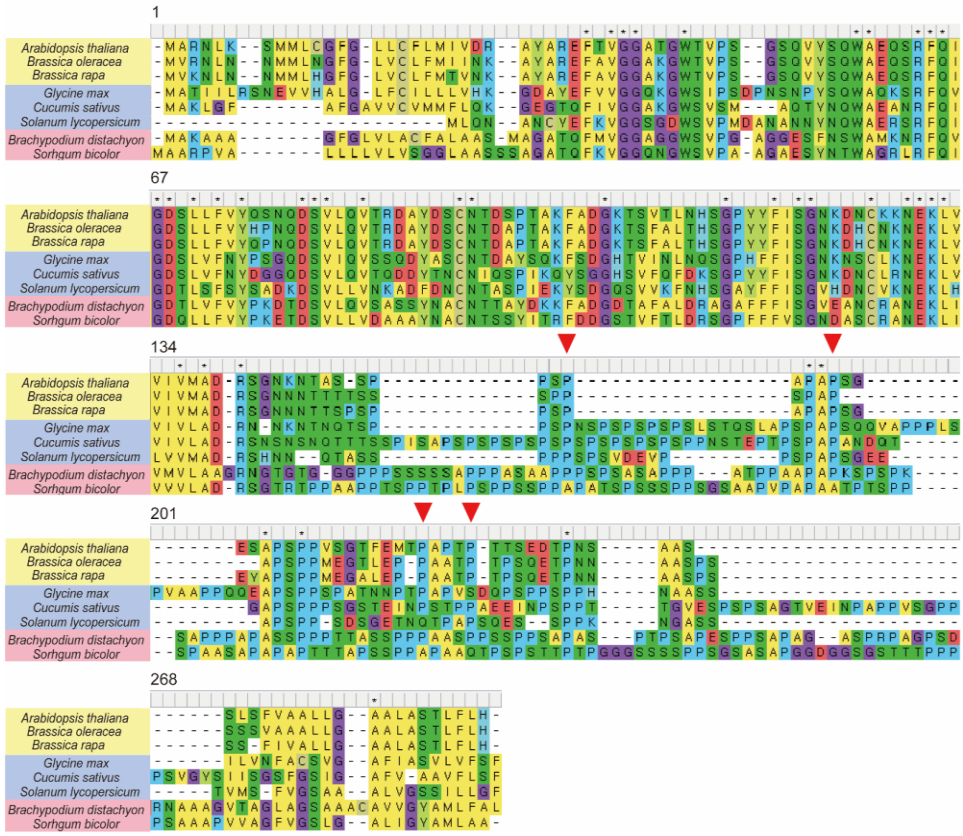

Fig 6. Sequence alignment of putative orthologues of RS6 antigen from species in this study. Amino acid sequences of SE-ENOD orthologues from plants used in the immunostaining were aligned in Mega X. A yellow box indicates sequences from *Arabidopsis thaliana* (AT3G20570.1), *Brassica oleracea capitata* (Bol026649), *Brassica rapa* (Brara.C03796.1) in the Brassicaceae family. A blue box indicates sequences from the eudicot species outside the Brassicaceae, *Solanum lycopersicum* (Solyc07g064240.3.1), *Cucumis sativus* (Cucsa.071940.1) and *Glycine max* (GlymaLee.12G181400.1). A red box indicates sequences from *Brachypodium distachyon* (Bradi3g04773.1) and *Sorhgum bicolor* (Sobic.010G231900.1). Amino acids conserved in all the sequences are marked in asterisks. Red arrow head indicated two proline-serine rich domains, first domain (PAPAP) and second domain (PAPTP).

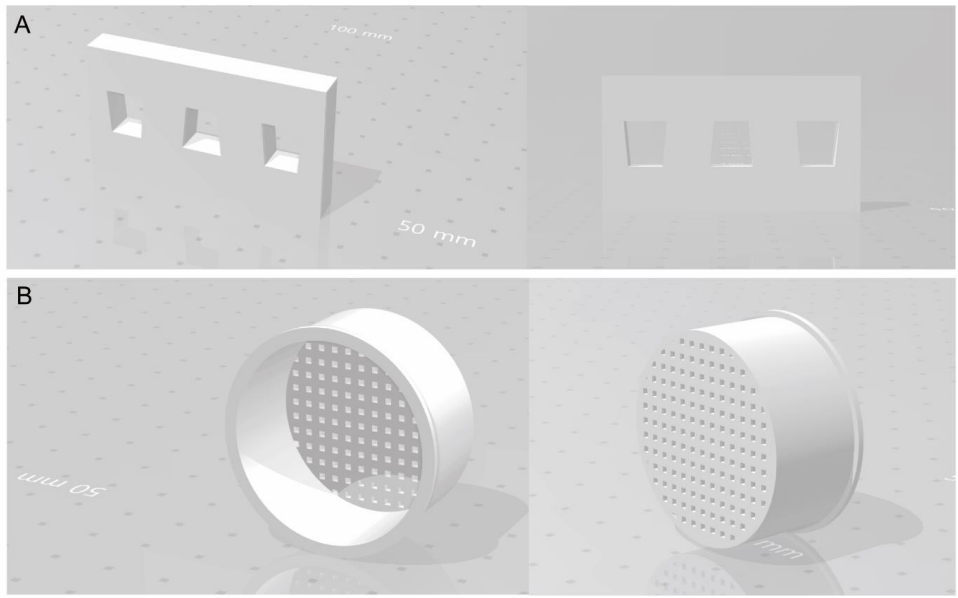

Supplemental Fig 1. Modeling for 3D printing. A-B Custom designed mold **(A)** and strainer **(B)** was generated by Fusion 360 software.